UiT The Arctic University of Norway

Department of Medical Biology, Faculty of Health Sciences.

Moving sperm forward

Benjamin Hellsten.

Master Thesis in Biomedicine, MBI-3911, May 2023.

Supervisor: Mona Nystad (PhD).

Co-Supervisors: Viktoria Emeline Swaty Finanger (MSc) and Azeem Ahmad (PhD).

Women's Health and Perinatology Research Group, Department of Clinical Medicine, Faculty of Health Sciences, UiT The Arctic University of Norway.

IVF-unit, Women's Clinic, Department of Obstetrics and Gynecology, University Hospital of North Norway.

Optical Nanoscopy, NT faculty Department of Physics and Technology, UiT The Arctic University of Norway.

Acknowledgements

I'd like to acknowledge the following individuals for their invaluable support and guidance through my master's degree:

First and foremost, I'd like to express my gratitude towards my main supervisor Mona Nystad. Mona's knowledge, encouragement and guidance was critical in helping me navigate and overcome the challenges this project posed. Her insightful feedback and constructive criticism have been important in shaping my work, I am grateful for the time and effort she devoted to the project.

I'd also like to thank my co-supervisor, Azeem Ahmad. His support and guidance in the microscopy section was instrumental for me to conduct the project. His deep understanding of the subject matter and his valuable feedback were integral for success in the project.

I am also deeply grateful to my co-supervisor, Viktoria Emeline Swaty Finanger, her insightful comments have majorly shaped the paper. Vikoria's support and encouragement have been inspiring in keeping me motivated and focused on improving the thesis.

I would like to extend my gratitude to the bioengineers at UNN for their collaboration and support on the project. Their contributions to the project have been valuable to my project, and they have enhanced my understanding on the subject matter.

Finally, I'd like to thank my parents for their support and encouragement throughout my academic journey. Their dedication has been a driving force and has helped in keeping me motivated though the journey. I am forever grateful for their unwavering support.

May, 2023

Benjamin Hellsten

Benjamin Hellsten

Abstract

Objective: The purpose of this study was to investigate a manual sperm sorting method (Swim-up) and a non-invasive microfluidics method (Zymot microfluidics) with emphasis on formation of reactive oxygen species (ROS) and DNA fragmentation as objective measurements of spermatozoa quality. Standard phase contrast imaging of spermatozoa was compared with quantitative phase contrast microscopy (QPM) imaging.

Study design: Anonymized spermatozoa samples (n=9) from healthy men in North Norway were sorted with the Swim-up method and Zymot microfluidics (Zymot; Gaithersburg Maryland, USA). Analysis of ROS was done with an Oxisperm II kit (Halotech; Madrid, Spain) and by measuring MDA levels (Sigma-Aldrich; St. Louis USA) of spermatozoa. DNA fragmentation was visualized with spermatozoa chromatin staining using a Halosperm G2 kit (Halotech; Madrid, Spain) in conjunction with a Nikon ECLIPSE E 200 phase microscope (Nikon; Tokyo, Japan). QPM analysis was done with an in-house microscope and software. An un-paired T-test and ROUT test was completed to identify P-values and outliers. The software used for this was *GraphPad Prism 9 version 9.0.0* (GraphPad; San Diego, California, USA)

Results: Native sperm and sperm plasma fractions had lower ROS levels in Swim-up samples compared to un-differentiated samples as analyzed with Oxisperm II, resulting in (P=0.0001). MDA-analysis showed that Swim-up and Zymot samples had lower ROS than Raw samples, showing a 0.05- and 0.7-fold difference respectively, resulting in P-value 0.0011 for Swim-up and P-value 0.0014 for Zymot. There was no significant difference in MDA levels between Swim-up and Zymot samples (P-value 0.6193). Swim-up and Zymot samples had a lower spermatozoa/ml than Raw samples, with the mean of Zymot and Swim-up being 460 and 877.7-fold lower. The resulting P-values were 0.001 for Zymot samples and <0.0001 for Swim-up samples. When comparing Swim-up and Zymot sample concentration, no difference was found as their datapoints were close to each other's mean value (P-value 0.0829). DNA fragmentation was lower in Zymot and Swim-up samples compared with Raw samples, with P-values <0.0001 and 0.0047 respectively. Upon comparison, DNA fragmentation was found to be lower in Zymot samples than Swim-up samples with a P-value of 0.0230. The DNA fragmentation in Zymot spermatozoa was 1.2-fold lower than Swim-up. Outlier testing revealed 1 outlier in the Swim-up sample in the MDA analysis, using Q=1.000%. No other outliers were found. QPM provided live video of differentiated spermatozoa and created a heat map giving a "3D" topographical image. Regular phase microscopy was able to capture singular spermatozoa

images stained with G2 DNA Fragmentation kit. QPM could not provide images of spermatozoa stained with the G2 DNA Fragmentation kit.

Conclusion: Levels of ROS were lower in Swim-up and Zymot sorted spermatozoa, indicating that these sorting methods can reduce ROS. MDA analysis showed no differences in ROS when comparing Swim-up and Zymot sorted spermatozoa. With regard to DNA fragmentation, it was demonstrated that Zymot isolated spermatozoa with less DNA fragmentation compared to Swim-up. QPM proved capable of live video data gathering of spermatozoa. However, quantitative analysis was hindered by lack of software tools. QPM was not able to capture high resolution images of DNA fragmentation due to the experimental setup being suboptimal.

Abbreviations

ART Assisted reproductive technology

DA Denaturing agent DA

DIC Differential interference contrast

EGF Epidermal growth factor

ICSI Intracytoplasmic sperm injection

IVF *In vitro* fertilization

LH Luteinising hormone

LS Lysis solution LS

MI Medium inlet

MSO Motile spermatozoa outlet

NA Numerical aperture

NMSO Non-motile spermatozoa outlet

PB1 First polar body

PB2 Second polar body

PBS Phosphate buffer saline

PCM Phase contrast microscopy

QPM Quantitative phase contrast microscopy

RAW Native sperm sample

ROS Reactive oxygen species

ROUT Robust regression and outlier remover

SCS Super coated slides

SD Standard deviation

SEM Standard error of mean

SI Spermatozoa inlet

TESE Testicular sperm extraction

ZP3 Zona pellucida glycoprotein 3

Table of Contents

List of Tables

List of Figures

1 Introduction

The demand for *in vitro* fertilization (IVF) and assisted reproductive technologies (ART) increase each year since infertility is a global health problem affecting 186 million individuals worldwide (1). ART include handling of sperm cells, oocytes (eggs) and embryos (2). Many of the laboratory methods are still manual and may introduce stress to the gametes (3-5). Consequently, there is a need for better non-harmful methods. One promising method is microfluidics for spermatozoa sorting.

Microscopic analysis of gametes and embryos are one of the cornerstones of IVF-treatment and one of the research focuses of the Women's Health and Perinatology Research Group at Department of Clinical Medicine at UiT the Arctic University of Norway. Their main emphasis is on translational and clinical research to the benefit for the IVF-patients which includes phase contrast imaging of sperm cell morphology, motility, and speed.

The Master thesis was performed at the Women's Health and Perinatology Research Group, Department of Clinical Medicine (UiT) in collaboration with the Optical Nanoscopy Research Group, Department of Physics and Technology (UiT). The aim of the collaboration was to shed light on the possible use of the newly developed quantitative phase contrast microscope (QPM) in a clinical setting using normal sperm samples from the IVF-clinic at UNN (Figure 1). The "manual method" of sperm sorting called Swim-up were used as a reference for the comparison of microfluidics sorting. To evaluate a possible negative effect of the separation methods such as DNA-fragmentation and production of reactive oxygen species (ROS) were measured. Two different strategies for ROS evaluation were used, one was a kit provided by Halotech that uses a preliminary grading scale to measure ROS. MDA marker was the second method chosen as a ROS indicator as MDA is correlated to ROS levels in a sample. DNA fragmentation was measured by visualisation of chromatin structure using a kit provided by Halotech through phase contrast microscopy. Samples from the different differentiation techniques were taken for QPM video analysis to show if QPM could be used to video live spermatozoa.

The preliminary studies started with learning the different separate techniques before the whole setup (Figure 1) was performed.

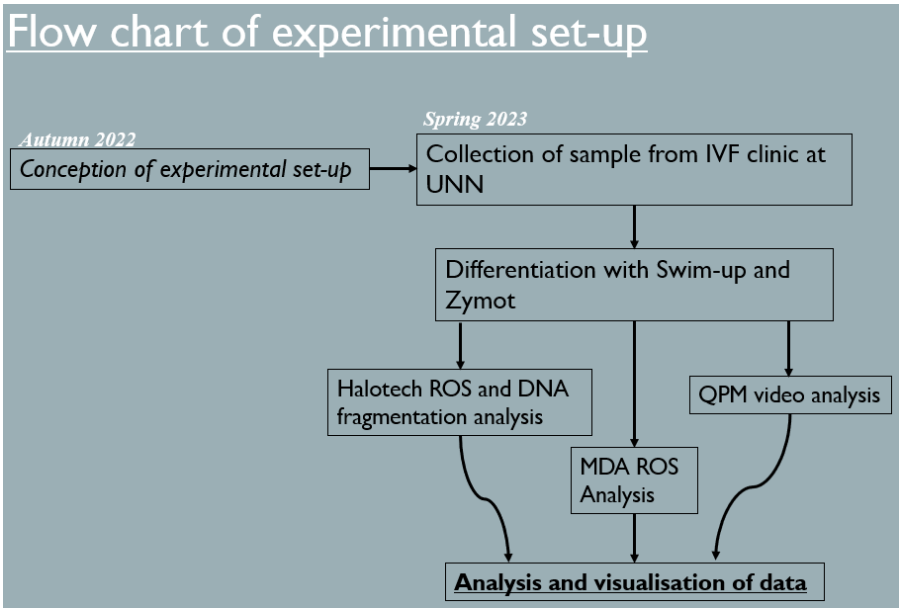

Figure 1:The master project setup*. The flowchart represents an overview of the project setup for the experimental plan. Stage one was conception of the experimental setup. This was followed by conducting the experiment. Collection of samples from the IVF clinic at UNN, followed by differentiation with Swim-up and Zymot techniques. Fractions from samples were subsequently taken for ROS and DNA analysis with the Halotech kits, MDA ROS analysis and QPM video analysis. Data collected was successively analyzed and visualized.*

1.1 Theoretical background

The following section outlines the theoretical background of this study.

Normal development of male- and female gametes are a prerequisite for fertilization and a natural development of the embryo (6, 7). The importance of knowing the intricacies of both cells is paramount to understanding fertility in broader aspects. To lay the foundation, the spermatozoa will be explained first.

1.2 The spermatozoa

Spermatozoa develop in the testicles within seminiferous tubules. At birth, these tubules contain simple round cells. These cells are transformed into mature spermatozoa during puberty (Figure 2 (A)) (8). Several mitotic cell divisions are needed before the spermatogonium is differentiated into a primary spermatocyte that undergoes meiosis (Figure 2(A)) creating a spermatid with 23 chromosomes (7, 8).

The sex determining chromosomes X and Y are also carried in the spermatozoon as number 23 (8). Presence of the Y-chromosome determines that the sex of the resulting child will be a male (7). The spermatid further differentiates into a spermatozoon with a head with a nucleus containing the haploid genome, a midpiece with the mitochondria, and a tail (Figure 2B and Figure 3). A spermatozoon is highly specialized to deliver paternal genes to the oocyte (9). To facilitate this, a spermatozoon has a unique form and structure to streamline the delivery prosses (9).

Figure 3 illustration of spermatogenesis in the human testis, shown below it illustrates the human spermatogenesis. A cross section of a seminiferous tubule is provided together with the maturation step of a spermatozoa.

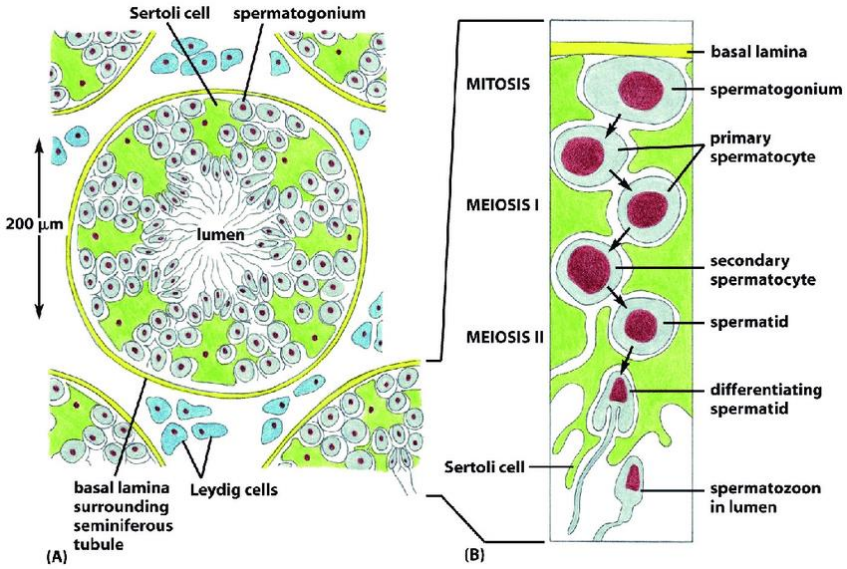

Figure 2: Illustration of spermatogenesis in the human testis. *A) One functional unit in the testis, called seminiferous tubule, is about 200 µm wide and is surrounded by a basal lamina and Leydig cells. B) To create a functional spermatozoon a spermatogonium must go through a reductive cell division to create gametes. This starts with mitosis to make primary spermatocytes for meiosis. In meiosis I the chromosomal content of the cell is halved. Secondary spermatocyte is formed and matured to a Spermatid. These differentiate and migrate to the lumen where the matured spermatozoon is released. Figure has been reproduced from (9)*

The spermatozoon has two main sections, the head, and the tail. Both sections are wrapped in a continuous plasma membrane (Figure 2A) (9, 10). Each section contain important structures related to the functioning of the spermatozoon (9). This is illustrated in the Figure 3 underneath.

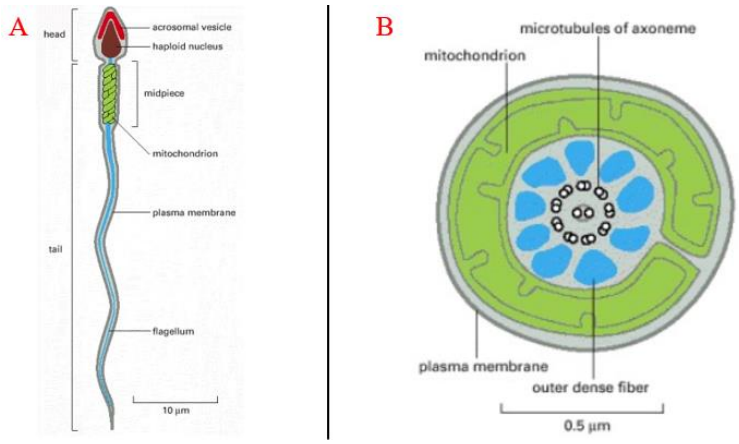

Figure 3: Illustration of a normal mature spermatozoa. *A) The distinct parts of the spermatozoa consist of two main sections named head and tail, with a plasma membrane surrounding the whole structure (grey). The head contains two sections, the acrosomal vesicle shown in red and a haploid nucleus colored in brown. The tail has three sections: a midpiece with mitochondria (green) that are inside the mid piece and a flagellum (blue). B) Cross section of the midpiece with four main sections the plasma membrane (grey), mitochondrion (green), outer dense fibers (blue) and microtubules of axoneme (white). Scalebars; 10 µm in A and 0.5µm in B. All Figures are reproduced from (9).*

The spermatozoan head contains two primary structures: an acrosomal vesicle and a haploid nucleus (9, 10). Inside of the acrosomal vesicle are hydrolyzing enzymes enabling the spermatozoon to penetrate the oocyte outer coating (zona pellucida) (9). Following penetration of the zona pellucida, the acrosome vesicle releases compounds facilitating spermatozoan binding, and fertilization (9, 10). Within the haploid nucleus in the spermatozoon head, paternal DNA is highly condensed to minimize volume and to keep it dormant, preventing transcription from occurring (9, 10). Wrapping of DNA into a tight structure is not done through histones as in somatic cells (9). Instead, the spermatozoon uses extremely positively charged proteins named protamine's to condense the DNA (9).

Tail and midpiece sections of a spermatozoon function as the motility unit, providing force for the spermatozoon to move in a directional manner (9). An outer plasma membrane covers the entirety of the spermatozoon, providing structural support and protection (Figure 3(B)) (9). In the center of the midpiece a high number of mitochondria are located (Figure 3*(B)*) (9). These mitochondria surround nine dense fibers (Figure 3(*B*)) (9). The midpiece center has nine

microtubule-doublets that enable movement by sliding past each other, thus, generating the required flagellar motion (9, 10).

Importantly, ATP needed for movement is created by the mitochondrion in the midpiece (9). They are positioned so that ATP can be easily provided to the microtubules, enabling the flagellar motion of the spermatozoon (9, 10). The bridge linking mitochondrion and microtubules are composed of dynein motor proteins that utilize the ATP to facilitate a sliding motion to generate propulsion (16). Together these structures constitute the main functional units in a spermatozoon.

Having explored the structures of the spermatozoon, it is imperative to get an overview of the oocyte structure to be able to understand the process of fertilization and the subject more comprehensively.

1.3 Oogenesis and fertilization

Normal development of the oocyte is crucial for successful fertilization by the spermatozoa (11, 12). Human oogenesis is special since the development and meiosis I starts in early foetal stages and can be divided into two arrest stages: First in prophase I until puberty and the second continues to the metaphase of meiosis division II. Upon fertilization meiosis continues past meiosis II in the oocyte (11). In the following section, the prosses of oogenesis will be presented in detail.

1.3.1 Oogenesis

Oocyte development starts in the foetal stage (12, 13). The diploid germline cells migrate and settle in the urogenital ridge in week 4-5 (13). These germ cells continue developing into oogonia (12). Approximately 1-2 months before birth, most of the seven million oogonia will undergo apoptosis (12). The remaining oogonia will enter meiosis I, these develop into primary oocytes (12). During meiosis I, the primary oocytes are arrested in prophase I after genome replication, prior to the first meiotic division (12). The primary oocytes stay in this arrest until puberty, where maturation is completed by hormonal signalling (12).

1.3.2 Maturation of the oocyte

Maturation of an oocyte starts with hormonal signalling (12). Two main pathways are followed, either indirectly through exposure of oocytes and ovarian follicles to luteinising hormone (LH) or direct with epidermal growth factors (EGF) (11).

Importantly, LH receptors are not present on oocytes or ovarian follicles. LH receptors are expressed on mural granuloca cells (11). These release EGF helping oocyte maturation and ovulation. (11, 14). EGF subsequently fosters cumulus cell expansion and consequently oocyte maturation and ovulation (11, 15).

Before ovulation one of the oocytes outgrows the other, where the outgrown oocyte is absorbed into the follicle (12). This prevents unwanted oocytes to reach full maturation, allowing only one oocyte to ovulate each month (12). The exact mechanism in this process is unknown, it is however believed that estrogen released by the maturing oocyte effects the hypothalamus to stop the release of follicle stimulating hormone, which is essential for oocyte maturation (12). This creates a positive feedback loop allowing one oocyte to mature while suppressing maturation of other oocytes (12).

Ovulation occurs roughly 14 days after menstruation in women with a 28 day sexual cycle (Figure 4) (12). It is categorised by a sudden surge in LH, causing a protrusion on the matured follicle called a stigma to form (12). Fluids exude from the stigma carrying the oocyte together with several granulose cells, to complete ovulation (12).

As illustrated, the female monthly cycle and oocyte maturation plays a crucial role for preparing the uterus for implantation and fertilization, the two main hormones responsible for this is estradiol and progesterone (Figure 4). Understanding the interplay between menstrual cycle and fertilization is critical for understanding the broader reproductive system.

Figure 4 shows the menstrual cycle. Figure 4 can be split into 3 main parts menstrual phase, profilative phase and secretory phase. In addition, the hormonal balance of estradol and progesterone together with the epithelial lining is described.

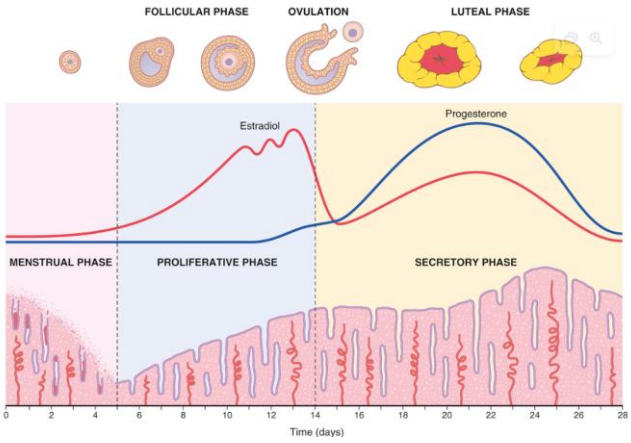

Figure 4: Describes the normal female menstrual cycle with attention to the release of eggs and hormones through time*. It presents the menstrual, proliferative, and secretory phases during which estradiol and progesterone levels vary. In parallel, ovulation punctuates the transition between the follicular and luteal phases. The cycle begins at the menstrual phase (day 0-4), where estradiol levels are above progesterone and slowly increase as the latter remains stable. Epithelial tissue is broken down and discarded during this time. The proliferative phase follows (day 5-14) and sees estradiol levels increase to a peak, with the endothelium increasing in thickness (day 13) whilst the follicular phase translates into ovulation and release of the ovum. Finally, the secretory phase (day 14-28) sees estradiol levels diminish to be below progesterone levels, as the latter increases. The two hormones evolve in a bell-shape in this period, peaking at day 23. Meanwhile, the ovaries are in the luteal phase. During this period the epithelial tissue sees little growth and peaks at day 25. At the end of the period, base levels are reached, and the cycle begins anew.*

Figure 4 describes the creation of an oocyte and how fertilization occurs. Firstly, the oocyte undergoes meiotic arrest in prophase I, after the genome has been replicated (7, 16). This state is called dictyate arrest (16). When puberty starts, a hormonal signaling cascade triggers the final maturation process (12, 16). Key hormones in this process are as follows, gonadotropins, luteinizing hormone and follicle-stimulating hormone, which promote completion of meiosis (16). When meiosis I is completed one set of homologous chromosomes are discarded into PB1 (16). The remaining chromosomes remain in the oocyte and constitute finished set (16). During meiosis II creates the mature oocyte, and is released during ovulation, to possibly be fertilized (16).

If fertilization occurs anaphase II commences, the sister chromatids are separated into PB2 (16). Pronuclear envelope is created to facilitate fusion of the maternal and paternal chromosomes, thus creating a full genome (16). After this occurrence the embryo undergoes mitosis to become a blastocyst, and fetal development starts(16).

Figure 5 shown below illustrates the maturation of an oocyte and fertilization. It has been split into three main parts Meiosis I, Meiosis II and Embryogenesis. Each of these parts have underlying layers explaining individual processes.

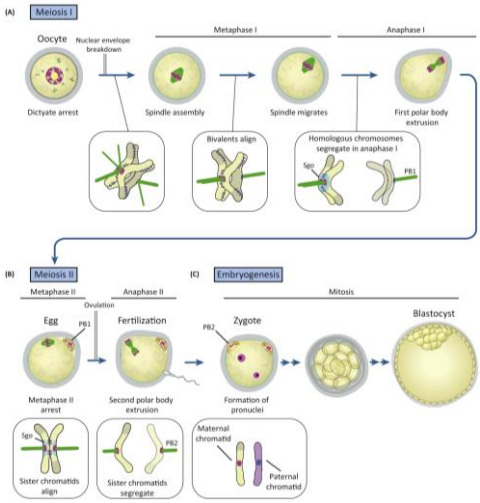

Figure 5:Illustration of egg maturation and fertilization. *A) Oocytes created in fetal development remain dormant for decades until puberty, in a phase named dictyate arrest. When puberty sets in hormonal signals comprising of gonadotropins, luteinizing hormone and follicle-stimulating hormone reactivate the oocytes to complete meiosis. Then meiosis one sets in and continues as described previously in Figure* 2. *When meiosis 1 is completed when one set of the homologous chromosomes are expelled into polar body 1 (PB1), the rest will remain in the oocyte. Further meiosis 2 occurs as described in Figure* 2 *creating a matured egg, which is released during ovulation to potentially be fertilized by a spermatozoon. When fertilization occurs, anaphase II is triggered, sister chromatids are then segregated into the egg and a second polar body (PB2). A pronuclear envelope the maternal and paternal chromosomes unite to create the full genome of the embryo. The embryo then continues with mitosis, becoming a blastocyst. The Figure has been reproduced from (16).*

Figure 5 shows the egg maturation and fertilization process. In section A, the oocyte is created however it remains dormant in dictyate arrest until puberty. When puberty start a hormonal cascade consisting of gonadotropins, luteinizing hormone and follicule stimulating hormone reactive the oocyte and causes it to continue with meiosis I and meiosis II. During Meiosis I the homologue chromosome pairs align in metaphase I and separate in anaphase during the first round of cell division. This is done through a spindle complex and is described in Figure 5. One pair of homologous chromosomes is conversely expelled as PB1. During meiosis II the sister chromatids align, and separation occurs, thus the matured oocyte is ready for fertilization. If fertilization occurs, anaphase II is triggered. The sister chromatids are segregated into the oocyte and PB2. A pronuclear envelope covers the maternal and paternal chromosomes to make a full genome. Thus the oocyte has been fertilized and the embryo undergoes mitosis becoming a blastocyst, in the embryogenesis phase (Figure 5).

1.3.3 Fertilization

Seminal fluid is integral in creating a favorable environment for the spermatozoa and fertilization, where pH and buffering capacity are vital (17). Seminal fluid pH is slightly basic, ranging from 7.3-8.7, protecting the spermatozoa from the acidic vaginal environment (pH≤4.5), facilitating migration into the pH-neutral cervical mucus (17). Moreover, spermatozoa have a high buffering capacity, thus it is unaffected by the acidic environment, through presence of citrate in the seminal fluid (17, 18). Additionally, citrate-ions are present in the seminal fluid, affecting the buffering capacity (17). Primarily these facilitate motility, acrosome creation and fertilization. Examples of other such important ions include calcium, zinc and magnesium that promote healthy spermatozoa function (17). While these substances effect the buffering capacity, other substances such as fructose, glucose and a plethora of proteins affect motility.

Fructose, glucose, and a diverse set of proteins play crucial roles in spermatozoa motility. Fructose and glucose act as sources of energy for the spermatozoa, accelerating motility (17). In addition, a diverse set of protein are shown to increase motility, with albumin being a key facilitator (17, 19). The final step in spermatozoa maturation is the process of capacitation.

Capacitation is an important step to complete maturing of the spermatozoa, which occur in the female genital tract (6). It encompasses two important processes: 1) alterations to the flagellar movement increasing the ability to penetrate the zona pellucida (outer oocyte layer) and 2) expression of zona pellucida glycoprotein 3 (ZP3) which aid in the binding of the spermatozoa to the zona pellucida of the mature oocyte (20). An overview of this process can be seen in Figure 6.

Figure below constitutes the steps necessary for successful fertilization. The steps of fertilization can be split into 8 distinct phases as described in Figure 6. The result is the fusion of the male and female pronucleus achieving fertilization.

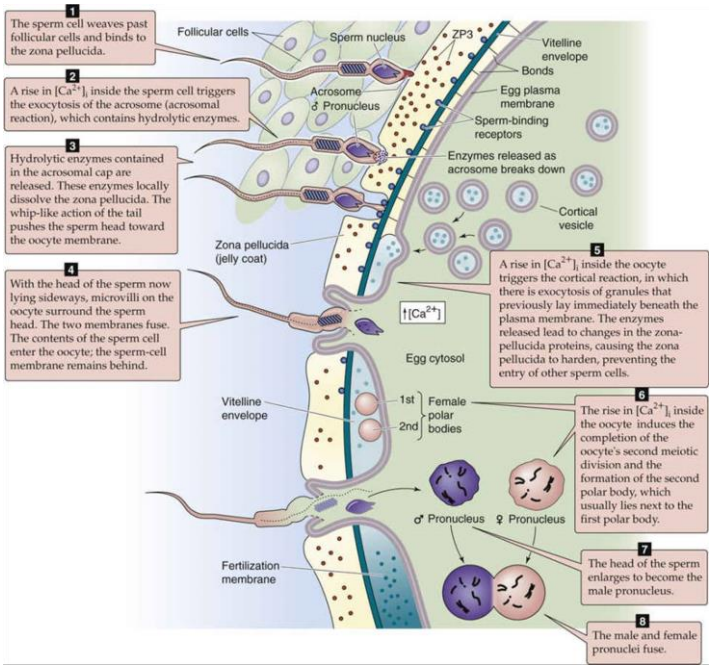

Figure 6: The fertilization process in humans. *Fertilization consists of eight steps. 1)The sperm cell passes the follicular cells and binds to the zona pellucida. 2) Rise in Ca^{2+} causes the sperm cell to release hydrolytic enzymes to help breakdown of the zona pellucida. 3) With the breakdown of the zona pellucida and the propulsion generated by the tail, the spermatozoon can go deeper into the oocyte. 4) When the spermatozoa have moved sufficiently through the membrane, the head fuses with the oocyte and the contents of the head are released 5) When the contents of the spermatozoa release into the oocyte they trigger the cortical reaction, this causes granules adjacent to the membrane to migrate into the zona pellucida, causing hardening of the membrane and preventing further spermatozoa binding. 6) rise in Ca^{2+} because of the previous release of contents, causes the completion of the second meiotic division, and formation of the PB2. 7) the head of the spermatozoa enlarges and becomes the male pronucleus. 8) the male and female pronuclei fuse. Figure was reproduced from (21).*

Many different substances and processes are involved in the binding of spermatozoa and oocyte (6). Oocyte and spermatozoa binding is enriched by ZP3, to create a strong fusion between the oocyte and spermatozoon (Figure 6) (22). An increase in Ca2+ causes the acrosome to release hydrolytic enzymes, which are necessary to break down the outer membrane of the oocyte. Together with flagellar movement of the spermatozoon, this drives the spermatozoon towards the inner membrane (Figure 6) (6, 21). Upon reaching the inner membrane the microvilli rich region fuses with the sideways oriented spermatozoon, releasing the contents of the spermatozoa head into the oocyte (21). Changes within the oocyte caused by the spike in Ca^{2+} trigger a cortical reaction (6, 21). This causes the membrane of the oocyte to harden, thus preventing other spermatozoa from binding to the membrane (6, 21). A rapid rise in Ca^{2+} causes the final maturation of the oocyte, in this fashion releasing it from meiotic arrest II and forming PB2 (Figure 6) (6, 21). Lastly, the spermatozoon head enlarges to become the pronucleus and subsequently fuses with the female pronucleus to complete fertilization (Figure 6) (6, 21).

In some circumstances the natural process described above might not be possible due to either male or female factor infertility. In such instances *In vitro* fertilization is an important tool to overcome these obstacles. In the section below *in vitro* fertilization will be explored as a practice in fertility treatment.

1.4 *In vitro* fertilization

In vitro fertilization is part of an umbrella term known as assisted reproductive technology which encompasses many technologies aimed at assisting couples in getting pregnant (23). ART methods in IVF account for 99% of all procedures (23, 24). IVF fertilization occurs i*n vitro* where the oocyte can be fertilized by a spermatozoon in a dish (23, 25). Initiated embryo development, the embryo is monitored in a microscope each day (23). If the embryo reaches sufficient condition, the embryo is transferred to the woman's uterus and the development continues *in vivo* (23). IVF as a procedure has had to undergo a lengthy development process to reach mainstream medicine.

IVF has become a widely accepted method for treating infertility. Involving manipulation of human gametes outside of the body. However, the development of modern IVF has been a lengthy process that started experimentally in the 1970s. The section below will outline the major developments that has led to modern IVF treatments.

1.5 History of *in vitro* fertilization

Before the late 1970s, women with non-functioning fallopian tubes where considered to be sterile (25). However, with the first human born using IVF technology in 1978, it marked the start of IVF for fertility treatments (26). Although experimental, at the time it underwent rapid development and refinement, with the success rate increasing from 6% in 1980 to 30% in 1983 (25, 27, 28).

Initially, surgical intervention was needed for IVF procedures (25). In the mid-1980s new ultrasound technology led to less intrusive oocyte retrieval methods (25). This developed to transvaginal ultrasound guided transvaginal follicle aspiration that became the standard method in the 1980s (29). This method reduced the number of lab-personnel needed, hospital expenses, risks, discomfort and procedure time from 2 hours to 15 minutes (25). IVF treatment became more standardized, and it became clear that male infertility was one of the next challenges (25).

IVF treatments relied on spermatozoa of sufficient quality including morphology, concentration, and motility (25). If these were insufficient IVF success would be impacted severely (25, 30). Development of intracytoplasmic sperm injection (ICSI) in the 1990s revolutionized male IVF technology. With the ability to select and inject spermatozoa into an oocyte, doctors could increase success rates dramatically (25, 31). ICSI achieved success rates of up to 70%, overcoming struggles presented by varying spermatozoon quality, as of 2003 55.6% of all treatments were of this type (25).

For males with non-viable spermatozoa in the ejaculate, a procedure called partial zona dissection was developed, this though had limited success (25). In the 1990s spermatozoon's could be collected from testicular tissue, known as testicular spermatozoon extraction (TESE) (32). TESE achieved a 70% fertilization success rate and required few spermatozoa of suboptimal quality, providing a treatment alternative to individuals with conditions that impact spermatozoon quality (25, 33). With these dramatic improvements in laboratory practices, it has led to IVF becoming a modern staple in medicine.

1.5.1 Modern in vitro fertilization

Since the first successful IVF birth in 1978, IVF and ART has made significant progress in treating female and male infertility, resulting in 2 million "IVF babies" born worldwide from 1978 to 2006 (25). Modern IVF treatment starts with blood tests and hormonal stimulation of the woman (Figure 7). Spermatozoa analysis and retrieval are performed to do either *in vitro* fertilization or ICSI. The embryo culture is then monitored, and an embryo of excellent quality is chosen for transfer to the woman.

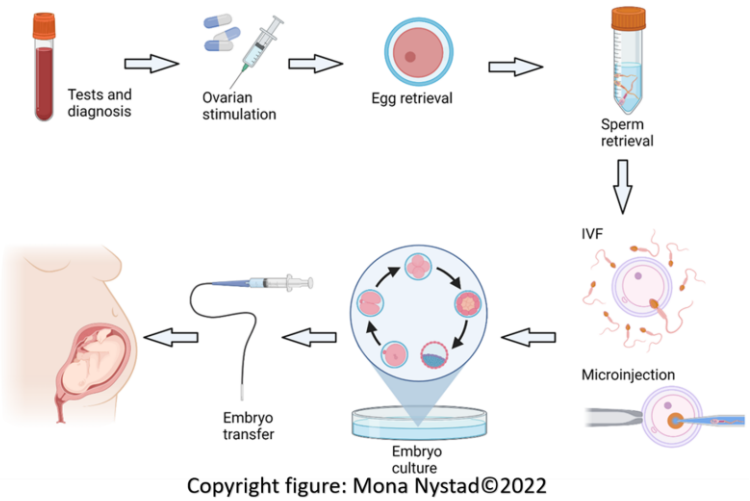

Figure 7*: *Showing stages of modern IVF treatment. *Diagnostic tests are first run to ensure proper treatment is selected. Egg and sperm retrieval is subsequently done for IVF procedures. The fertilized oocyte is placed in an embryo culture and transferred to the womb for maturation.*

As shown in Figure 7 Modern IVF procedures are multistep, requiring highly trained personnel (25). Even as the procedure is difficult IVF however accounts for 4.5% of births in Europe and 1.6% in the USA, demonstrating IVF and ART importance (23-25). IVF has proved monumental in helping patients suffering from fertility problems. To reach optimal success chances, spermatozoa of high quality are needed. To select spermatozoa of good quality IVF clinics routinely do spermatozoa sample evaluations.

1.6 Basic semen sample evaluation

1.6.1 Spermatozoa motility

Spermatozoa motility is an important factor for fertilization success, motility is however greatly affected by age in the male (30). Motility of spermatozoa decreases with 0.6% per year in males (34, 35). Over a 20 year period, this can amount to a 12% decrease in motility (30). It is believed that the age of a male doesn't affect the spermatozoa directly, instead effecting fertility indirectly through prostate and the epididymis (30).

Spermatozoa motility is developed when the spermatozoa goes through the prostate and epididymis (30). It is, therefore, believed that a decrease in motility is due to the decrease in function of the prostate glands and epididymis, causing changes in mitochondrial function by altering cAMP-induced tyrosine phosphorylation cascade that is responsible for the rapid movement of the spermatozoa flagellum (36, 37).

It is important to consider additional characteristics when evaluating Spermatozoa. Spermatozoa concentration is an important factor in determining fertility, as low concentrations significantly hinder successful fertilization. The section below describes in brief how spermatozoa concentration is affected in males.

1.6.2 Spermatozoa concentration

Spermatozoa concentration when first studied in 1969, observed that in males 20-30 years of age, 90% of seminiferous tubules contained spermatids (38). In males 40-50 years of age only 50% of seminiferous tubules contained spermatids, dropping to 10% in males older than 80 (39). However, spermatozoa concentration is the least consistent parameter, with studies finding contradicting results, showing both decreases and increases in concentration with age (34, 40).

Samples with large concentrations of spermatozoa do not guarantee successful fertilization. Spermatozoa morphology is therefore an important parameter when analyzing spermatozoa. Morphology refers to the size, shape, and structural characteristics of the spermatozoa. The section below describes how spermatozoa morphology is affected by factors such as hormones and reactive oxygen species (ROS) in males.

1.6.3 Spermatozoa morphology

Spermatozoan morphology decreases during male ageing, with a reduction of up to 0.9% per year (34, 41, 42). This translates to a total global decline of 18% from 1988 to 2007 (34, 41, 42). Hormonal changes and the body's intrinsic inability to remove ROS contribute to this pattern (43). In the ageing male, gonadotropin levels increase while testosterone levels decrease with the decline of leyding cells (12, 43-45). Additionally, the Intrinsic capacity of the body to remove ROS reduces with age (46, 47). The build-up of ROS can lead to inadequate spermatozoa formation in the testis by damaging DNA in gametes (47, 48). This potentially creates spermatozoa with abnormalities in the ageing male.

When describing spermatozoa with potential abnormalities, common guidelines are followed from the WHO. These guidelines ensure that abnormal spermatozoa are categorized correctly. A description of the WHO criteria is provided below, to give an insight into abnormal spermatozoa.

1.7 Abnormal spermatozoa

WHO manual, provides an easy to access repertoire of definitions and categorization on abnormalities related to spermatozoa (49). This ensures consistent conclusions with laboratory testing of samples (49). It also helps the scientific community ensuring transparency and ease of communication (49).

There are many different subclasses of abnormal spermatozoa conditions detailed in the WHO manual, some of these are mentioned in this chapter.

1.7.1 Azoospermia

Azoospermia is a condition were a male does not produce viable spermatozoa, representing 15% of all male infertility cases. (50). It can be split into two classes, obstructive and non-obstructive azoospermia. Obstructive azoospermia describes the condition were no spermatozoa are present in the seminal fluid because of an obstruction (50). Non-obstructive azoospermia, spermatozoa are not present in the seminal fluid because of abnormal spermatozoa production (50). Azoospermia does not however describe morphological abnormalities.

As azoospermia refers strictly to the condition where a male does not produce any spermatozoa in seminal plasma, it does not relate to abnormal spermatozoa morphology. Abnormal morphology in spermatozoa describe a variety of conditions. These are categorized by the WHO and are described in the section below.

1.7.2 Abnormal morphology

In Figure 8 abnormal spermatozoa morphology is shown. There are four main areas of defects encompassing the major areas of a spermatozoon, head, neck-midpiece, tail, and cytoplasmic defects (49). Importantly, these are then split into a variety of subcategories as seen in Figure 8 (49).

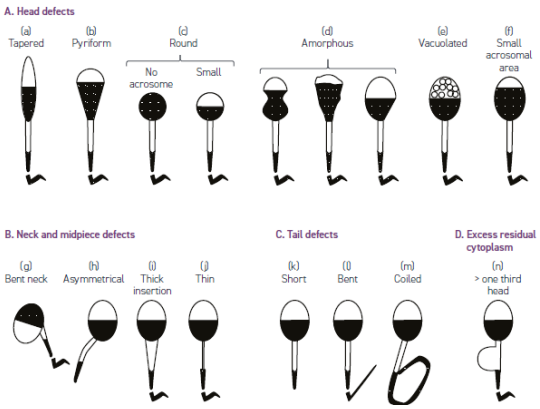

Figure 8*: *Illustration of different classes of abnormal spermatozoa. *The Figure is divided into sections A, B, C and D with subsections in each. A contains six subsections describing different head defects a sperm can have. The six sections are as follows, Tapered, Pyriform, Round, Amorphous, Vacuolated and Small acrosomal area, these are labelled A-F, respectively. Section B contains neck and midpiece defects and contain four subcategories such as bent neck, asymmetrical, thick intersection and thin, they are labelled G-J. From there is section C that contains tail defects, labelled as short, bent, and coiled, shown in subsections K though M. Section D named excess residual cytoplasm, contains only one abnormality named one third head, labelled as n. The Figure was taken from WHO laboratory manual for the examination and processing of human semen* (49).

Abnormalities in spermatozoa can be related to the head, midpiece, neck section, tail defects, cytoplasm with each affecting the spermatozoa differently (Figure 8). Head defects are the biggest class with nine different subclasses. The second biggest class of defects are the neck and midpiece defects with four being illustrated in Figure 8. Second to last are tail defects, as three defects of this kind are illustrated in Figure 8. Excess residual cytoplasm defects describe only one condition and is illustrated in Figure 8.

Importantly, spermatozoa with defects often suffer from more than one, making fertilization even more unlikely (51). If over 25% of all spermatozoa in a sample have one or more of these defects clinical sterility is often assumed (52). Supplement 8 shows what's considered a normal spermatozoa and what's considered an abnormal spermatozoa as the WHO laboratory manual defines it (49).

A normal spermatozoa has strict morphological criteria set by the standard WHO report (49). According to WHO, a normal spermatozoa head is characterized by being smooth, regularly shaped, and slightly oval. A spermatozoon's head should not contain any vesicles, except the acrosome region that should encompass 40-70% of total head volume (49). Abnormal spermatozoa can have an acrosome bigger or smaller than 40-70% (49). Changes to head shape, length, width, presence of vacuoles, and the occurrence of more than one head is considered abnormal (49). Any combination of these is also considered abnormal (49). When considering when each individual section of a spermatozoon the WHO states the following.

A spermatozoon's midsection should be about the same length and thinner than the head, in addition to having the same plain alignment as the head (49). Irregularities in the midpiece include, shape, thickness, incorrect plain alignment, or any combination of the above (49).

The tail section of a spermatozoa should be 10 times the length of the head, and slightly irregular without clear breaks (49). Abnormalities such as shortness or an irregular thickness, shape, or multiple tails is an indication of abnormal development (49).

Cytoplasmic globules can be present in spermatozoa; however, they should cover less than 1/3 of the spermatozoa head size (49). Cytoplasmic globules are considered abnormal when the droplets are over 1/3 of spermatozoa head size (49).

As described in the above sections, spermatozoa suffer from a variety of abnormalities. In IVF procedures it is therefore paramount to select the healthy fraction from a sample. To achieve this a variety of preparation techniques have been developed to select healthy spermatozoa.

1.8 Existing spermatozoa preparation techniques

Purification of spermatozoa is a crucial step in IVF (25, 49). As it improves the quality of the spermatozoa sample and fertility rates of patients (25, 49). Therefore, it's important that IVF clinics have a good practice using the best and least damaging methods of spermatozoa purification (49). The approach each separation technique uses varies; IVF clinics need to have the expertise to select the appropriate one for individual patient needs.

There are various approaches to separate spermatozoa from the sperm fluid (25, 49). Principles of separation differ between methods (49). It can be as simple as adding medium and gently centrifuging the sample to induce a separation of spermatozoa from the seminal fluid (49). More complicated approaches take advantage of the density difference between normal and abnormal spermatozoa samples (49). The most common techniques used to differentiate spermatozoa in IVF clinics are described below.

1.8.1 Simple wash

The simple wash method is commonly used on spermatozoa of ideal quality and quantity, as it contains as few steps of manipulation as possible, to reduce the creation of ROS (49). ROS can negatively affect DNA quality and motility of spermatozoa (47, 49). Initially, the simple wash requires extensive liquification of the spermatozoa (49). After which the liquified spermatozoa are mixed with additional medium and centrifuged minimally (49). When phase separation occurs, the sample can be collected for downstream applications (49).

Simple wash is a straightforward technique used mostly for ideal spermatozoa. When samples are of subpar quality, more complicated sorting techniques are needed to select the healthy fraction, such as density gradient centrifugation.

1.8.2 Density gradient centrifugation

Density gradient centrifugation (DGS) is the separation of spermatozoa based on density (49). Morphologically normal spermatozoa have a density of 1.10g/ml, while abnormal spermatozoa have densities between 1.06g/ml and 1.09g/ml (49, 53). This difference is enough to discriminate normal from abnormal spermatozoa after centrifugation (49, 53). To minimize stress on spermatozoa and avoid ROS formation, centrifugation of the sample is done at the lowest speed possible (49, 53). DGS produces a gradient through the centrifugation of the sample that is either continuous or discontinuous.

DGS is either continuous or discontinuous (49). DGS involves separating different components of semen based on their densities into distinct layers including seminal plasma, white blood cells, debris, abnormal non-motile sperm, interphase proteins, and viable and motile sperm (49). The separated layers can be used for various purposes, such as fertility treatments or research (49, 54). When selecting the type of DGS, it is important for IVF clinics to be aware of what each gradient consists of. Since the continuous and discontinuous gradients are fundamentally different.

As suggested, a continuous gradient does not have "defined" layers in the same manner as a discontinuous gradient does, where each layer of the gradient is placed on top of each other (49, 53). In the first layer of the discontinuous gradient, there is the seminal plasma that resembles a clear liquid, in the next layer there is a small sheet of white blood cells and debris (53). The third layer, consists of abnormal non-motile sperm, this portion is called the 45% phase (Figure 9) (53). The 45^{th} percentile denote the amount of diluted silane coted silicate particles needed to produce the given gradient (Figure 9) (55). This principle is illustrated in Figure 9. In the discontinuous gradient a lower phase is also present.

In the lower phase of the discontinuous gradient the viable motile spermatozoa are located (53). These sperm are in the 90% gradient, meaning there is a substantial amount of diluted silicate particles (Figure 9)(55). The 45% phase and 90% phase are separated by a thin interphase layer consisting of a mix of protein (figure 9) (53). Phase separation and the creation of separating layers and sorting is shown in Figure 9. Figure below shows the principle of density gradient centrifugation. The phases are described and how much each phase constitutes of a test tube.

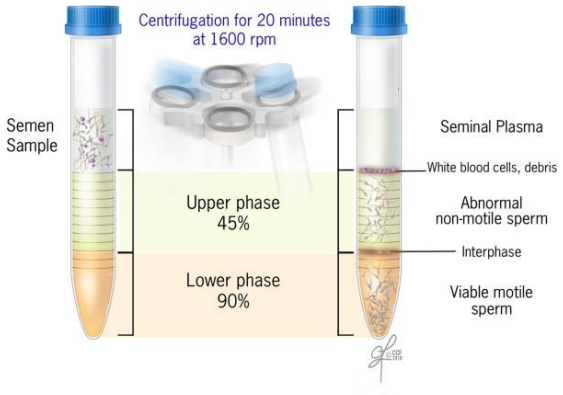

Figure 9: Showing DGS and phase sections. *Mediums are poured into the vessel in the following sequence, 90%, 45% phase and finally the sample, this is shown in the right section of the Figure. After centrifugation for 20min at 1600rpm, a separation is induced. Sections from top to bottom are as follows Seminal plasma, white blood cells and debris, abnormal non-motile sperm, interphase, and viable motile sperm. This is shown in the right hand of the Figure.* ***Figure*** *is reproduced from (53**).***

As an alternative to DGS, Swim-up can be used, the technique uses the intrinsic movement of healthy spermatozoa to differentiate samples. This technique is described in the section below.

1.8.3 The swim-up protocol

Swim-up is one of the most common techniques for separating spermatozoa (Figure 10). The Swim-up protocol is based on the intrinsic motility of the spermatozoa to differentiate a sample (49). A spermatozoa pellet is created through gentle centrifugation, with two overlapping mediums gently placed over the pellet after centrifugation (49). The top layer medium contains an environment that is favourable for spermatozoa, spermatozoa will migrate to this layer from the bottom, i.e. they will “Swim-up” (49). The migration of the spermatozoa is the mechanism behind Swim-up.

This migration enables selection of spermatozoa, as only a spermatozoa with the best motility and without morphological abnormalities will migrate into the nourishing medium (49, 54). This is shown in Figure 10 when gathering spermatozoa from the top layer medium, it’s important to take the area furthest away from the bottom layer, as the spermatozoa will have the best motility and morphology (49, 54).

Figure 10 below shows the layout of a Swim-up sample. Notice how the liquified sample after incubation migrates to the upper section of medium. The reaction tube is also placed on a slight angle to allow the maximum amount of surface area for collection.

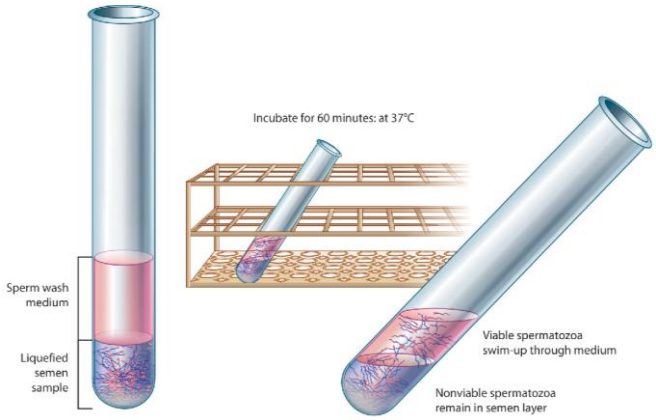

***Figure 10**: **Principle behind the Swim-up method**. The Figure shows the sample after the first round of centrifugation. Tube furthest to the right shows the overlapping mediums. Bottom layer contains the liquified spermatozoa while the top layer is SpermWash medium, rich in nutrients. Furthermore, the sample is incubated at an angle for 60min at 37°c. After incubation, motile spermatozoa migrate to the top layer while immotile spermatozoa remain at the bottom layer. Figure has been reproduced from (54).*

Figure 10 shows the swim-up reaction tube after centrifugation. Centrifugation causes spermatozoa to be pooled at the bottom of the reaction vessel, as seen in Figure 10. The pooled sample is incubated at 37°c at an angle, to allow swim-up of spermatozoa. After incubation the highly motile spermatozoa are collected from the top section of the sample. Further IVF procedures such as an extended examination are possible.

When differentiation of a spermatozoa sample is completed, an extended examination can be done to gather additional characteristics. These examinations vary between the needs of each individual sample but often include analysis of ROS quantities and chromatin structure. These two parameters are described below.

1.9 Extended examination of spermatozoa

1.9.1 DNA fragmentation

DNA fragmentation is a debated topic in male infertility. The intrinsic inadequacy of spermatozoa to protect against oxidative stress is a contributing factor to DNA fragmentation (56). Poor chromatin structure exposes particularly the peripheral DNA, the loose structure around histone protein in this area causes the DNA to be susceptible to fragmentations through ROS (56). Outside factors also contribute to DNA fragmentation (56). Animal models have shown that DNA fragmentation increases with age, where it's thought to be driven by a decrease in epididymal antioxidant capacity, increasing oxidative stress. (30, 57, 58). In addition, during sample preparation any centrifugation or handling of samples can cause DNA fragmentation through ROS creation (49). Studies correlate oxidative stress and subsequent DNA fragmentation with male infertility (4). Therefore, some IVF clinics have adopted screening methods for oxidative stress and DNA fragmentation to explain male infertility (30).

DNA fragmentation can be caused by various endogenous and exogenous factors. One of the factors leading to oxidative stress is ROS. ROS induce DNA breaks and modifications of bases leading to DNA Fragmentation. Thus, ROS has been an important topic in male fertility categorization. The sections below details what roles ROS have in male fertility.

1.9.2 Oxidative stress

Oxidative stress (OS) has been shown to be a major factor in male infertility, with 30%-40% of infertile men showing high ROS levels in seminal plasma (46, 47, 57). OS can in brief be described as the body's inability to detoxify a given tissue of ROS (4, 47). Consequently, if the body's OS capacity is lower than the amount of ROS created at a given time, it can exist freely in a biological system, and create damage to tissues (4, 46, 47). The sources of ROS can vary between endogenous and exogenous sources in the body (47).

ROS can come from both endogenous sources and exogenous sources (47). Endogenous sources of ROS include leukocytes, immature spermatozoa, capacitation, and varicocele (47). Exogenous sources include smoking, alcohol, radiation, and toxins (47). These sources of ROS culminate in two distinct pathways that play both pathological and physiological roles (47). The pathological role of ROS is lipid oxidation, apoptosis, and DNA damage, which all interferes with male infertility (47). Physiological roles of ROS are important regarding spermatozoa

since it may influence capacitation, hyperactivation, sperm-oocyte binding, and the acrosome reaction (47, 59-62).

As mentioned, ROS has intrinsic roles in fertility. Capacitation of spermatozoa happens through a controlled low concentration of ROS initiating gene changes and upregulation of cAMP, thus preparing the sperm for hyperactivation (62). ROS's role in hyperactivation is essential to creating the cAMP cascade that leads to the spermatozoa being highly motile, consequently facilitating fertilization (59). With regards to sperm-oocyte binding, ROS has been shown to increase the membrane fluidity (61). ROS cleaves the secondary fatty acid from phospholipids in the cell membrane, thus, increasing fluidity and promoting fusion between oocytes and spermatozoa (60). In connection with the acrosome reaction, ROS promotes phosphorylation of plasma membrane proteins in the spermatozoa, increasing extracellular calcium and promoting the reaction (61). These major events are crucial for fertilization and normal spermatozoa function (47). Highlighting the importance of ROS in fertility, ROS has two main pathways of creation in the male body.

Importantly, all these events have the common need for ROS to be a catalyst. ROS can be produced in two ways: through NADPH in the plasma membrane or NADH in the spermatozoan mitochondria (47). ROS in its most common structure is O_2^-, which is created when O_2 reacts with itself. O_2^- can then generate H_2O_2 through dismutation. If transition metals such as copper or iron are present, H_2O_2 can react with them to produce OH^-, a highly reactive compound that can cause peroxidation of lipids, damage to spermatozoa membranes and significant DNA damage, which can lower fertility (Figure 11) (47). This process can be seen in Figure 10.

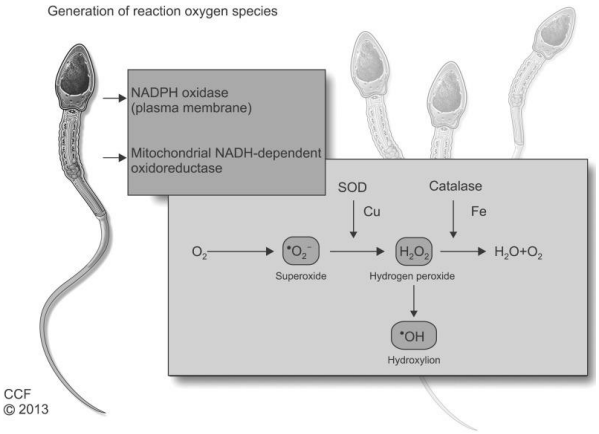

Figure 11: Formation of ROS in spermatozoa: *There are two main ways for ROS to be created, either though NADPH in the plasma membrane or NADH found in the mitochondria. ROS most generic form, O_2 reacts with itself to create O_2^-. O_2^- then reacts with itself though dismutation to generate H_2O_2. If transition metals such as copper or iron are present. When H_2O_2 reacts with either iron or copper they produce OH^-, an extremely potent compound, responsible for peroxidation of lipids, destroying the spermatozoa membrane. In addition, OH^- can cause large amount of DNA damage lowering fertility. Figure is reproduced from (47).*

As shown in the Figure 11, ROS has two main sources of formation in spermatozoa. The two pathways are through NADPH in the plasma membrane, or NADH in mitochondria. However, the products created though the cascade shown in Figure 11. ROS can react with transition metals and create potent oxidisers, potentially leading to DNA damage. It is important in IVF to subsequently remove ROS from a sample, as it could reduce fertility chances. The efficiency the common methods have in removing ROS can be seen in Figure 12.

Figure below describes how different spermatozoa sorting methods impact DNA fragmentation. The methods compare a Raw sample referred to as Centric, Density gradient, Swim-up and Microfluidics.

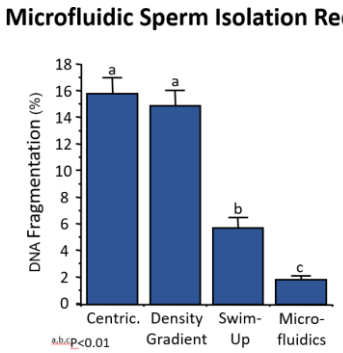

Figure 12: Showing impact on DNA fragmentation based on different sorting methods*. The y-axis on the Figure shows the percentage DNA fragmentation, X-axis denotes what method is shown. Methods shown are Centric (Raw sample), density gradient, Swim-up and microfluidics. Mean DNA fragmentation of the different methods are as follows, centric is 15.5%, density gradient 15%, Swim-up 5.5% and microfluidics 2%. A decrease can be observed between the centric and density gradient methods compared to Swim-up and microfluidics. Figure has been reproduced from (63).*

Figure 12 shows a markable difference in DNA fragmentation based on sorting technique. A scale in % is shown on the Y-axis, while the methods are described on the X-axis. A decrease in DNA fragmentation can be seen between Centric, Density gradient, Swim-up and Microfluidics.

As described ROS are highly reactive molecules that play various physiological roles in spermatozoa. However, excessive ROS can have a negative effect leading to decreased fertility. An emerging technology in ROS removal is Microfluidics. The segment below will detail how microfluidic systems function.

1.10 Microfluidics

Microfluidics, also known as “lab on a chip”, is a highly flexible technology that manipulates fluids that range from 10^{-9} to 10^{-18} liters through channels (64-66). As a technology it has driven advancements in drug discovery and IVF technology (64, 66). Four key areas of influence for microfluidics are biodefence, molecular analysis, biology, and microelectronics (65).

Microfluidics have been particularly impactful molecular biology and biology (65, 67, 68). Development of electrophoresis and gas-phase chromatography in a capillary system fundamentally changed biochemical analysis (65). With advancements of high resolution

detection systems based on lasers and optical sensors, small quantities of a sample were needed to gather data (65). This pushed development of novel smaller systems to complement these advancements e.g., microfluidic devices (65). When molecular biology gained momentum with the development of DNA-sequencing and genomics in the 1980s (65). These two major new fields of research required new detection technologies, where one of the systems to play a major part were microfluidics (65, 68). The sector impacting microfluidics together with molecular biology has been microelectronics, resulting in polymer being used as a fabrication material (65).

Microelectronics has impacted the development of microfluidics. Techniques like photolithography has been successfully applied in microelectronic systems, in silicon electronics (65). Moreover, it was hoped that microfluidics might provide similar success (65, 69). The first attempts to use microfluidics in microelectronics devices were fabricated in silicone or glass, which had limited use as existing micro electrical systems from polymer proved better (65). New microfluidic devises would take advantage of this advancement in polymer manufacturing, leading to cheaper and easier analysis than silicone and glass counterparts (65). Thus, polymer became the standard way to produce microfluidic devises, a crucial step for biology, lowering cost and increasing accessibility (65, 69).

Main advantages of microfluidics over traditional laboratory techniques are the limited reagents are needed, low cost, high sensitivity, resolution, and limited space are needed for analysis (70, 71). An overlooked advantage is that fluids in small confined spaces and in small volumes enable an unprecedented control over molecules and concentrations (65).

As microfluidics devises can manipulate lesser amounts of fluid, with a high degree of precision, it has been explored as a potential technique in IVF. Sections will below explore microfluidics as a tool in IVF.

1.10.1 Microfluidic devices as a tool in IVF

Traditional methods of spermatozoa selection, such as DGS or Swim-up, can provide spermatozoa with high DNA fragmentation and a comparatively low yield from the total sample (49, 72). Microfluidic devises have been created to differentiate high quality spermatozoa from low quality spermatozoa (72, 73). The method of separation varies between manufacturers but can include principles such as laminar flow systems and membrane filters (72, 73).

One of the separation techniques used in microfluidics is a pore principle. This technique requires spermatozoa to swim through pores designed only solely for morphologically correct spermatozoa. Thus, differentiation is possible, the segment below explains the principle of the method.

1.10.2 Microfluidic devices utilizing the pore principle.

Microfluidic devises using a pore principle have been created (72). In practical terms the spermatozoa are sorted through a pore-barrier (72). Spermatozoa in the semen chamber swim upwards to a separate chamber by chemotaxis, shown in Figure 13 (74). Spermatozoa are, therefore, Swimming against gravity to get to the upper chamber through the 3-8 μm pores, meaning undesirable spermatozoa of lesser quality will not pass through (72). The sorting prosses of a pore based microfluidic device is described below in Figure 13. Note how the device only consists of a retrieval chamber and a semen chamber separated by a filter (pores).

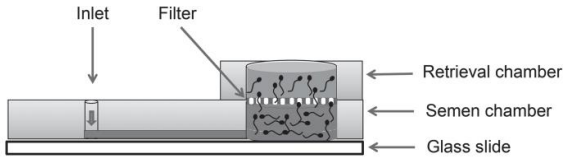

***Figure 13**: **A schematic describing spermatozoa sorting with a microfluidic device using the pore principle**. From the left, the microfluidic unit comprises a spermatozoa inlet. Subsequently, there is a filtration component that possesses perforations for the differentiation of spermatozoa. At the lower portion of the microfluidic device lies a glass slide that serves as the unit's base. On top of the slide, there is a semen compartment that accommodates both motile and non-motile spermatozoa. The retrieval compartment, which comprises solely motile spermatozoa, is situated above the semen compartment. This illustration was adapted from the original source (72).*

The limitation to the devise is that two pores can be joined together unintentionally, potentially creating a pore twice the 8 μm maximum size, enabling unwanted spermatozoa to pass through (72). Pass-through frequency of spermatozoa is proportional to the number of pores on the filter (72). Samples with a high volume of spermatozoa will therefore need more time for all viable spermatozoa to pass through (72). Looking past these caveats, this system provides up to a 10% better yield than Swim-up, in suboptimal conditions for isolation (72). In favourable conditions the device can isolate 58%, while Swim-up technique can only isolate >20% of viable spermatozoa (49, 72). Showing the prowess of microfluidics in IVF.

Microfluidics has thus emerged as a powerful tool in IVF, capable of isolating spermatozoa with a high degree of precision. However, to visualise the quality of the differentiated fraction one must use a microscope. Phase contrast microscopy can be used to achieve this, below is the

description of how phase contrast microscopy creates a high resolution, capable of imaging spermatozoa.

1.11 Microscopy

1.11.1 Bright field microscopy

Bright field microscopy uses transmitted light to observe specimens. In this technique, the light passes directly through the sample, which absorbs or scatters the light to varying degrees depending on its composition and structure (75). The resulting image is a two-dimensional representation of the specimen, with features appearing as dark or light areas depending on their ability to absorb or scatter light (75). Bright field microscopy is useful for visualizing cells and tissues, but it may not be effective at highlighting subtle structural features or differences between cells (75). Bright field microscopy often fails to generate high-contrast images of cells (75, 76). This is because cells are highly transparent, and regular bright field microscopy relies on differences in light absorption and scattering to generate contrast in the image (76). Since cells do not strongly absorb or scatter light, it can be challenging to visualize them effectively using this technique (76). Therefore, a more sensitive imaging technique was developed to aid imaging of biological samples named phase contras microscopy (PCM).

1.11.2 Phase contrast microscopy

PCM was developed by Dutch physicist Frits Zernike in 1955 and is widely regarded as a major innovation in the field of microscopy (77). PCM is a powerful imaging technique used to enhance the contrast of transparent or low-contrast samples, such as cells, tissues, and microorganisms, allowing for better visualization of their internal structures and features (78). PCM utilizes the phase shift that occurs when light passes through a transparent object to generate contrast in the image (78).

In PCM, the light source is split into two beams, one passing directly through a specimen, and the other passing through a phase plate (Figure 14) (78). The two beams are then recombined, producing an interference pattern that can be captured by the microscope's objective lens and imaged onto the detector (Figure 14) (78).

The phase plate creates a phase shift in the light passing through the specimen, converting differences in refractive index into intensity variations that can be detected and amplified by

the microscope (78). This allows for visualization of internal cellular structures that are otherwise difficult to see using traditional bright field microscopy (78).

PCM has several advantages over other imaging techniques. It is non-destructive and non-invasive, allowing for imaging of live cells and tissues without affecting their morphology or function (78). It also allows for the visualization of fine structural details that are not visible with other imaging techniques, making it a valuable tool for research in cell biology, microbiology, and materials science (78).

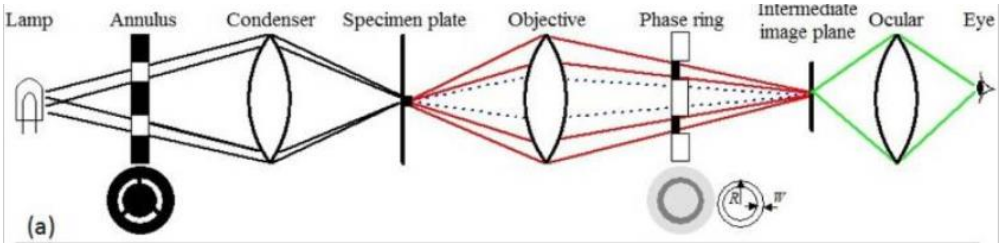

***Figure 14*: Depicting the configuration of a PCM**. Firstly, the sample is illuminated by a lamp. Light travels through the annulus also known as the annular ring. Light then travels through a condenser that focuses the light on the specimen. Light will then depending on the thickness refract and either pass though the phase ring or omit it. The light then travels through the intermediate image plate to focus the light before it passes through the ocular to get refocused into the eye or camera. Image is recreated from (78).

PCM operates by utilizing two key components, the phase ring and the annular ring, which work together to produce higher resolution images (78). The annular ring is located in the condenser portion of the microscope and illuminates the specimen with light (78). As light passes through the specimen, it undergoes a phase shift, which can depend on the thickness and refractive index of the sample (78). The phase ring is located in the objective lens and interacts with the refracted light, enhancing its phase shift and creating an interference pattern (78).

The phase shift created by the sample causes light that hits the phase ring to appear dark in the resulting image (78). Conversely, regions where refracted light fails to hit the phase ring will appear bright (78). This creates contrast in the image, allowing for the visualization of fine details within the specimen that would otherwise be difficult to observe (78).

One advantage of PCM is that it is non-invasive and non-destructive, allowing for the observation of live cells and tissues without damaging them (78). Additionally, it provides high resolution images of transparent samples without the need for staining or other sample preparation techniques, which can alter the sample's morphology or function (78).

1.11.3 Differential interference contrast microscopy

DIC, also known as Nomarski interference contrast or simply Nomarski microscopy, is an advanced form of light microscopy that provides high-resolution images of transparent or low-contrast samples (79). DIC was developed in the 1950s by Georges Nomarski and has since become a widely used technique in the field of microscopy (79).

DIC operates by utilizing polarized light to create interference patterns that enhance contrast in the image (79). The sample is illuminated with a beam of polarized light that is split into two beams by a prism. The two beams of light then pass through different areas of the sample, creating phase shifts due to differences in thickness and refractive index (80). The two beams of light are then recombined and passed through a second prism, creating interference patterns that enhance contrast in the image (79, 80).

DIC microscopy produces images with high contrast and three-dimensional (3D) appearance, making it a valuable tool for observing the morphology and structure of cells, tissues, and other transparent specimens (79, 80). It is especially useful for imaging live cells and tissues, as it is a non-invasive technique that does not require staining or other sample preparation methods that could affect the sample's morphology or function (81).

1.11.4 Quantitative phase contrast microscopy

QPM research is relatively new, shown in 1999 as a viable method for gathering quantitative data with microscopy (82). QPM arose from the fact that the two most popular techniques for imaging in phase contrast microscopy, Zernike’s and Nomarski methods, were good for producing images but not gathering quantifiable data (82). The main drawback of the Zernike method are the two ordinary forms of artefacts produced, named “shading” and “halo effects”, making gathering quantitative data impractical (83). The Nomarski method isn’t held back by the same problems as the Zernike method, instead the main limitation is the intricacy involved in gathering the data, requiring complex processing and signal evaluation (82). This led to the development of QPM, where the main advantage of the method is that the phase division equals modulo 2π when compared to the phase division on the sample, which in practice means that an image generated should be artifact-free and suitable for quantitative measurements such as topography (82). below in Figure 15 a simplified view comparing QPM to regular bright field microscopy is presented.

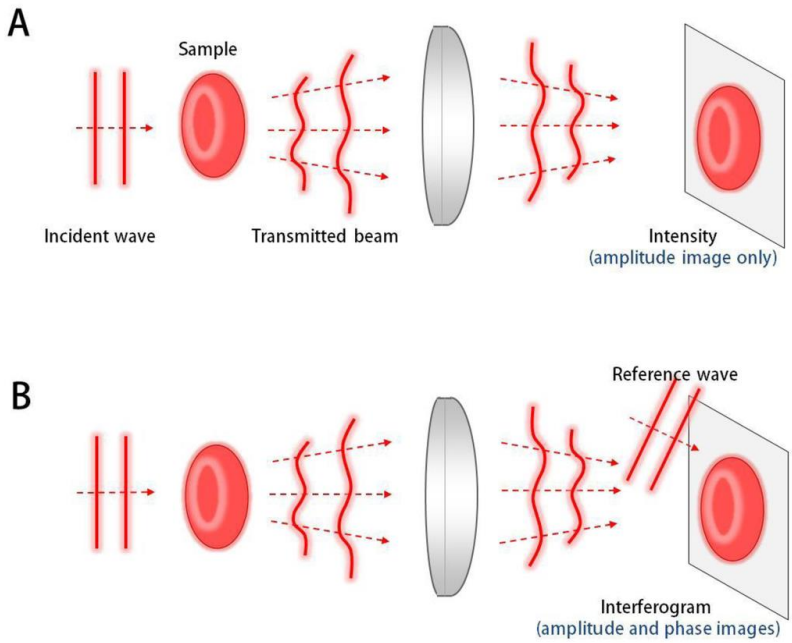

Figure 15: Showing the theory of QPM compared to bright field microscopy. *Figure A shows how a conventional bright field imaging system works. The incident wave travels through the sample and thus becomes the transmitted beam. The transmitted beam gets focused through a lens into a sensor for imaging. The only information gained from bright field imaging is light intensity, otherwise known as the amplitude. B shows the principle behind QPM. QPM imaging starts with an incident wave, that passes through a sample. Thus, it becomes a transmitted beam, this gets focused though a lens, and directed to an optical sensor. But in addition to this a reference wave is incorporated into the image, this gives us phase information on the sample. Figure has been taken from* (84).

QPM uses the theory of interferometry to measure a given optical field. Interferometry is the phenomenon of interference within waves (84). Most biological samples are translucent in regular visible light, thus little contrast is provided. Nevertheless, even if a sample is transparent, it provides an optical delay which serves as a imaging contrast in QPM (84). Principles behind the method can be seen in Figure 15.

QPI systems based on interferometry are widely used today (84). However, these systems suffer from a variety of problems that can impede data gathering (84). Parameters such as vibrations, temperature gradients, airflow will deteriorate QPI measurements by increasing the phase noise (84).

A way to mitigate this is through actively stabilized phase-shifting low-coherence interferometry, by measuring the refractive and thickness of a sample (84). Principle behind the technique is the light beam is split into two parts, one that travels through the sample and one that doesn't (84). These two light sources interfere with each other producing dark and light regions that correspond to interference fringes (84).

To improve accuracy on the sample, the phase of the light waves is shifted by small increments between each measurement (84). This removes unwanted interference in the light wave and reduces noise and potential errors in the sample (84). The last part of the name "low-coherence" refers to using a light source with a small coherence length (84). Meaning that only a small fraction of a sample is imaged at a given time, this allows for a more precise measurement of the samples properties (84). QPM has therefore provided researchers with powerful imaging platform capable of gathering quantitative data.

QPM has emerged as a powerful tool in investigating biological samples. By measuring the phase shift of light, quantitative information can be extracted. This has led to QPM having numerous applications in biology. Described below are some of QPM applications in biology.

1.11.5 QPM in biology

QPM provides label free imaging to characterise structures in living cells that brightfield microscopy is not capable of. For instance, the topology of cells can be measured easily, something that brightfield microscopy does not allow. The chemical makeup of cells can be assessed, in the case of red blood cells concentration of haemoglobin can be measured through QPM (85). Perhaps the biggest advantage of QPM is the study of cellular activities. While it is hard to observe changes directly inside of the cell, membrane fluctuations can be quantitatively measured with QPM (86). Data gathered can thus be correlated directly to chemical or physiological changes within the cell (85). However, conducting this analysis on higher order eukaryotic cells as opposed to red blood cells remains challenging (86). This is due to the complicated 3D morphology eukaryotic cells possess (86). However, QPM still has advantages compared to phase contrast imaging, or more traditional methods in biology.

One of the big advantages of the QPM system is the ability to visualize cells and structures within cells, without using fluorescent labelling techniques (87, 88). Circumventing the limitations of fluorescent microscopy, which suffers from phototoxicity and photobleaching. QPM takes advantage of different refractive indexes to accomplish this (88). Metals such as gold have high refractive indexes, compared to biomaterial, thus, using 3D refractive index tomograms visualization of internal organelles is possible, without using fluorescence (88).

Limitation in QPM is not being able to identify and locate targets that are smaller than the lowest detectable diffraction size (89). Although, this limitation can also be mediated through the integration of other techniques, such as phase and intensity measurements (89).

2 Aim and objectives

The overall aim of this Master's thesis was to compare microfluidic technology in sperm sorting with a traditional sperm sorting method called Swim-up.

The specific objectives were:

- Comparison of the Zymot microfluidic system and the Swim-up technique.
- Implement ROS-analysis and DNA-fragmentation as objective analysis methods to evaluate which of the sorting methods, i.e. Swim-up and microfluidics from Zymot, are the most gentle methods for use in IVF- and ICSI treatment.
- Comparison of Halotech Oxisperm II and MDA analysis to evaluate differences and potential pros and cons in each method.
- Comparison of QPM against standard phase contrast imaging

3 Materials and methods

In this project healthy sperm samples from anonymous donors were recruited from the IVF clinic at the University Hospital of North Norway. All participants were patients who were enrolled for routine laboratory testing as part of their medical care. Prior to enrollment into the study, all participants were informed about the nature and purpose of the study by the bioengineers at the IVF clinic before they provided informed consent (S1 in Supplementary information). All samples were anonymized before enrollment into the research study.

Basic examination of sperm samples according to WHO recommendations were performed by the bioengineers at the IVF clinic as part of routine laboratory testing (49). The data gathered included volume, concertation/ml, viscosity, aggregation, motility (%) and degree of motility.

Table S2 in Supplementary information provides a detailed list of all the equipment, reagents and solutions used for this study. In the section below a brief description of the methods are described. Full protocols are available in supplementary information (S4-6) The different

methods used for examination of the spermatozoa samples in this research project are shown in Figure 16.

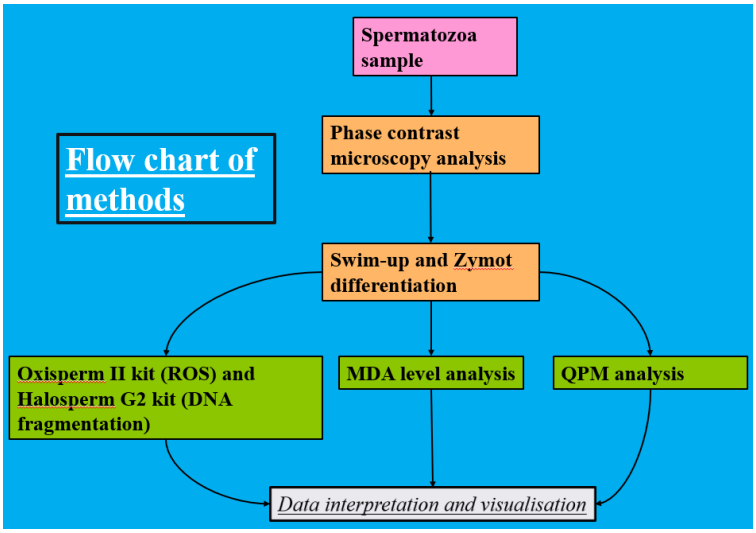

Figure 16: showing a flowchart of the experiments done in this study*. The experimental setup can be split into 7 distinct parts. Gathering of spermatozoa seen in pink. Preliminary analysis and differentiation seen in orange. Analysis types as can be seen in the green fraction of the Figure. Lastly analysis and interpretation seen in the white section.*

3.1 Clinical evaluation and phase contrast microscopy of spermatozoa samples

Spermatozoa samples were liquified for 10-30min in a MR-1 Mini-rocker Shaker (BioSan; Riga ,Latvia) for 25 oscillations/min. Spermatozoa viscosity was measured by observation of droplets from a Polyethylene disposable transfer pipette (fisher scientific; Massachusetts, USA) using the WHO criteria (49). Total volume (ml) was also noted for each sample. A duplicate of 10ul of spermatozoa sample was placed on microscopy slides (Thermo fisher; Massachusetts, USA) with cover slips (fisher scientific; Massachusetts, USA) and examined in a Nikon ECLIPSE E 200 Phase contrast microscope (Nikon; Tokyo, Japan). Sperm number (sperm/ml), motility (grade and % of motile sperm cells) and aggregation were estimated using 20× magnification and 40× magnification objective.

3.2 Swim-up

Samples were liquified on a in a MR-1 Mini-rocker Shaker (BioSan; Riga, Latvia) at 20-25 revolutions a minute for 10-30 minutes. Sample was subsequently evaluated in accordance with WHO 2021, if the sample was within standard parameters the following was done. 3x the sample volume equivalent in SpermWash was added. The sample was subsequently rocked for

10min. After, the sample was divided into two Nunc tubes (Thermo Scientific™; Massachusetts, USA). Tubes were placed in a Rotina 420R centrifuge (Hettich; Kirchlengern, Germany) and spun at 1500rpm for 10 minutes. The supernatant was removed to eliminate any potential contaminants in the seminal plasma. 1ml of Fertmedium (CooperSurgical®; Connecticut, USA) was added to each tube and mixed thoroughly, then centrifuged in a Rotina 420R centrifuge for 5min at 1200rpm. The remaining supernatant was removed carefully, 1.5ml of Fertmedium (CooperSurgical®; Connecticut, USA) was added over the pellet carefully, to not disturb the pellet. Samples was placed for incubation in a Forma™ Series II Water-Jacketed CO_2 Incubator (Thermo Scientific™, Massachusetts, USA) at 37 ^oC, 5% CO_2 for 2 hours. After incubation, 0.7 ml of the top section was taken for further analysis.

3.3 Zymot

Initially, the sample was liquified with a MR-1 Mini-rocker Shaker (BioSan; Riga, Latvia) at 20-25 revolutions a minute for 10-30 minutes, 850 µl was taken with a BD Luer-Lok™ 1-mL syringe (BD; New Jersey, USA). A tight seal is achieved, and the sample was injected without creating air bubbles that might impede sorting. The upper collection chamber was primed with 750 µl of SpermWash ORIGIO (CooperSurgical®; Connecticut, USA). The collection outlet was also primed with SpermWash ORIGIO. Priming of the chambers is done to allow differentiated spermatozoa to migrate into the upper section for collection before incubation in a Forma™ Series II Water-Jacketed CO_2 Incubator (Thermo Scientific™; Massachusetts, USA) for 30 minutes at 37 ^oC and 5% CO_2 to allow for sorting. When incubation was finished 500 µl of the sample was collected for downstream applications.

3.4 Halosperm G2 DNA Fragmentation

Agarose was melted in a Husqvarna Microwave dine (Husqvarna; Stockholm, Sweden). Denaturing agent (Halotec; Madrid, Spain) (DA) and lysis solution (Halotec; Madrid, Spain) (LS) were placed in room temperature. Sample was measured, with a maximum number of spermatozoa at 20 million/ml, if more spermatozoa was present, the sample was diluted. 50 µl of the sample was pipetted into Eppendorf tubes (Eppendorf; Hamburg, Germany) containing agarose gel, mixing was performed. 8 µl of the mix was pipetted onto super coated slides (Halotec;Madrid, Spain) (SCS) and spread using a coverslip (fisher scientific; Massachusetts, USA).

The SCS was then placed on a pre-cooled (4^{o}C) plastic block in a refrigerator (Electrolux; Stockholm, Sweden) to solidify the agarose. After removal from the refrigerator, the coverslip was gently removed, and additional sample treatment was performed under a fume hood (Phenix Control Corpuration; Massachusetts, USA). DA solution was added, covering the entire sample, and incubated for 7 minutes. Any residue of reagents was gently removed. LS was added and incubated for 20 minutes to allow lysis. LS reagent was gently removed after incubation. SCS was washed with distilled water for 5 minutes to remove any remaining reagents. SCS was prepared for staining, it was dehydrated by being placed in 70% and Ethanol Emparata ACS (Sigma-Aldrich® Solutions; Missouri, USA) for 2 minutes each.

Eosin (Halotec; Madrid, Spain) staining solution was added to the sample and incubated for 7 minutes, staining supporting structures in a cell, such as cytoplasm and collagen. After staining it was gently removed. Thiazine staining solution (Halotec; Madrid, Spain) was then added and incubated for 7 minutes to stain the DNA, any excess reagent was removed. Slides were subsequently microscoped with a Nikon ECLIPSE E 200 (Nikon; Tokyo, Japan) with Nikon 10X/0,25, Nikon 20X/0,4 and Nikon 40X/0,55 (Nikon; Tokyo, Japan) magnification and photographed with a HDMI16MDPX–HDMI 6MegaPixel Microscope camera by (DeltaPix; Ballerup, Denmark), subsequently placed in storage at -4 ^{o}C.

3.5 ROS analysis with Halotech Oxisperm II

10 µl of a neat sperm sample was transferred to an Eppendorf Safe-Lock Tube (Eppendorf; Hamburg, Germany). A separate Eppendorf Safe-Lock Tube was prepared with net spermatozoa, meaning spermatozoa due for purification. Net spermatozoa (Raw) contained 10^{6} spermatozoa; it was centrifuged in a Biofuge 13 (Sepatech; Hanau, Germany) at 6000g for 10min to separate the seminal plasma. Seminal plasma was transferred to an Eppendorf Safe-Lock Tube. The spermatozoa pellet was resuspended in 50 µl of phosphate buffer saline (PBS) and kept at 22 ^{o}C for 3 min. Moreover, the spermatozoa pellet was centrifuged two additional times at the previous setting, the supernatant was removed each time and resuspended in 50 µl of PBS. This ensured that the spermatozoa pellet was clean. In the second round of centrifugation, the supernatant was removed and 10 µl of OSIIS sperm reactivity (Halotech; Madrid, Spain) was added and incubated for 5min. Subsequently, 5 µl of each sample was added to a OSIIRS reactive membrane (Halotech;Madrid, Spain). ROS was measured for the following fractions neat sample, seminal plasma sample, sperm sample, positive, and negative

control. The negative control was PBS. OSIIRS reactive membrane was incubated for 15min in a light sealed container to allow colour development. Colour of the reactivity sheet was then compared with the provided colour scheme. The reactivity sheet is provided below with an explanation.

Background for analysis of Oxisperm II is the scale provided is from the manufacturer and can be seen in Figure 17.

Figure 17: showing grading levels for oxidative stress in samples*. Level 1 signifies no oxidative stress in a sample. Level 2 signifies a slight presence of ROS in a sample. Thirdly a purple colour indicates a moderate presence of ROS. Lastly level 4 implies a high presence of ROS in the sample.*

ROS quantification is presented in Figure 17. The Figure is taken from the protocol provided by Halotec. ROS is quantified into four levels, level one shows no ROS formation while level four signifies high degree of ROS formation. A higher level of ROS will be seen as a darker colour in the sample reaction area.

3.6 MDA ROS level analysis

Analysis of spermatozoa commenced as soon as the sample was donated to the clinic at UNN to ensure the most accurate results. The protocol followed is the standard company protocol, with the sample preparation section being slightly changed to accommodate spermatozoa preparation.

Spermatozoa consisting of $2*10^6$ cells, was sonicated with a VCX-130 sonicator (Vibra-Cell™; Connecticut, USA) 8 times on ice. Settings used for sonication were 100% aptitude at 20khz for 8 second with a 30 second rest period in between sonication sets. Sonication was done to ensure proper dissolution of the spermatozoa membrane. After sonication, 300 µl of MDA lysis

buffer containing 3X BHT (Sigma-Aldrich®; Missouri, USA) was added to further break down spermatozoa products. Centrifugation followed, at 13000g for 10min in a Biofuge 13 (Septech; Hanau, Germany) to remove insoluble material. 200 µl of the resulting supernatant was used for further analysis of ROS.

To prepare the 96-well Clear Flat Bottom TC-treated Culture Microplate (Falcon®; New York, USA) a fresh standard curve was prepared for each assay run. 4.17 M MDA standard solution (Sigma-Aldrich®; Missouri, USA) was diluted with purified water to a make a 0.1 M MDA standard solution. This dilution was further reduced to a concentration of 2 mM. The MDA standard was then prepared in accordance to *Table* 1.

Table 1*: *Preparation of MDA standard. *Table containing the MDA standard for the colorimetric assay, the Table is split into four rows and seven columns. Top row shows the well number, 2mM MDA standard, Purified Water and MDA (nmole/well) in total five wells in duplicate were created for the standard.*

Well	2 mM MDA Standard	Purified Water	MDA (nmole/well)
1	10 µL	190 µL	20
2	8 µL	192 µL	16
3	6 µL	194 µL	12
4	4 µL	196 µL	8
5	2 µL	198 µL	4
6		200 µL	0

ROS in spermatozoa samples was determined by analysis of malondialdehyde (MDA) content. 600 µl of TBA solution (Sigma-Aldrich®; Missouri, USA) was added to the standard and samples, this was incubated in an Eppendorf ThermoMixer® C (Eppendorf ; Hamburg, Germany) at 95 ^{o}C for 60min and cooled in an ice bath for 10min. This induces the colour change indicative of ROS content. MDA content of each sample was determined through spectrophotometry with an Epoch 96-well reader (Thermo Scientific™; Massachusetts, USA) by measuring colorimetric absorbance at 532 nm. A more intense colour would indicate a higher amount of MDA correlating to higher ROS. Results obtained were then compared to an MDA standard curve.

3.7 QPM microscopy analysis

Figure 18 describes the process needed to obtain QPM data. QPM analysis can be split into seven distinct phases. Sample preparation, QPM system set up and system adjustment. This was done in accordance to pre-established in-house procedures. Acquisition of images of video on the QPM system was done promptly after system adjustment. The acquisition is done digitally where the researcher can see the sample on a screen through a camera. When the sample is in focus the researcher navigates software to acquire images. Phase reconstruction of gathered data was completed with a premade algorithm and computer software detailed in (90). Data visualisation and analysis was subsequently preformed on the reconstructed images. Videos were made with imageJ version 1.54d (National Institute of Health, Maryland, USA).

A flow chart of the process involved in QPM analysis is provided in Figure 18. The chart is split into seven distinct parts giving an insight into QPM analysis.

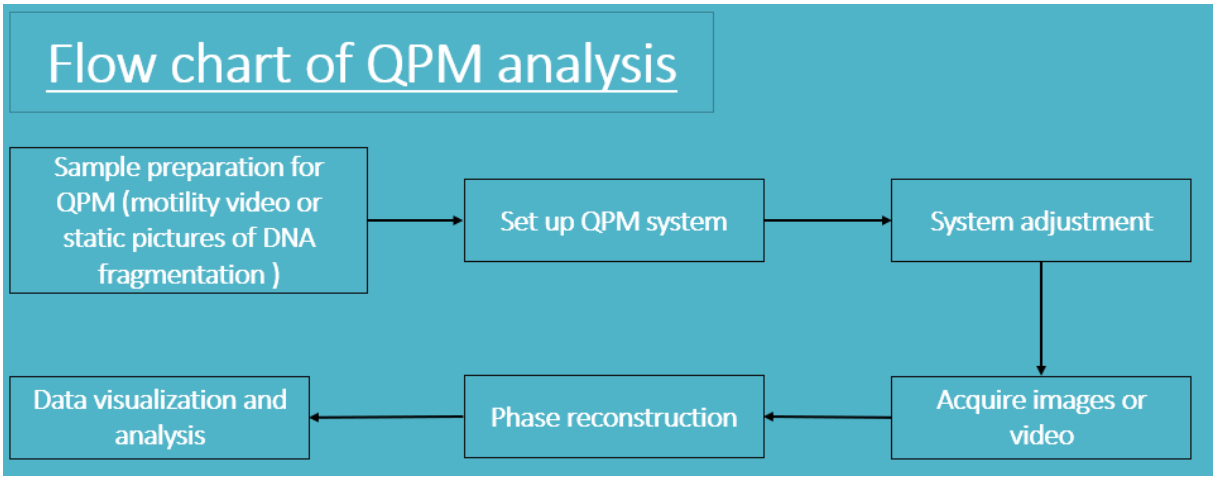

***Figure 18**: **Flow chart of QPM analysis**. The Figure depicts seven steps needed to conduct a QPM analysis of spermatozoa. Flow of the chart is depicted by the direction of the arrows. Firstly, sample preparation was done in accordance to preestablished protocols. After preparation of samples the QPM system was set up for either image or video procurement. System was adjusted to give the best quality of images. After adjustment, images or video was procured. Phase reconstruction was done with a pre-made algorithm, the details of mathematical complexities can be found in* (90)*. Data visualisation and analysis of the reconstructed images was then completed.*

Sample preparation included Swim-up and Zymot sorting chip in addition to an unprepared native sample (Raw) sample. After sorting the QPM system was set up in accordance with previous established methods. Samples for video analysis where prepared on silicon wafers and contained in a polymer chamber. Silicon wafers were chosen to increase the contrast of the interferometric data by matching the intensity in the object and the reference beam.

Objective lenses chosen were 20×_0.45NA_532nm, 60×_0.9NAand 60X_1.2NA (Olympus; Tokyo, Japan). 20× and 60× relate to the magnification of the lens, while the NA corresponds to the numerical aperture (NA). Numerical aperture determines the resolving power of the microscope, meaning the higher NA a higher resolution image is acquired. The interferogram is created by the use of polarized light. Meaning the light-waves were normalized to a single plain. This light wave was subsequently split into two by a prism and directed towards the sample. These beams passed different areas of the sample, the beams were recombined together to a single light source. The delta between these two beams were used to calculate interference patterns, the resulting fringes were optimised in the QPM system to yield high contrast data. Images were acquired with a digital camera by Hamamatsu (Hamamatsu, Japan) stacks 3 containing 510 images in each stack. Video was taken at 32 frames per second.

If DNA fragmentation sample images were to be collected, sample preparation followed the DNA fragmentation protocol. Images were gathered following the same principle as video, with the noticeable difference being only single images being gathered. A detailed description of the program and image transformation is described below.

To retrieve phase information about the spermatozoon, a Fourier transform of the image was done, decomposing the gathered images into the basic frequencies. Transformation of the image was done to remove unwanted background noise and select only first order peak of the Fourier spectrum. After filtering, an inverse Fourier transformation was performed to reconstruct the image as a 2D array of numbers. This allows the phase profile of the sample to be measured. A phase map was created, that represents the optical path difference between each point on the map. This corresponds to the phase shift of light that had gone through the spermatozoon. The phase shift between the spermatozoon and surrounding medium was used to calculate the optical path difference, this provided information about topology and morphology.

Several morphological parameters were used in the categorization of spermatozoa, these were taken from (90). Firstly, the surface area of the spermatozoa head was categorised, subsequently data related to volume was gathered. Surface to volume ratios were calculated. These provided the morphological parameters for the reconstruction algorithm to reconstruct the spermatozoon successfully. To enable a more accurate recreation of the spermatozoon texture parameters were also considered.

Texture parameters used in the re-construction algorithm were calculated from the following paper (90) . Specific texture parameters that were used included mean, variance, kurtosis, skewness, entropy and, energy (90). Mean corresponds to the phase distribution over the spermatozoa head, a decrease of this parameter would signify a flattening of the head (90). Variance as a texture parameter signifies the spread of datapoints over the sample (90). Kurtosis and skewness, categorise asymmetry and regularity in the phase distribution of the spermatozoa head (90). Entropy predicts the growth of randomness in the phase distribution across the spermatozoa head (90). Last parameter chosen was energy, this forecasts the increase in heterogeneity in the phase distribution of the spermatozoa head (90).

3.8 Statistics

Statistical analysis and illustration were performed with the statistical software *GraphPad Prism 9 version 9.0.0* by GraphPad (San Diego, California, USA). The P-value was calculated with an unpaired t-test, outlier removal was done with robust regression and outlier remover (ROUT). All data of $P<0.05$ was deemed as statistically significant and indicated with "*". Data presented is ± standard error of mean (SEM).

4 Results

4.1 Preliminary spermatozoa analysis

Table 2 shows the results gathered by the bioengineers at UNN. Variables tested were Concentration (10^6/ml), Viscosity, Motility% and Motility grade. The parameters calculated were as follows *Median, Mean, standard deviation (SD) and Range.* for volume these variables were calculated *Median*: 1,90, *Mean*: 2,23, *SD*: 1,16 and *Range*: 2,50. Concentration of the spermatozoa samples were found to be the following *Median*:100, *Mean*:108,33, *SD*:53,019 and *Range*: 160. Viscosity was characterized as *Median: 1*, *Mean 1,77, SD: 0.91* and *Range: 2*. The Motility percentage of the total samples were as follows *Median:* 0,70, *Mean: 0,71, SD: 0,11 and Range 0,40.* Motility grade of all the samples was categorized to be the following *Median*: 3, *Mean:* 2,55, *SD* 0,49 *and Range* 1. These values are presented in Table 2.

Table 2: Showing results from all preliminary analysis done by the bioengineers at UNN. *The sample size is (n=9) Variables measured at the UNN hospital were Volume, Concentration (10^6/ml), Viscosity, Motility% and Motility grade. Parameters calculated were Median, Mean and Range.*

Variable	*Median*	*Mean*	*SD*	*Range*
Volume	1,90	2,23	1,16	2,50
Concentration (10^6/ml)	100	108,33	53,01	160
Viscocity	1,00	1,77	0,91	2,00
Motility%	0,70	0,71	0,11	0,40
Motility grade	3,00	2,55	0,49	1,00

4.2 Phase contrast imaging of spermatozoa samples

Figure 19 shows a Raw sample shortly after being given to the clinic at UNN. In Figure 19 examples of a Raw sample can be seen. The pictures are taken on 40×/55 magnification. **A1-Raw-40X** shows a Raw sample. Spermatozoa heads can be seen as small white/translucent objects connected to a black pin. Tail and midpiece sections can be seen as thin black lines. A large number of artifacts can be seen in the sample. These include headpieces, tail sections, and potential cell fragments.

B1-Raw-40X shows a Raw sample. Head sections can be identified by white/translucent ovals connected to a black pin. Tail and midpiece sections can be identified as a black line connected to the translucent ovals. Artifacts are present around the spermatozoa. These artifacts are but not limited to tail section pieces, head sections and cell fragments.

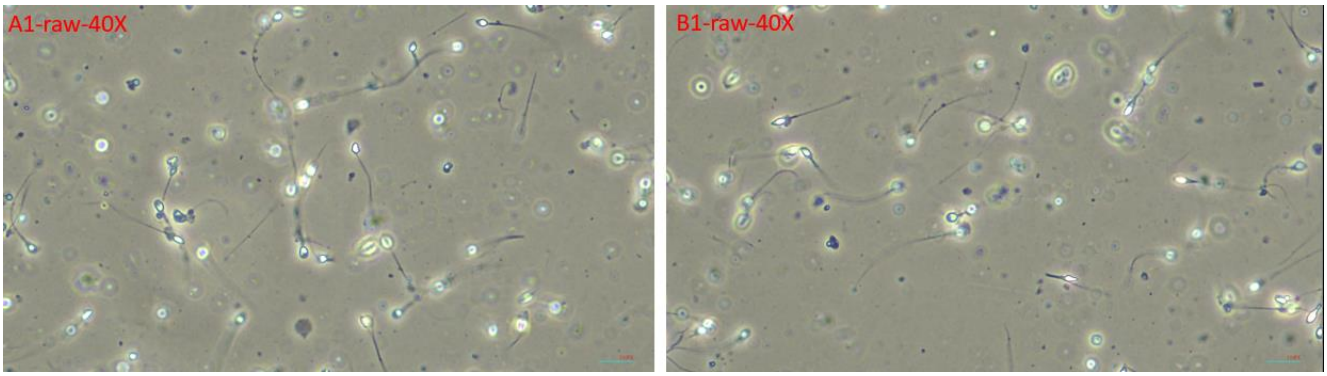

Figure 19*: *Showing examples of spermatozoa through a phase contrast microscope. *Pictures are taken of Raw sample spermatozoa samples. From left to right the picture shows samples **A1** and **B1**. Both pictures are taken on 40X/0,55 magnification. Both pictures contain a high number of artefacts in the sample. **A1-Raw-40x** shows a Raw sample, a plethora of regular spermatozoa are shown, artifacts can also be seen. **B1-Raw-40x** shows a Raw sample containing a plethora of spermatozoa, artifacts in the sample can also be seen.*

4.3 Halosperm G2 DNA Fragmentation, significantly less DNA fragmentation in Swim-up and Zymot spermatozoa

The following figure 20 illustrates DNA fragmentation of spermatozoa from a Raw sample, Swim-up and Zymot microfluidic sorting. These are seen from left to right in Figure 20. Magnification of samples is shown from top to bottom as 10×/0,25, 20×/0,4 and 40×/0,55. A scalebar is given in the bottom right corner of the photo, while the name of the sample, together with the technique and magnification is shown in the top left corner. All techniques have artefacts present on the photo.

Sample A1

Raw Swim-up Zymot

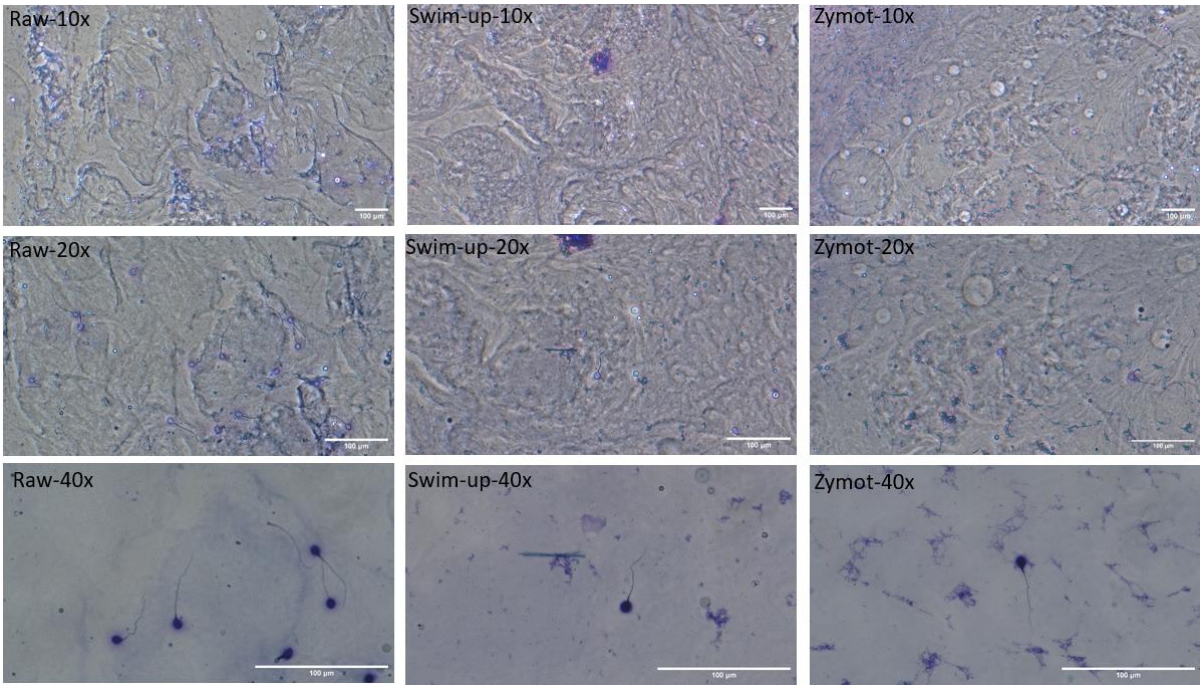

Figure 20: Shows a spermatozoa sample stained for DNA fragmentation*. All pictures have a 100μm scale at the bottom right. The rows from left to right show a Raw sample, Swim-up and Zymot. The magnification for the Figure from top to bottom is 10X/0,25, 20X/0,4 and 40X/0,55. All pictures show a fluctuating degree of artifact in the frame.* ***Raw-10x*** *shows spermatozoa, with a halo around the head.* ***Raw-20x*** *shows the same sample with more visible halos.* ***Raw-40x*** *displays several spermatozoa with halos around the head. A spermatozoon tail is also visible in the centre right, and a curled spermatozoon can be seen bottom right.* ***Swim-up-10X*** *shows a singular spermatozoon in the centre of the frame, with a visible pink artifact at the top centre of the frame. There is no halo around the spermatozoon.* ***Swim-up-20X*** *shows spermatozoa in centre of the frame, no halo is visible.* ***Swim-up-40X*** *numerous artifacts are visible, and spermatozoon doesn't not show a halo.* ***Zymot-10x*** *singular spermatozoon in centre of the frame, with artifacts present. No halo can be seen.* ***Zymot-20X*** *shows the abovementioned spermatozoon, no halo can be seen around the head, artifacts are still present. In the centre of* ***Zymot-40x*** *the spermatozoon is seen with no halo around the head.*

In **Raw-10X,** multiple spermatozoa are visible, along with a high degree of artefacts in the photo. **Raw-20X** provides a clearer view of **Raw-10X** spermatozoa, halo can be seen around the head. Artifacts can be seen surrounding the spermatozoa. **Raw-40X**, multiple spermatozoa can be seen, with, varying degrees halo around each head. It is also noticeable that spermatozoa are missing its head.

Swim-up 10X shows a singular spermatozoon in the centre of the frame. Numerous artifacts can be seen around the sample, no halo can be seen. In **Swim-up-20X** a more magnified view can be seen of the spermatozoon. Sample is on the centre of the frame, various artifacts can be seen, no halo is observed. Lastly, **Swim-up-40x** provides the highest magnified view of the spermatozoon. Artifacts can be seen around the spermatozoon, with, no halo around the spermatozoon head.

Zymot-10X, two spermatozoa are visible in the sample, one is situated in centre of the frame while the other is located slightly off to the right. The peripheral spermatozoon has a partially damaged tail, and several artifacts can be observed. Note how a halo can be seen. **Zymot-20X** provides a closer view of the aforementioned spermatozoa, note how there is a slight halo around each spermatozoon. Artifacts can also be observed. Lastly, **Zymot-40X** shows a singular spermatozoon, a halo can be seen around the head of the spermatozoa. Artefacts can also be seen in vicinity of the spermatozoon.

Figure 21 illustrates DNA fragmentation in a Raw sample, Swim-up and Zymot spermatozoa sorting techniques as presented below, from left to right Raw sample, Swim-up and Zymot. Magnification of the samples from top to bottom are 10×/0,25, 20×/0,4 and 40×/0,55, with all techniques exhibiting some degree of artefacts on the photo. A scalebar is provided in the bottom right corner of the photo, while the name of each sample, together with the technique and magnification is shown in the top left corner.

Sample B1

Raw Swim-up Zymot

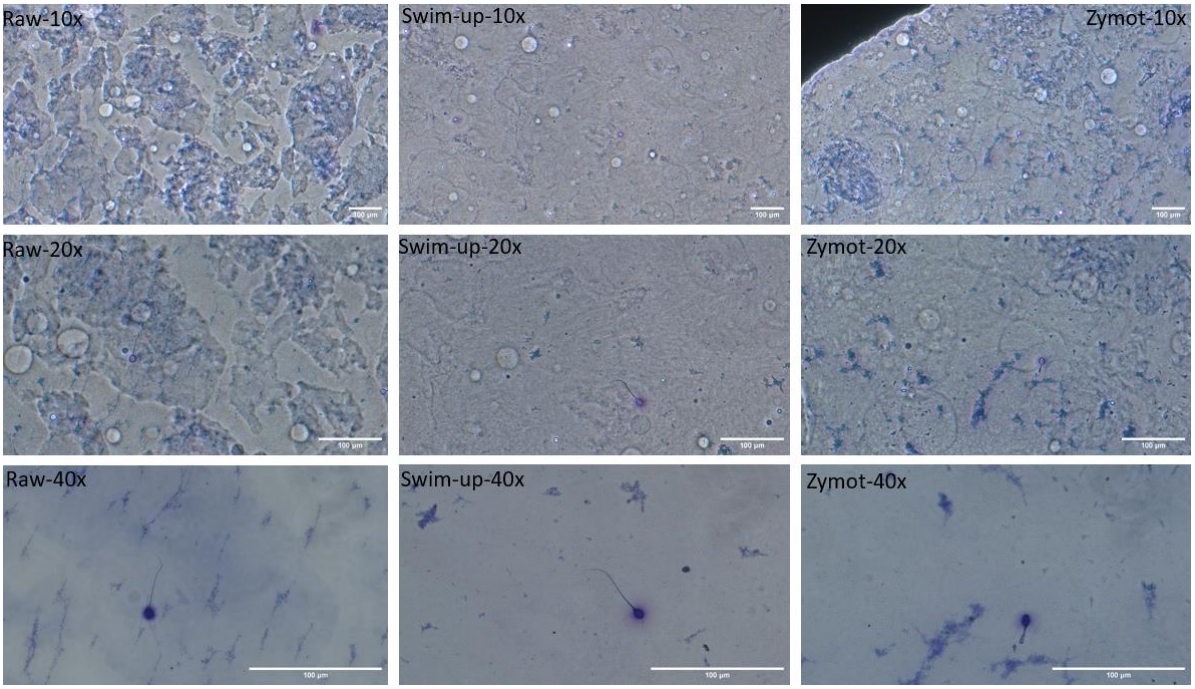

Figure 21: Displays spermatozoa stained for DNA fragmentation*. all pictures include a 100µm scale at the bottom right and display a Raw sample, Swim-up, and Zymot in rows from left to right. The magnification for all samples from top to bottom is 10X/0,25, 20X/0,4, and 40X/0,55, all of which exhibit some degree of artifacts around each sample.* ***Raw-10x*** *image displays a spermatozoon, with no halo around the head.* ***Raw-20x*** *shows the same spermatozoon with no halo.* ***Raw-40x*** *exemplifies the spermatozoon, it shows no halo.* ***Swim-up-10X*** *indicates a singular spermatozoon at the centre, with a halo around the head.* ***Swim-up-20X*** *shows same spermatozoon in centre with a halo. In* ***Swim-up-40X*** *the spermatozoon is in the centre of the frame and has clear halo around itself.* ***Zymot-10x*** *shows a singular curled spermatozoon in the centre with a halo. with edge of the slide visible in the top left corner.* ***Zymot-20X*** *shows the abovementioned spermatozoon, a halo can be seen around the head.* ***Zymot-40x*** *as before, shows a curled spermatozoon with a halo around the head.*

Raw-10X shows spermatozoa; one in the centre of the photo, and one centre left. Notice the high degree of artefacts in the photo. No halo can be seen. In, **Raw-20X** a magnified view of **Raw-10X** is shown, a spermatozoon is shown in the centre while the head of the leftmost is also present. A slight halo is observed and, artifacts can be seen around the spermatozoa. **Raw-40X**, shows a singular spermatozoon in centre. Artifacts can be seen while, no halo is observed.

Swim-up 10X displays one spermatozoon in the centre of the frame, a segment of a head can be seen in the left section of the frame. Artifacts surround the sample, and a halo can be observed over both heads. **Swim-up-20X** is a more magnified view of the spermatozoon. In centre of the frame, with a halo and some visible artifacts. **Swim-up-40x** shows a clear view of

the spermatozoon in the centre of the sample, with a strong halo around it and artifacts present in the sample.

Zymot-10X displays two spermatozoa in sample, one is in the centre with an abnormal tail while the head section of another is located in the top section of the photo. Each head has a halo, artifacts can be seen in the sample including the edge of the slide in the top left corner. **Zymot-20X** shows a single spermatozoon in the centre with an abnormal tail, and a halo can be seen around the head, with artifacts seen in the sample. **Zymot-40X** details a singular spermatozoon, with a halo around the head, and a damaged tailpiece, with Artefacts in the vicinity of the spermatozoon.

Figure 22 displays DNA fragmentation among Raw sample, Swim-up and Zymot spermatozoa sorting techniques from left to right in Figure 22. Samples are magnified at 10×/0,25, 20×/0,4 and 40×/0,55 from top to bottom. All techniques show artefacts in the sample. A scalebar is provided in the bottom right corner of the photo, while the name of each sample, together with the technique and magnification is shown in the top left corner.

Sample C1

Raw Swim-up Zymot

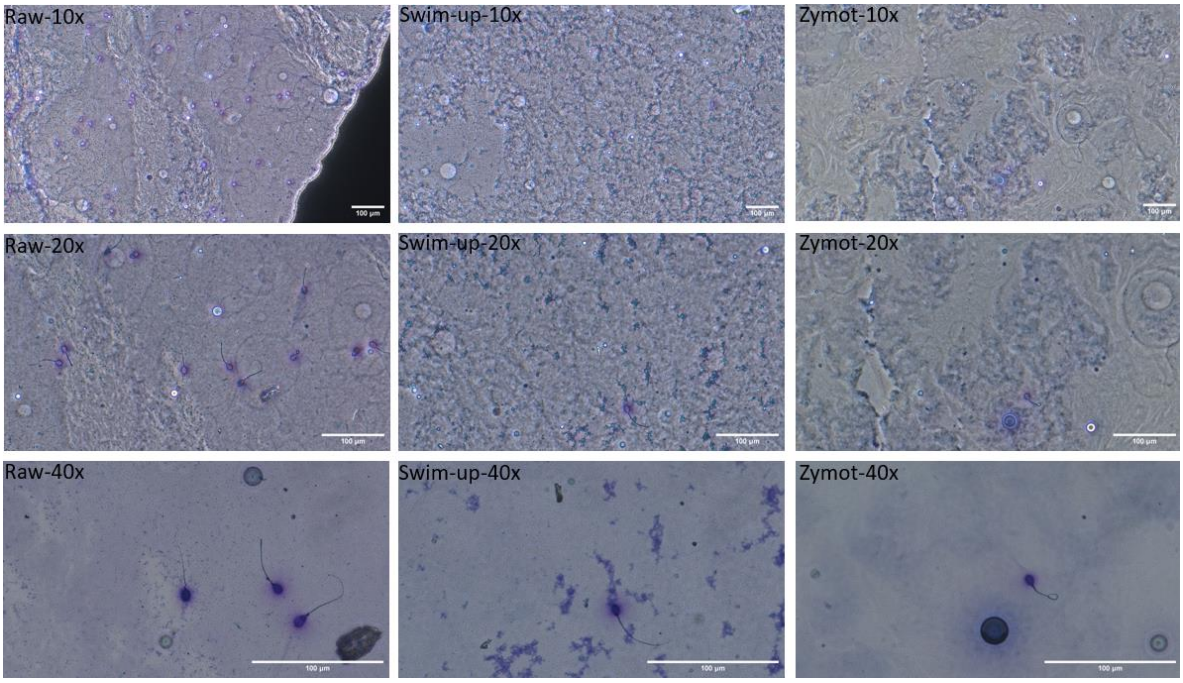

Figure 22: Exhibits a spermatozoa sample stained for DNA fragmentation*. Images have a 100µm scale at the bottom right. The rows from left to right show Raw sample, Swim-up and Zymot. Magnification of the samples from top to bottom is 10X/0,25, 20X/0,4 and 40X/0,55.* ***Raw-10x*** *displays several spermatozoa, with varying amounts of halo around the head, some also lack a tale.* ***Raw-20x*** *shows the same sample with more visible heads and halos.* ***Raw-40x*** *exemplifies three spermatozoa, all of which have a halo.* ***Swim-up-10X*** *indicates a spermatozoon at the centre, with a halo.* ***Swim-up-20X*** *shows the previous spermatozoon, a halo is seen. In* ***Swim-up-40X*** *presents the spermatozoon in the lower portion of the image, with a halo visible.* ***Zymot-10x*** *shows a singular curled spermatozoon in the centre of the frame, with a halo around the head.* ***Zymot-20X*** *same spermatozoon, halo is shown around the head.* ***Zymot-40x*** *shows previous spermatozoon, a curled tail can be observed together with a halo.*

Raw-10X shows multiple spermatozoa together with sections of heads, there is a high degree of artefacts in the photo, a halo is seen around all the spermatozoa. **Raw-20X** shows a clearer halo around head sections of the spermatozoa, with visible artifacts. **Raw-40X**, displays multiple spermatozoa, with a strong halo around each head and artifacts present in the sample.

Swim-up 10X shows a spermatozoon in the centre, several artifacts can be seen around the sample, with a halo being present. **Swim-up-20X** shows a spermatozoon in the centre. Halo can be seen around the head; artifacts can also be seen. **Swim-up-40x** shows the spermatozoon located in the centre. The spermatozoon shows a clear halo around it. Artefacts can be observed around the spermatozoon.

In **Zymot-10X,** a singular spermatozoon with an abnormal tail is shown in the lower centre of the photo. A slight halo above the head can be seen, and several artifacts can be seen in the sample. **Zymot-20X** shows a spermatozoon in the centre an abnormal tail. A halo can be seen around the head, artifacts can also be seen. **Zymot-40X** exhibits a singular spermatozoon with a halo around the head, and the tailpiece is damaged. Additionally, artefacts can also be seen in vicinity of the spermatozoon.

To get a more objective overview of DNA fragmentation a categorization of Spermatozoa resembling ***A1-Swim-up*** in Figure 23 are used for categorising a sample for DNA fragmentation. Conversely spermatozoa resembling ***B1-Swim-up-40X*** in Figure 23 were categorised as not having DNA fragmentation. Subsequently the findings are presented in Figure 25 as a percentage number of spermatozoa that have DNA fragmentation from the total sample.

Figure 23 below shows the background for categorization of DNA fragmentation in this study. Magnification of the photo is 40×/0,55, the left picture shown a spermatozoon without DNA fragmentation while the right picture shows one with fragmentation.

Background for categorisation of DNA fragmentation

Spermatozoon with halo Spermatozoon lacking halo

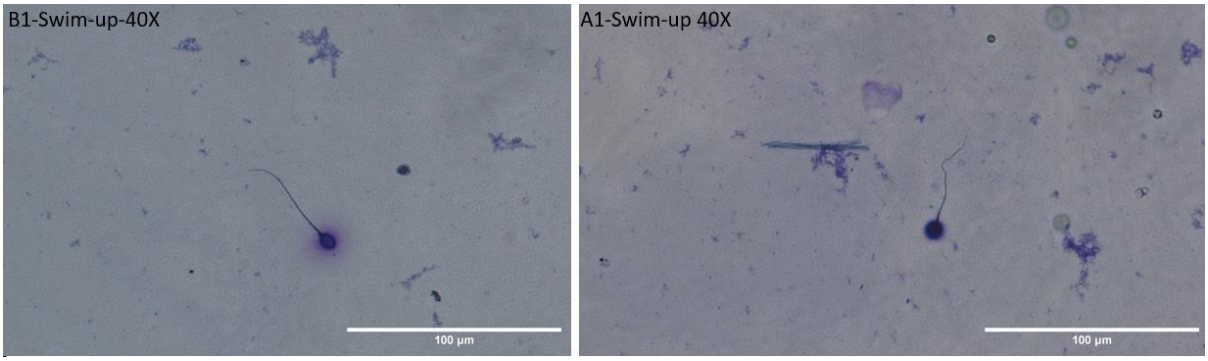

Figure 23: Description of background for categorization of ROS % in samples. *The Figure has a scalebar denoting 100µm at the bottom right corner. Top left section of the Figure shows the name of the sample together with the magnification 40X/0,55.* ***B1-Swim-up-40X*** *shows a spermatozoon with a clear halo around it, several artefacts can also be seen. Notice the hue around the spermatozoon head.* ***A1-Swim-up 40X*** *indicates a spermatozoon with no hue around the head, artifacts can be seen around the sample.*

The background for categorisation of DNA fragmentation is presented in Figure 23, each Figure has a scalebar at the bottom left that depicts 100µ*m*. Magnification of each sample is 40×/0,55, additionally artifacts are present in both photos. Names of the samples is shown in the top left corner of the photo. **B1-Swim-up-40X** shows a spermatozoon that doesn't have DNA fragmentation, this can be observed through the halo above the spermatozoon head. **A1-Swim-up-40X** shows a spermatozoon that does have DNA fragmentation. Visualization of this can be observed through the lack of a halo above the spermatozoon head.

4.4 ROS categorisation with Oxisperm II in Raw sample and Swim-up

4.4.1 Lower levels of ROS in Swim-up samples compared to a Raw sample of spermatozoa with Oxisperm II kit

Figure 24 shown below is an example of how the results from the Halotec Oxisperm II kit. Left side of the Figure shows the results from a Swim-up procedure, while the right Figure shows the results from a Raw sample.

Figure 24: Example of Halotec ROS kit categorization*. The Figure displays Oxisperm II ROS kits from Halotec, with the right picture showing a Swim-up test and the left showing Raw sample results. The testing section is divided into four categories N, SP, S and C. The N section of the test denotes the neat spermatozoa sample i.e., the Raw sample. SP section is for the seminal plasma fraction, while the S section is for cleaned fraction or net spermatozoa. C is meant for the control. Swim-up test results are shown in the right photo, with no color change observed in all test columns. Left shows the Raw test results, a color change can be seen in N and SP, indicating a ROS level of 2-3 (per Figure 24.) … However, no color change is observed in P and C sections.*

Figure 24 displays the results from the Oxisperm II kit. Reaction areas are divided into N (neat spermatozoa sample), SP (seminal plasma fraction) S (cleaned spermatozoa fraction), and C (control). Left section shows Swim-up results with no color change in any reaction area. Right section shows Raw sample results, areas N and SP display a level of 2-3 ROS formation (Figure 24) with, sections S and C showing no color change.

4.5 Significant differences in Oxisperm II, MDA ROS analysis, Halosperm G2 DNA fragmentation and spermatozoa/ml between spermatozoa sorting techniques

Figure 25 visualises the different results gathered in this study. Results depicted in the four graphs of the Figure 25 are ROS categorisation with Halotech kit and MDA, marked as A and B correspondingly. Furthermore, DNA fragmentation and concentration of spermatozoa is visualised and marked as C and D.

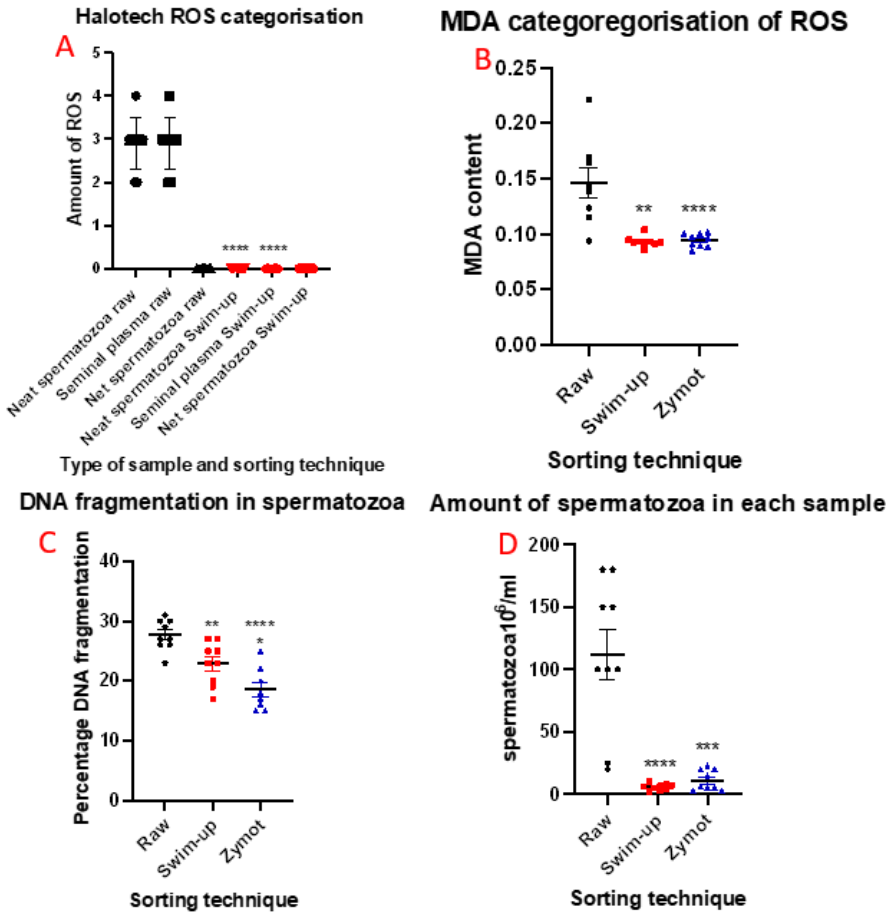

Figure 25: Categorization of Raw, Swim-up and Zymot differentiated spermatozoa samples*. The X axis shows the sorting technique and the Raw sample. Y-axis shows the content measured, from the left to the right graph this is MDA content, spermatozoa10^6/ml and percentage of DNA fragmentation. The error bars show the standard error from mean, individual datapoints are also shown as circles (Raw; n=8-9), squares (Swim-up; n=9) and triangles (Zymot; n=8-9) for each column.* ***A****, T-test compared Swim-up and Zymot differentiation together with Raw with the use of the Halotech kit. ***P<0.01 for neat spermatozoa Swim-up vs neat spermatozoa Raw, ***P<0.001 for Seminal plasma Swim-up vs seminal plasma Raw.* ***B****, T-test to compare spermatozoa differentiation through MDA content. Raw vs Swim-up **P<0.01, Raw vs Zymot ****P<0.0001.* ***C****, T-test comparing DNA fragmentation percentage between Raw, Swim-up and Zymot differentiated samples. **P<0.01 Raw vs Swim-up, Raw vs Zymot ****P<0.0001, Swim-up vs Zymot *p<0.05.* ***D****, T-test comparing concentration of spermatozoa (10^6/ml), ****P<0.0001 Swim-up vs Raw and ***P<0.001 Zymot vs Raw.*

Figure 25 **A** shows the results from the Halotech ROS categorization, between Swim-up and Raw samples comparing respectively neat spermatozoa, seminal plasma and net spermatozoa. The graph only shows a statistical difference when comparing neat spermatozoa and seminal plasma. The resulting P-value for neat spermatozoa and seminal plasma was for both 0.0001. An outlier ROUT test was conducted with no outliers detected with a value of 1.000%. No statistical difference was found between neat spermatozoa samples.

Figure 25 **B** illustrates results from the MDA categorization of ROS, between Raw, Swim-up and Zymot categorized samples. Graph shows the large variability in MDA content for Raw samples. It can be observed that one of the Raw samples is within the SEM of the Swim-up and Zymot samples. A statistical difference is shown in the graph between Swim-up and Raw samples and Zymot and Raw samples. The resulting P-value was respectively 0.0011 and 0.0014. A ROUT test was performed to identify outliers with a Q value of 1.000%, only one statistical outlier was found in Swim-up spermatozoa samples. The mean ROS in Swim-up samples was observed 1.57-fold lower compared to Raw sample. Similarly, when comparting the means of Raw and Zymot differentiated samples, the mean ROS in Zymot samples was 1.55-fold lower than Raw sample. No statistical difference was found between Zymot and Swim-up differentiated samples, with means of each column being contained in the SEM. The resulting P-value between Zymot and Swim-up was 0.6193.

In Figure 25 **C** demonstrates the difference in DNA fragmentation between Raw spermatozoa and Swim-up and Zymot differentiated samples. A statistical difference was found between Swim-up and Raw samples, Zymot and Raw and Zymot and Swim-up samples. Swim-up and Raw samples have values that go inside the SEM of the respective columns. Zymot differentiated spermatozoa has values contained in the SEM of Swim-up respectively, Swim-up has two values in the SEM of Zymot differentiation. The mean of Zymot was 1.5-fold lower than Raw samples. The mean of Zymot was found to be 1,2-fold lower than Swim-up. Mean of Swim-up compared to Raw samples was found to be 1.2085-fold lower. A T-test was done comparing each differentiation technique. The P-value obtained when comparing Swim-up to Raw samples was 0.0047, P-value obtained when comparing Zymot to Raw samples was <0.0001, when comparing Zymot to Swim-up samples the P-value obtained was 0.0230. Whilst categorizing for outliers with a ROUT test with a Q-value of 1.000% resulted in no outliers being found.

Figure 25 **D** shows the number of spermatozoa in 10^6/ml, between Raw, Swim-up and Zymot differentiation of spermatozoa. A statistical difference was found between the Raw and Swim-up differentiated samples and Raw and Swim-up differentiated samples. A high degree of variability was observed in Raw samples, with two data points being close to the SEM of Swim-up and Zymot. Mean of Zymot samples was found to be 460-fold lower than Raw samples. Mean of Swim-up samples was found to be 877.7-fold lower than Raw samples. A T-test was done between Raw and Swim-up, this resulted in a P-value of P<0.0001. When comparing Raw to Zymot with a T-test the P-value result was 0.001. While comparing Zymot and Swim-up the T-test resulted in a P-value of 0.0829. A ROUT test was done to categorize outliers with no being found, using a Q-value of 1.000%.

4.6 QPM Video exerts of Raw, swim-up and zymot spermatozoa

Figure 26 shows the single frames from 60X_NA09_532nm videos. All exerts are from the same sample. The parameters chosen for visualization are 60× magnification, 09 numerical aperture and taken at a wavelength of 532nm. Frames shown are from left to right Raw, Swim-up and Zymot. A 10 μ*m* scale is shown in the bottom left of each image and heatmap is shown on the right of the Figure depicted in radians.

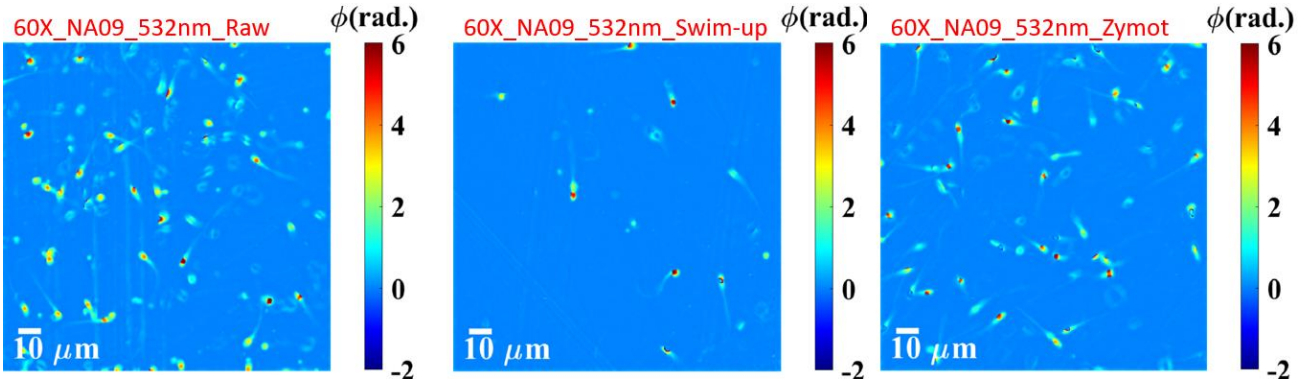

Figure 26: Frames from QPM videos showing different spermatozoa differentiation techniques. *Top sections of each Figure show the magnification, aperture, light used and differentiation technique. Bottom left corner shows a 10μm, right side shows a heat map scale in radians. The concentration of spermatozoa in Raw, Swim-up and Zymot was, 150mil/ml, 5mil/ml and 22mil/ml respectively.* ***60x_NA09_532_Raw*** *shows a Raw sample. A high number of spermatozoa are observed. Spermatozoa head sections are illustrated as a red colour, while the midpiece can be observed as a more yellow/green colour. Artifacts can be seen between the spermatozoa. Long parallel lines in the background are scratches in the silicon wafer.* ***60X_NA09_532nm_Swim_up*** *shows a Swim-up sample, with few spermatozoa in frame. Spermatozoa heads can be seen with a clear red colour, one can be seen on the right with a green head section. Tail and midpiece sections are shown in yellow/green. Some artifacts can be observed in the background of the Figure. Long parallel lines in the lower left section are scratches on the silicon wafer.* ***60X_NA09_532nm_Zymot*** *shows a Zymot differentiated sample. Many spermatozoa are shown. Spermatozoa heads are shown in red colour, Tail and midpiece sections are shown in yellow/green. Some artifacts can be observed in between the spermatozoa.*

60X_NA09_532nm_Raw shows a Raw sample of spermatozoa at 60× magnification, with a 09 aperture at 532nm wavelength. A large number of spermatozoa is shown as the sample concentration was 150mil spermatozoa/ml. Head sections of spermatozoa can be seen in red, midpiece and tail sections are shown in green/yellow. Artifacts are shown between the spermatozoa samples. Parallel lines in the middle of the sampler are scratches in the polymer wafer.

60X_NA09_532nm_Swim-up shows a Swim-up differentiated sample at 60× magnification, with a 09 aperture at 532nm wavelength. Few spermatozoa can be observed, as the sample concentration was 5mil spermatozoa/ml. Head sections of the spermatozoa are illustrated in red to a light green color. Midpiece and tail sections are displayed in a yellow to green color. The noticeable long lines in the bottom left of the Figure are marks in the silicon wafer.

60X_NA09_532nm_Zymot displays a sample differentiated with the Zymot microfluidics system. Sample is shown in 60× magnification, 09 aperture and 532nm light. A high number of spermatozoa can be observed. Sample concentration was measured to be 22mil spermatozoa/ml. Spermatozoa heads can be illustrated in red, while the midpiece and the tail section are illustrated in yellow and green. A few artifacts are observed around the spermatozoa. Long parallel lines running the length of the picture are scratches in the silicon wafer.

4.7 QPM DNA-fragmentation of Swim-up differentiated spermatozoa

Figure 27 shows the reconstruction of spermatozoa without DNA fragmentation. The magnification used was 20X, 07 numerical aperture and light used was 532nm. Differentiation technique shown is Swim-up. A scale of 10 μ*m* is shown on the bottom left corner. A scale in radians is shown on the right side of the Figure.

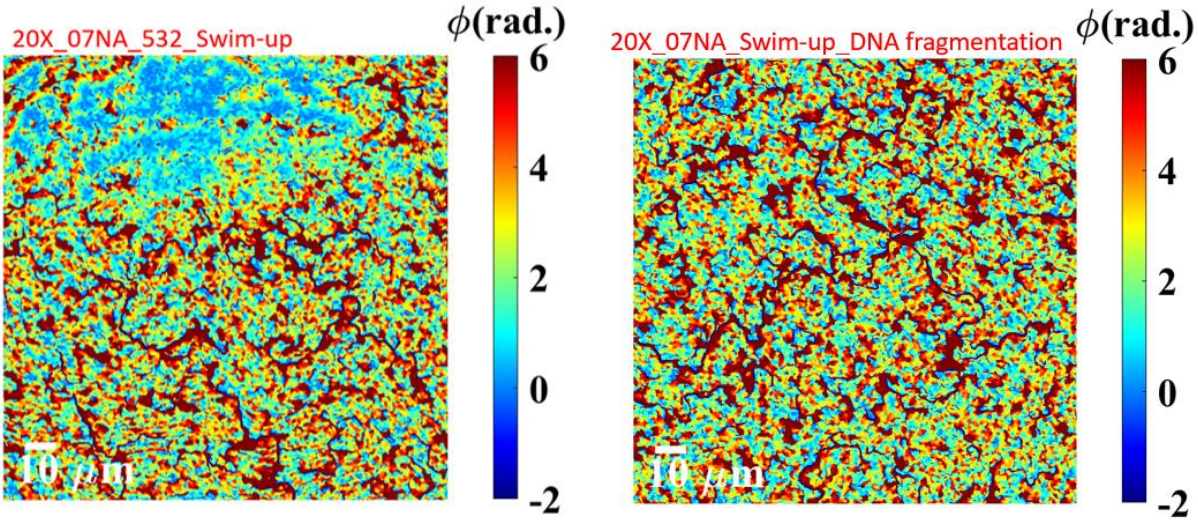

Figure 27: Showing DNA fragmentation in spermatozoa Swim-up*. A scale can be seen on the right side in radians. A scale for reference is placed on the left bottom corner, indicating 10μm. The scale of the photo is 20X, and light wavelength is 532nm. Numerical aperture is 0.7. No spermatozoa can be seen in both photos. Artifacts can be observed over the entirety of both figures.*

Figure 27 shows the reconstruction of QPM images on spermatozoa demonstrated with or without DNA fragmentation on the left. The rigth section shows a sample containing DNA fragmentation. A heat map scale in radiants is shown on the right side of the Figure, while on the left bottom a scale bar depicting 10μm is shown. No spermatozoa in both photos are observed, artifacts are presented over the entirety of the photos.

5 Discussion

This study used phase contrast microscopy to compare DNA fragmentation using Halosperm G2 kit in a Raw, Swim-up and Zymot differentiated spermatozoa. When comparing Swim-up and Zymot sorting systems this study found that Zymot was able to isolate spermatozoa with less DNA fragmentation. Showing that microfluidics is a potent remover of suboptimal spermatozoa. This is consistent with previous findings contrasting the two techniques (3, 91-93). When comparing Swim-up and Zymot to the reference Raw sample, both techniques isolated spermatozoa with less DNA fragmentation. Demonstrating that these techniques can separate subpopulations of spermatozoa from a Raw sample with more intact DNA. Potentially because spermatozoa with DNA fragmentation show less motility and these categorization techniques use motility-based sorting (94, 95). This is consistent with previous studies that show similar trends when contrasting the aforementioned sorting techniques (3, 94-96). This is not to say that this method of categorizing DNA fragmentation has some limitations.

Halosperm G2 kit does not detect double stranded DNA breaks in matrix attachment regions (97). These types of breaks are highly damaging for the spermatozoa, reduceing fertility rates (97, 98). However, it is also important to note that this categorisation of DNA fragmentation is subjective and relies on researcher observations. Therefore, the results are only indicative of a trend in DNA fragmentation.

DNA fragmentation has been shown as a critical factor in male fertility. To visualise DNA fragmentation changes between the Swim-up, Zymot and Raw samples phase contrast microscopy was used. The appropriate magnification was used to obtain the highest quality images. The magnification should be high enough to distinguish spermatozoa with or without DNA fragmentation. While avoiding interference that can impede analysis, in the following paragraphs the appropriate magnification is discussed with the results from this study.

This study found that using 40× magnification lends itself the best for analysis of DNA fragmentation in spermatozoa. 40× magnification reduced seen artifacts in the sample leading to more accurate analysis. 40× magnification made it simple to differentiate between spermatozoa that show DNA fragmentation and those that do not. When contrasting this to 10× magnification the following was noted

10× magnification when observing DNA fragmentation was not suitable for analysis, due to the mounting agar used, which produced numerous artifacts hindering analysis. In addition, the halo formation is hard to see in 10×, making the 10× magnification unsuitable. Significant differences were noted between 10× and 20× magnifications.

20× magnification provides greater insight to DNA fragmentation. DNA fragmentation is more apparent in the 20× pictures, consequently 20× lends itself as a better analysis tool. However, 20× magnification does not overcome the challenges of artifact formation. As with 10× magnification, 20× magnification is impaired by artifact formation in this study.

While phase contrast microscopy is common when analyzing DNA fragmentation and spermatozoa in live cells, it has limited capacity to provide quantitative information. To overcome this challenge QPM microscopy was used to gather data from live spermatozoa and stained for DNA fragmentation.

This study was able to take live video of spermatozoa with the use of QPM technology. The study was able to use the collected video samples from both Raw, Zymot and Swim-up sorted spermatozoa to generate a heat map and conversely a “3D” topographical image of the spermatozoa. Similar videos have been published attempting to categorize the spermatozoa niche with QPM (99). However, articles have not categorized sorting techniques in IVF, only showing the potential of QPM in gathering data on fast moving spermatozoa in Raw samples (99, 100). Analysis of the spermatozoon video based on morphological, or motility characteristics, could not be achieved due to time constraints and lack of custom video analysis tools.

While QPM has been shown in this paper as a promising tool to image live spermatozoa. QPM was also attempted to be used in quantification of DNA fragmentation. As the system has potential to provide quantitative data. The categorization of DNA fragmentation was unsuccessful. Spermatozoa were mounted on SCS, this decreases the number of refractions achieved. If the samples could have been mounted on silicon wafers a higher resolution image could have been procured, and analysis could potentially have been done. The programing software is also not optimized for the imaging of DNA fragmentation; thus, reconstruction was impaired. Regular phase microscopy therefore provided better results than QPM in this regard.

However, as QPM technology matures it is likely that QPM will be able to overcome the obstacles shown in the study, thus potentially outperforming regular phase contrast imaging.

This study used a molecular biology approach to categorize ROS formation in Raw, Swim-up and Zymot samples. The significant results of these analyses are discussed in the sections below.

This study found statistically significant results between neat and seminal plasma fractions of Raw and Swim-up samples. However, the study was not able to show statistically significant results when comparing net seminal plasma fractions of Raw and Swim-up samples.

Measured ROS was identical for neat and seminal plasma fractions in Raw samples, suggesting that ROS is present in the isolated plasma fraction. Spermatozoa samples differentiated with Swim-up did not show any ROS in net fractions. This suggests Swim-up technique does not generate ROS in isolated spermatozoa.

Importantly the Oxisperm II kit only measures ROS through the creation of nitro blue tetrazolium in reaction to O_2 (101). This limits the Oxisperm II kit in providing a comprehensive measurement of all ROS species in a sample (102). Therefore, a sample could potentially have large undetectable ROS fractions (102). The Oxisperm II used to categorise ROS is subjective. Primarily because it relies on a scale provided in the kit itself. To gather more empirical data MDA levels were measured to further categorise ROS in spermatozoa.

This paper shows that MDA levels are significantly lower in Zymot, and Swim-up sorted spermatozoa compared to Raw samples, indicating lower ROS levels. However, when comparing Swim-up and Zymot no statistically significant result was found. Showing that the ROS created during centrifugation in Swim-up is not detected with MDA measurements. An explanation could be that the reactions needed to create MDA have not occurred, thus this assay would not pick up ROS in the sample even if a substantial fraction was present (103). Nonetheless this papers data suggests that Zymot and Swim-up are potent removers of ROS in spermatozoa samples. This study reinforces earlier published articles that have not been able to show centrifugation as a novel creator of ROS (53, 104). While also contradicting previous studies that have shown that centrifugation can create ROS in spermatozoa samples (72, 105). A potential reason is the sample size of our study with n=9, with a larger sample size the study

could compare MDA levels more accurately and reach a more robust conclusion about ROS formation. MDA itself can also be created through other enzymatic reactions in the body (106). Meaning that it may not accurately reflect the amount of lipid peroxidation. Thus, results gathered with the method should complement other analysis techniques to get an accurate picture of ROS. When differentiating the samples for MDA analysis, the data showed a markable decrease in the concentration of spermatozoa. These differences in concentration are described in the section below.

This study measured the number of spermatozoa (10^6/ml) in Raw, Swim-up, and Zymot samples. Both techniques resulted in statistically significant decreases in spermatozoa numbers. Compared to Raw samples, Zymot sorted samples showed a statistically significant decrease in the number of spermatozoa per ml. This is likely due to the fact that microfluidics systems filter out morphologically abnormal spermatozoa (3). Similarly, Swim-up showed a significant decrease in number of spermatozoa concentration/ml compared to the Raw samples. Meaning they isolate subpopulations from the sample, this has been highlighted in previous articles (107, 108). This study found no statistical difference in spermatozoa concentration between Swim-up and Zymot microfluidics differentiated spermatozoa. Similar results have been shown in studies comparing different sorting methods (107). It is important to note that Zymot microfluidics system had a higher mean spermatozoa/ml than Swim-up. However, it did not produce a statistical difference. An explanation for these findings could be the sample size of this study n=9, perhaps a clearer trend would be achieved with a bigger sample size.

As to the application of Oxisperm II, Halosperm G2 and MDA categorisation in an IVF setting the following can be said. When conducting the study, it was experienced that the Oxisperm II and Halosperm G2 were user friendly and required only standard lab equipment. The volumes needed for analysis were also not enough to impede further analysis with the sample. The results gathered from Oxisperm II and Halosperm G2 are subjective due to a lack of quantitative data and rely on the observations by the staff. Due to this, only potential trends can be elucidated, and more robust methods need to be used to confirm them.

MDA categorisation uses standard lab equipment, and the procedure is relatively easy to complete. Though, it requires chemicals typically not found in an IVF lab, such as 1-butanol, lysis buffer and BHT. Small microparticles from the chemicals can impact fertility by

decreasing air quality(109). No studies have been done to show how the chemicals used in MDA categorization may impact fertility success. However, it would not be surprising if it would have a negative impact considering the wide array of chemicals that do so (109). MDA categorization does provide the user with empirical data leaving little room for wrongful interpretation. However, the potential negative consequences this method can have on an IVF clinic though chemicals used, relegates it to research only. When comparing the Zymot and Swim-up method in a IVF clinic context the following can be said.

Swim-up itself is a technique that most IVF labs have the capacity to perform. Labs are well versed in the technique and bioengineers are well versed in the procedure, requiring minimal training. However, Swim-up requires to 2-3 hours to perform the entire protocol. Zymot microfluidics is similarly easy to perform. The required materials to conduct the procedure is already standard lab equipment in an IVF lab. The main advantage of Zymot microfluidics comes from the time saved, as the procedure takes 30min, as opposed to 2-3 hours with Swim-up. Thus, this study found that Zymot gives comparable results to Swim-up and better results when comparing DNA fragmentation. IVF clinics can, therefore, easily introduce the Zymot as an alternative sorting method. Increasing throughput and efficiency in daily processes. This study provides the following insight and conclusion.

6 Conclusion

This study showed that differentiation techniques such as Swim-up and Zymot produce less DNA fragmentation compared to Raw samples. When comparing the techniques, Zymot was shown to produce less DNA fragmentation. When analysing DNA fragmentation 40× magnification was found to be most effective for analysis. QPM was shown to be able to video live spermatozoa differentiated differently, QPM was shown to not be able of imaging DNA fragmented spermatozoa. Instead, regular phase microscopy proved adequate for this. This paper was not able to do statistical analysis of QPM results, because of lack of analysis tools. This study showed that there are differences in ROS neat and seminal plasma ROS between Raw and Swim-up techniques using Oxisperm II. When analysing MDA levels the study showed lower MDA levels in Swim-up and Zymot differentiated compared with Raw samples. The kits Oxisperm II, Halosperm G2 would be a beneficial supplement to IVF clinics while MDA categorisation is relegated to researchers. When comparing the sorting methods, the study

found Zymot to be easily implementable into IVF clinics, offering similar or better results than Swim-up while providing substantial time saving.

7 Future perspectives

Spermatozoa sorting remains a relevant topic for discussion in IVF since many of the current methods introduce DNA fragmentation and reactive oxygen species. Microfluidics has been shown in multiple papers too enable sorting of normal from abnormal spermatozoa from other cells in the sample (3, 93, 107, 110). Furthermore, it can produce spermatozoa with superior characteristics than more traditional methods in IVF. However, one of the limitations of microfluidics is the lack of standardization. Efforts should be made to compare clinical studies of microfluidic systems. This would enable researchers to standardize the technique and make it easier to apply in clinics. It is important to mention broader applications of microfluidics. Oocyte sorting in IVF as a potential area in microfluidics, have been shown as proof of concept in animal studies (111). Two methods have been explored in oocyte sorting, one uses a comparable laminar flow principle to spermatozoa sorting, for separation of good and bad quality oocytes (111). Another possibility is an electrical charge method named di-electrophoresis (112). Di-electrophoresis takes advantage of the fact that healthy oocytes moves faster in a charged enclosed microfluidics system compared to unhealthy ones, allowing one to distinguish between them (112). Unfortunately, the possibilities of expansion of microfluidic systems and exploration of the most suitable method for spermatozoa sorting, remains outside the scope of this study.

Notably, DNA fragmentation is an influential marker for fertilization rates and correct embryo development. DNA fragmentation has been correlated with aneuploidy, fertilization, and implantation rates as well as development of the fetus (113-115). IVF clinics should therefore consider implementing measurement techniques for DNA fragmentation in human spermatozoa, as this would potentially benefit the patients greatly.

Furter quantitative analysis is needed to be performed with QPM microscopes, relatively little data has been published with the use of QPM. Articles published in PubMed containing the words “QPM and Spermatozoa” are 56 from 1982 to 2023. To be able to understand the potential of QPM in IVF more quantitative studies are needed (116). Tools for analysis of spermatozoa utilizing QPM data will be vital if the technology is to be moved past research and

into IVF clinics. Development of such tools will potentially take years and need robust datasets as a foundation. The potential gains however if proved as a viable concept and technique, could be large for the IVF field, and could drastically lower analysis times and increase accuracy of the analysis.

8 References

1. Boivin J, Bunting L, Collins JA, Nygren KG. International estimates of infertility prevalence and treatment-seeking: potential need and demand for infertility medical care. Hum Reprod. 2007;22(6):1506-12.
2. Zegers-Hochschild F, Adamson GD, de Mouzon J, Ishihara O, Mansour R, Nygren K, et al. International Committee for Monitoring Assisted Reproductive Technology (ICMART) and the World Health Organization (WHO) revised glossary of ART terminology, 2009. Fertil Steril. 2009;92(5):1520-4.
3. Quinn MM, Jalalian L, Ribeiro S, Ona K, Demirci U, Cedars MI, et al. Microfluidic sorting selects sperm for clinical use with reduced DNA damage compared to density gradient centrifugation with swim-up in split semen samples. Hum Reprod. 2018;33(8):1388-93.
4. Wright C, Milne S, Leeson H. Sperm DNA damage caused by oxidative stress: modifiable clinical, lifestyle and nutritional factors in male infertility. Reprod Biomed Online. 2014;28(6):684-703.
5. Agarwal A, Maldonado Rosas I, Anagnostopoulou C, Cannarella R, Boitrelle F, Munoz LV, et al. Oxidative Stress and Assisted Reproduction: A Comprehensive Review of Its Pathophysiological Role and Strategies for Optimizing Embryo Culture Environment. Antioxidants (Basel). 2022;11(3).
6. Georgadaki K, Khoury N, Spandidos DA, Zoumpourlis V. The molecular basis of fertilization (Review). Int J Mol Med. 2016;38(4):979-86.
7. Alberts B, Johnson A, Lewis J, Raff M, Roberts K, Walter P. Molecular Biology of the Cell 4th edition. New York: Garland Science; 2002.
8. Suede SH, Malik A, Sapra A. Histology, Spermatogenesis. StatPearls. Treasure Island (FL): StatPearls Publishing

9. Alberts B, Johnson A, J L. Molecular Biology of the Cell. 2002. In: Molecular Biology of the Cell [Internet]. New York: Garland Science. Available from: https://www.ncbi.nlm.nih.gov/books/NBK26914/.
10. Aitken RJ. Human spermatozoa: revelations on the road to conception. F1000Prime Rep. 2013;5:39.
11. Jamnongjit M, Hammes SR. Oocyte maturation: the coming of age of a germ cell. Semin Reprod Med. 2005;23(3):234-41.
12. Hall J, Hall M. Medical Physiology 14th ed. Canada: Elyse O'grandy; 2021. 1056 p.
13. diZerega GS, Hodgen GD. Folliculogenesis in the primate ovarian cycle. Endocr Rev. 1981;2(1):27-49.
14. Peng XR, Hsueh AJ, LaPolt PS, Bjersing L, Ny T. Localization of luteinizing hormone receptor messenger ribonucleic acid expression in ovarian cell types during follicle development and ovulation. Endocrinology. 1991;129(6):3200-7.
15. Downs SM, Daniel SA, Eppig JJ. Induction of maturation in cumulus cell-enclosed mouse oocytes by follicle-stimulating hormone and epidermal growth factor: evidence for a positive stimulus of somatic cell origin. J Exp Zool. 1988;245(1):86-96.
16. Webster A, Schuh M. Mechanisms of Aneuploidy in Human Eggs. Trends in cell biology. 2017;27 1:55-68.

17. Owen D, Katz D. A Review of the Physical and Chemical Properties of Human Semen and the Formulation of a Semen Simulant. Journal of andrology. 2005;26:459-69.
18. Kavanagh JP. Sodium, potassium, calcium, magnesium, zinc, citrate and chloride content of human prostatic and seminal fluid. J Reprod Fertil. 1985;75(1):35-41.
19. Carpino A, Siciliano L. Unaltered protein pattern/genital tract secretion marker levels in seminal plasma of highly viscous human ejaculates. Arch Androl. 1998;41(1):31-5.
20. Evans JP, Florman HM. The state of the union: the cell biology of fertilization. Nat Cell Biol. 2002;4 Suppl:s57-63.
21. Boron W, Boulapep E. Medical Physiology. 3: Elsevier - Health Sciences Division; 2016.
22. Evans JP. The molecular basis of sperm-oocyte membrane interactions during mammalian fertilization. Hum Reprod Update. 2002;8(4):297-311.
23. Choe J, Archer JS, Shanks AL. In Vitro Fertilization. StatPearls. Treasure Island (FL): StatPearls Publishing

24. Sunderam S, Kissin DM, Crawford SB, Folger SG, Boulet SL, Warner L, et al. Assisted Reproductive Technology Surveillance - United States, 2015. MMWR Surveill Summ. 2018;67(3):1-28.
25. Wang J, Sauer MV. In vitro fertilization (IVF): a review of 3 decades of clinical innovation and technological advancement. Ther Clin Risk Manag. 2006;2(4):355-64.
26. Steptoe PC, Edwards RG. Reimplantation of a human embryo with subsequent tubal pregnancy. Lancet. 1976;1(7965):880-2.
27. Edwards RG, Steptoe PC, Purdy JM. Establishing full-term human pregnancies using cleaving embryos grown in vitro. Br J Obstet Gynaecol. 1980;87(9):737-56.
28. Edwards RG, Steptoe PC. Current status of in-vitro fertilisation and implantation of human embryos. Lancet. 1983;2(8362):1265-9.
29. Dellenbach P, Nisand I, Moreau L, Feger B, Plumere C, Gerlinger P. Transvaginal sonographically controlled follicle puncture for oocyte retrieval. Fertil Steril. 1985;44(5):656-62.
30. Harris ID, Fronczak C, Roth L, Meacham RB. Fertility and the aging male. Rev Urol. 2011;13(4):e184-90.
31. Palermo G, Joris H, Devroey P, Van Steirteghem AC. Pregnancies after intracytoplasmic injection of single spermatozoon into an oocyte. Lancet. 1992;340(8810):17-8.
32. Craft I, Bennett V, Nicholson N. Fertilising ability of testicular spermatozoa. Lancet. 1993;342(8875):864.
33. Staessen C, Coonen E, Van Assche E, Tournaye H, Joris H, Devroey P, et al. Preimplantation diagnosis for X and Y normality in embryos from three Klinefelter patients. Hum Reprod. 1996;11(8):1650-3.
34. Auger J, Kunstmann JM, Czyglik F, Jouannet P. Decline in semen quality among fertile men in Paris during the past 20 years. N Engl J Med. 1995;332(5):281-5.
35. Fisch H, Goluboff ET, Olson JH, Feldshuh J, Broder SJ, Barad DH. Semen analyses in 1,283 men from the United States over a 25-year period: no decline in quality. Fertil Steril. 1996;65(5):1009-14.
36. Sartorius GA, Nieschlag E. Paternal age and reproduction. Hum Reprod Update. 2010;16(1):65-79.

37. Aitken RJ, Nixon B, Lin M, Koppers AJ, Lee YH, Baker MA. Proteomic changes in mammalian spermatozoa during epididymal maturation. Asian J Androl. 2007;9(4):554-64.
38. Bonde JP, Kold Jensen T, Brixen Larsen S, Abell A, Scheike T, Hjollund NH, et al. Year of birth and sperm count in 10 Danish occupational studies. Scand J Work Environ Health. 1998;24(5):407-13.
39. Sasano N, Ichijo S. Vascular patterns of the human testis with special reference to its senile changes. Tohoku J Exp Med. 1969;99(3):269-80.
40. Schwartz D, Mayaux MJ, Spira A, Moscato ML, Jouannet P, Czyglik F, et al. Semen characteristics as a function of age in 833 fertile men. Fertil Steril. 1983;39(4):530-5.
41. Andolz P, Bielsa MA, Vila J. Evolution of semen quality in North-eastern Spain: a study in 22,759 infertile men over a 36 year period. Hum Reprod. 1999;14(3):731-5.
42. Bujan L, Mieusset R, Mondinat C, Mansat A, Pontonnier F. Sperm morphology in fertile men and its age related variation. Andrologia. 1988;20(2):121-8.
43. Pino V, Sanz A, Valdés N, Crosby J, Mackenna A. The effects of aging on semen parameters and sperm DNA fragmentation. JBRA Assist Reprod. 2020;24(1):82-6.
44. NEAVES WB, Johnson L, Porter JC, PARKER JR CR, PETTY CS. Leydig cell numbers, daily sperm production, and serum gonadotropin levels in aging men. The Journal of Clinical Endocrinology & Metabolism. 1984;59(4):756-63.
45. Johnson L, Petty C, Neaves W. Influence of age on sperm production and testicular weights in men. Reproduction. 1984;70(1):211-8.
46. Lanzafame FM, La Vignera S, Vicari E, Calogero AE. Oxidative stress and medical antioxidant treatment in male infertility. Reprod Biomed Online. 2009;19(5):638-59.
47. Agarwal A, Virk G, Ong C, du Plessis SS. Effect of oxidative stress on male reproduction. World J Mens Health. 2014;32(1):1-17.
48. Kong A, Frigge ML, Masson G, Besenbacher S, Sulem P, Magnusson G, et al. Rate of de novo mutations and the importance of father's age to disease risk. Nature. 2012;488(7412):471-5.
49. laboratory manual for the examination and processing of human semen. World health Organisation; 2021 27.07.2021.
50. Wosnitzer M, Goldstein M, Hardy MP. Review of Azoospermia. Spermatogenesis. 2014;4:e28218.
51. Auger J. Assessing human sperm morphology: top models, underdogs or biometrics? Asian J Androl. 2010;12(1):36-46.
52. Puerta Suárez J, du Plessis SS, Cardona Maya WD. Spermatozoa: A Historical Perspective. Int J Fertil Steril. 2018;12(3):182-90.
53. Malvezzi H, Sharma R, Agarwal A, Abuzenadah AM, Abu-Elmagd M. Sperm quality after density gradient centrifugation with three commercially available media: a controlled trial. Reprod Biol Endocrinol. 2014;12:121.
54. Beydola T, Sharma R, Lee W, Agarwal A. Sperm preparation and selection techniques. In Male Infertility Practice. 2013:244-51.
55. Hawksley. Gynotec SpermTec Silica Gradient 45%, 80% & 100% [Electronic]. United Kingdom Hawksley; 2023 [cited 2023 30.01]. Manufacturer storefront to buy separateing medium for sperm IVF sorting]. Available from: https://hawksley.co.uk/products/spermtec-silica-gradient-45-80-100.
56. Karavolos S. Sperm DNA Fragmentation. Semin Reprod Med. 2021;39(5-06):194-9.
57. Cocuzza M, Athayde KS, Agarwal A, Sharma R, Pagani R, Lucon AM, et al. Age-related increase of reactive oxygen species in neat semen in healthy fertile men. Urology. 2008;71(3):490-4.

58. Zubkova EV, Robaire B. Effects of ageing on spermatozoal chromatin and its sensitivity to in vivo and in vitro oxidative challenge in the Brown Norway rat. Hum Reprod. 2006;21(11):2901-10.
59. Makker K, Agarwal A, Sharma R. Oxidative stress & male infertility. Indian Journal of Medical Research. 2009;129(4):357-67.
60. Calamera J, Buffone M, Ollero M, Alvarez J, Doncel G. Superoxide dismutase content and fatty acid composition in subsets of human spermatozoa from normozoospermic, asthenozoospermic, and polyzoospermic semen samples. Molecular Reproduction and Development: Incorporating Gamete Research. 2003;66(4):422-30.
61. Bansal AK, Bilaspuri G. Impacts of oxidative stress and antioxidants on semen functions. Veterinary medicine international. 2011;2011.
62. Suarez SS. Control of hyperactivation in sperm. Human reproduction update. 2008;14(6):647-57.
63. Schulte R, Chung Y, Ohl D, Takayama S, Smith G. Microfluidic sperm sorting device provides a novel method for selecting motile sperm with higher DNA integrity. Fertility and sterility. 2007;88:S76.
64. Alias AB, Huang HY, Yao DJ. A Review on Microfluidics: An Aid to Assisted Reproductive Technology. Molecules. 2021;26(14).
65. Whitesides GM. The origins and the future of microfluidics. Nature. 2006;442(7101):368-73.
66. Dittrich PS, Manz A. Lab-on-a-chip: microfluidics in drug discovery. Nat Rev Drug Discov. 2006;5(3):210-8.
67. Beebe DJ, Mensing GA, Walker GM. Physics and applications of microfluidics in biology. Annu Rev Biomed Eng. 2002;4:261-86.
68. Lu C, Verbridge SS. Microfluidic methods for molecular biology: Springer; 2016.
69. Hou X, Zhang YS, Santiago GT-d, Alvarez MM, Ribas J, Jonas SJ, et al. Interplay between materials and microfluidics. Nature Reviews Materials. 2017;2(5):17016.
70. Manz A, Harrison DJ, Verpoorte EMJ, Fettinger JC, Paulus A, Lüdi H, et al. Planar chips technology for miniaturization and integration of separation techniques into monitoring systems: Capillary electrophoresis on a chip. Journal of Chromatography A. 1992;593(1):253-8.
71. Scheler O, Postek W, Garstecki P. Recent developments of microfluidics as a tool for biotechnology and microbiology. Curr Opin Biotechnol. 2019;55:60-7.
72. Asghar W, Velasco V, Kingsley JL, Shoukat MS, Shafiee H, Anchan RM, et al. Selection of functional human sperm with higher DNA integrity and fewer reactive oxygen species. Adv Healthc Mater. 2014;3(10):1671-9.
73. Phiphattanaphiphop C, Leksakul K, Phatthanakun R, Khamlor T. A novel microfluidic chip-based sperm-sorting device constructed using design of experiment method. Sci Rep. 2020;10(1):17143.
74. Bahat A, Eisenbach M. Sperm thermotaxis. Mol Cell Endocrinol. 2006;252(1-2):115-9.
75. Mualla F, Aubreville M, Maier A. Microscopy. In: Maier A, Steidl S, Christlein V, Hornegger J, editors. Medical Imaging Systems: An Introductory Guide. Cham (CH): Springer

76. Wang G, Fang N. Chapter four - Detecting and Tracking Nonfluorescent Nanoparticle Probes in Live Cells. In: conn PM, editor. Methods in Enzymology. 504: Academic Press; 2012. p. 83-108.
77. Zernike F. How I discovered phase contrast. Science. 1955;121(3141):345-9.
78. Yin Z, Kanade T, Chen M. Understanding the phase contrast optics to restore artifact-free microscopy images for segmentation. Med Image Anal. 2012;16(5):1047-62.
79. Murphy DB, Davidson MW. Fundamentals of light microscopy and electronic imaging: John Wiley & Sons; 2012.
80. Preza C, Snyder DL, Conchello J-A. Theoretical development and experimental evaluation of imaging models for differential-interference-contrast microscopy. J Opt Soc Am A. 1999;16(9):2185-99.
81. Wang X, Wang H, Wang J, Liu X, Hao H, Tan YS, et al. Single-shot isotropic differential interference contrast microscopy. Nature Communications. 2023;14(1):2063.
82. Cuche E, Bevilacqua F, Depeursinge C. Digital holography for quantitative phase-contrast imaging. Opt Lett. 1999;24(5):291-3.
83. Gleyzes P, Boccara AC, Saint-Jalmes H. Multichannel Nomarski microscope with polarization modulation: performance and applications. Opt Lett. 1997;22(20):1529-31.
84. Lee K, Kim K, Jung J, Heo J, Cho S, Lee S, et al. Quantitative Phase Imaging Techniques for the Study of Cell Pathophysiology: From Principles to Applications. Sensors. 2013;13(4):4170-91.
85. Ahmad A, Dubey V, Singh VR, Tinguely J-C, Øie CI, Wolfson DL, et al. Quantitative phase microscopy of red blood cells during planar trapping and propulsion. Lab on a Chip. 2018;18(19):3025-36.
86. Lee S, Lee JY, Park CS, Kim DY. Detrended fluctuation analysis of membrane flickering in discocyte and spherocyte red blood cells using quantitative phase microscopy. J Biomed Opt. 2011;16(7):076009.
87. Kim DNH, Lim AA, Teitell MA. Rapid, label-free classification of tumor-reactive T cell killing with quantitative phase microscopy and machine learning. Scientific Reports. 2021;11(1):19448.
88. Ozaki Y, Yamada H, Kikuchi H, Hirotsu A, Murakami T, Matsumoto T, et al. Label-free classification of cells based on supervised machine learning of subcellular structures. PLoS One. 2019;14(1):e0211347.
89. Micó V, Zheng J, Garcia J, Zalevsky Z, Gao P. Resolution enhancement in quantitative phase microscopy. Adv Opt Photon. 2019;11(1):135-214.
90. Dubey V, Popova D, Ahmad A, Acharya G, Basnet P, Mehta DS, et al. Partially spatially coherent digital holographic microscopy and machine learning for quantitative analysis of human spermatozoa under oxidative stress condition. Scientific Reports. 2019;9(1):3564.
91. Younglai EV, Holt D, Brown P, Jurisicova A, Casper RF. Sperm swim-up techniques and DNA fragmentation. Hum Reprod. 2001;16(9):1950-3.
92. Santiso R, Tamayo M, Gosálvez J, Meseguer M, Garrido N, Fernández JL. Swim-up procedure selects spermatozoa with longer telomere length. Mutat Res. 2010;688(1-2):88-90.
93. Shirota K, Yotsumoto F, Itoh H, Obama H, Hidaka N, Nakajima K, et al. Separation efficiency of a microfluidic sperm sorter to minimize sperm DNA damage. Fertil Steril. 2016;105(2):315-21.e1.
94. Zini A, Finelli A, Phang D, Jarvi K. Influence of semen processing technique on human sperm DNA integrity. Urology. 2000;56(6):1081-4.

95. Oguz Y, Guler I, Erdem A, Mutlu MF, Gumuslu S, Oktem M, et al. The effect of swim-up and gradient sperm preparation techniques on deoxyribonucleic acid (DNA) fragmentation in subfertile patients. J Assist Reprod Genet. 2018;35(6):1083-9.
96. Lara-Cerrillo S, Urda Muñoz C, de la Casa Heras M, Camacho Fernández-Pacheco S, Gijón de la Santa J, Lacruz-Ruiz T, et al. Microfluidic sperm sorting improves ICSI outcomes in patients with increased values of Double-Strand Breaks in sperm DNA. Revista Internacional de Andrología. 2023;21(1):100338.
97. Ribas-Maynou J, Benet J. Single and Double Strand Sperm DNA Damage: Different Reproductive Effects on Male Fertility. Genes (Basel). 2019;10(2).
98. Garolla A, Cosci I, Bertoldo A, Sartini B, Boudjema E, Foresta C. DNA double strand breaks in human spermatozoa can be predictive for assisted reproductive outcome. Reprod Biomed Online. 2015;31(1):100-7.
99. Kamieniczna M, Stachowska E, Augustynowicz A, Woźniak T, Kurpisz MK. Human live spermatozoa morphology assessment using digital holographic microscopy. Scientific Reports. 2022;12(1):4846.
100. Poola PK, Jayaraman V, Chaithanya K, Rao D, John R. Quantitative label-free technique for morphological evaluation of human sperm—a promising tool in semen evaluation. OSA Continuum. 2018;1(4):1215-25.
101. Aitken RJ. Nitroblue tetrazolium (NBT) assay. Reprod Biomed Online. 2018;36(1):90-1.
102. Castleton PE, Deluao JC, Sharkey DJ, McPherson NO. Measuring reactive oxygen species in semen for Male preconception care: A scientist perspective. Antioxidants. 2022;11(2):264.
103. Morales M, Munné-Bosch S. Malondialdehyde: Facts and Artifacts. Plant Physiology. 2019;180(3):1246-50.
104. Wang M, Sun J, Wang L, Gao X, Lu X, Wu Z, et al. Assessment of density gradient centrifugation (DGC) and sperm chromatin dispersion (SCD) measurements in couples with male factor infertility undergoing ICSI. J Assist Reprod Genet. 2014;31(12):1655-63.
105. Salam L, Rahim AI, Al-Kawaz U. Which is matter in centrifugation based Reactive Oxygen Species (ROS) production? force or time? 2020:6405-8.
106. Tsikas D. Assessment of lipid peroxidation by measuring malondialdehyde (MDA) and relatives in biological samples: Analytical and biological challenges. Analytical Biochemistry. 2017;524:13-30.
107. Gode F, Gürbüz AS, Tamer B, Pala I, Isik AZ. The Effects of Microfluidic Sperm Sorting, Density Gradient and Swim-up Methods on Semen Oxidation Reduction Potential. Urol J. 2020;17(4):397-401.
108. ÅKERLÖF E, Fredricsson B, Gustafson O, Lunell N, Nylund L, Rosenborg L, et al. Sperm count and motility influence the results of human fertilization in vitro. International journal of andrology. 1991;14(2):79-86.
109. Khoudja RY, Xu Y, Li T, Zhou C. Better IVF outcomes following improvements in laboratory air quality. J Assist Reprod Genet. 2013;30(1):69-76.
110. Pujol A, García-Peiró A, Ribas-Maynou J, Lafuente R, Mataró D, Vassena R. A microfluidic sperm-sorting device reduces the proportion of sperm with double-stranded DNA fragmentation. Zygote. 2022;30(2):200-5.
111. Iwasaki W, Yamanaka K, Sugiyama D, Teshima Y, Briones-Nagata MP, Maeki M, et al. Simple separation of good quality bovine oocytes using a microfluidic device. Scientific Reports. 2018;8(1):14273.

112. Choi W, Kim J-S, Lee D-H, Lee K-K, Koo D-B, Park J-K. Dielectrophoretic oocyte selection chip for in vitro fertilization. Biomedical Microdevices. 2008;10(3):337-45.
113. Chavez SL, Loewke KE, Han J, Moussavi F, Colls P, Munne S, et al. Dynamic blastomere behaviour reflects human embryo ploidy by the four-cell stage. Nat Commun. 2012;3:1251.
114. Hnida C, Engenheiro E, Ziebe S. Computer‐controlled, multilevel, morphometric analysis of blastomere size as biomarker of fragmentation and multinuclearity in human embryos. Human Reproduction. 2004;19(2):288-93.
115. Racowsky C, Stern JE, Gibbons WE, Behr B, Pomeroy KO, Biggers JD. National collection of embryo morphology data into Society for Assisted Reproductive Technology Clinic Outcomes Reporting System: associations among day 3 cell number, fragmentation and blastomere asymmetry, and live birth rate. Fertility and sterility. 2011;95(6):1985-9.
116. Komori K, Tsujimura A, Ishijima S, Tanjapatkul P, Fujita K, Matsuoka Y, et al. Comparative study of Sperm Motility Analysis System and conventional microscopic semen analysis. Reprod Med Biol. 2006;5(3):195-200.

Supplementary information

S1 Consent scheme

UNIVERSITETSSYKEHUSET NORD-NORGE
DAVVI-NORGGA UNIVERSITEHTABUOHCCEVIESSU

HELSE NORD

Samtykkeskjema for bruk av biologisk materiale

Avdeling: IVF-poliklinikken, Kvinneklinikken, K3K, Universitetssykehuset Nord-Norge

Ansvarlig person/Prosjektleder: Fag- og forskningsleder Mona Nystad

Formål med bruk av prøven:

Prøven skal brukes til:

- Intern validering av metoder ved IVF-poliklinikken.
- Forskningsprosjekter som går ut på å forbedre metoder som i dag benyttes på IVF-poliklinikken. Eksempel på forskningsprosjekt er utvikling av nye spermieseparerings-metoder og utvikling av nye mikroskop i samarbeid med UiT Norges arktiske universitet. Resultatene fra forskningsprosjektene kan bli publisert i vitenskapelige tidsskrifter. Siden prøven fra deg er anonymisert kan ikke resultatene kobles tilbake til deg.

Hva skjer med prøven:

Prøven anonymiseres.

Samtykke til at prøven med biologisk materiale kan brukes til de ovenfor nevnte punktene.

……	……..
Signatur/dato prosjektleder	Signatur/dato giver

Table S2: List of equipment, reagents and solutions

Table showing the Reagents and components of the methods used in the study. *The Table is split into Equipment, company, reference and objective.*

Equipment	**Company**	**Reference number**	**Objective**
phase contrast microscopy of spermatozoa samples			
Nikon ECLIPSE E 200	Nikon		*Microscopy of samples*
Polyethylen Disposable transfer pipette	fisher scientific	SO1213	Gauage *viscosity of samples*
HDMI16MDPX–HDMI 6MegaPixel Microscope camera	DeltaPix		*Photography of samples*
Coverslip	fisher scientific	12333128	*Dispersion of samples*
Microscope slide	Thermo scientific	AAAA000001##12E	surface to microscope from
Nikon 10X/0,25	Nikon		*Magnification of sample*
Nikon 20X/0,4	Nikon		*Magnification of sample*
Nikon 40X/0,55	Nikon		*Magnification of sample*
MR-1 Mini-Rocker Shaker	BioSan	BS-010152-AAG	Liquification of samples
Microscopy slides	Thermo scientific	Ref: AAAA000001##12E	*Surface to spread sample over*
Swim-up			
Nunc-tubes	Thermo Scientific™	Ref:337846	*Reaction vessel*

Fertimedium	CooperSurgical®	Ref: ART-3001	*Creation of a favorable environment for spermatozoa differentiation*
SpermWash ORIGIO	ORIGIO	Ref: 84050060A	*Washing of sample*
MR-1 Mini-Rocker Shaker	BioSan	BS-010152-AAG	Liquification of samples
Rotina 420R	Hettich	Ref: 4706	*Centrifugation of sample*
Forma™ Series II Water-Jacketed CO2 Incubator, 184L	Thermo Scientific™	Ref: 3110	*Incubation of sample in favorable conditions for differentiation*
Zymot			
Zymot microfluidics chip	Zymot	Ref: ZMH0850 LOT: Z21122202013	*Spermatozoa sorting by pore principle*
SpermWash ORIGIO	CooperSurgical®	Ref: 84050060A LOT: 220422-005953	*To allow for differentiation of the sample*
Eppendorf tube	Eppendorf	Ref: 0030120086	*Reaction vessel*
Coverslip	fisher scientific	12333128	*Dispersion of samples*
MR-1 Mini-Rocker Shaker	BioSan	BS-010152-AAG	Liquification of samples
BD Luer-Lok™ 1-mL syringe	BD	Ref: 309628	*Transfer and collection of samples*
Halosperm G2			
Halosperm G2 (kit)	Halotech	Ref:HT-HSG2	
Agarose cell support	Halotech	Ref: ACD Lot: G2 2230	*Fasten the spermatozoon to the super coated slide*

Super-coated slides	Halotech	Ref: SCS Lot: G2 2230	*Provides a surface for staining and microscopy of spermatozoon*
Eppendorf tubes	Halotech	Ref: Lot: G2 2230	*Reaction vessel*
Denaturant agent	Halotech	Ref: DA Lot: G2 2230	*Breakdown of chromatin structure to allow visualization*
Lysis solution	Halotech	Ref: LS Lot: G2 2230	*Lysis of spermatozoa membrane*
Eosin staining solution	Halotech	Ref: SSA Lot: G2 2230	*Staining of protein for DNA visualization*
Thiazine staining solution	Halotech	Ref: SSB Lot: G2 2230	*Staining of nucleic acids*
Husqvarna Microwave dine			*Melting of agar*
Ethanol absolute Emparata ACS	Sigma-Aldrich® Solutions	Ref: 1.07017	*De-hydration of samples*
70% ethanol			*De-hydration of samples*
Nikon ECLIPSE E 200	Nikon		*Microscopy of samples*
HDMI16MDPX–HDMI 6MegaPixel Microscope camera	DeltaPix		*Photography of samples*
Coverslip	fisher scientific	12333128	*Dispersion of samples*

Nikon 10X/0,25	Nikon		*Magnification of sample*
Nikon 20X/0,4	Nikon		*Magnification of sample*
Nikon 40X/0,55	Nikon		*Magnification of sample*
Electrolux refrigerator	Electrolux	Ref: EN340000AOW	Cooling of agar
Fume Hood	Phoenix Controls Corporation	Ref:FMH400-I	Ventilation of sample area
Oxisperm II ROS analysis			
Oxisperm II	Halotech	Ref: 90521 Lot:OS20II 2220317	
OSIIRS reactive membrane	Halotech	Ref: RS Lot: OSOII 2230	*Reaction vessel*
OSIIS sperm reactivity solution	Halotech	Ref: IS Lot:OS20II	*Substance needed to produce color change*
Phosphate buffered saline	Sigma-Aldrich®	Ref: MFCD00131855	*Negative control*
Biofuge 13	Sepatech	Ref: 3695	*Centrifugation of samples*
Eppendorf Safe-Lock Tubes	Eppendorf	Ref: 0030121872	*Reaction vessel*
MDA ROS level analysis			
MDA Lysis Buffer	Sigma-Aldrich®	Ref: MAK085A	*Breakdown of spermatozoa membrane and proteins*
Phosphotungstic Acid Solution	Sigma-Aldrich®	Ref: MAK085B	*Induce a color change*
BHT, 100X	Sigma-Aldrich®	Ref: MAK085C	*Stabilizer to prevent oxidation*

TBA	Sigma-Aldrich®	Ref: MAK085D	
MDA Standard, 4.17 M	Sigma-Aldrich®	Ref: MAK085E	*Known marker for oxidative stress*
VCX-130 sonicator	Vibra-Cell™	Ref: 42786L	*Breakdown of spermatozoa membrane*
Biofuge 13	Sepatech	Ref: 3695	*Centrifugation of samples*
Epoch 96-well reader	Thermo Scientific™	ref:171122113	*Gathering of absorption data*
96-well Clear Flat Bottom TC-treated Culture Microplate	Falcon	Ref: 353072	*Used for color participation*
Eppendorf ThermoMixer® C	Eppendrof	Ref: 5382000015	*Machine to allow for color precipitation*
Electrolux refrigerator	electrolux	Ref: EN340000AOW	*Cooling of samples*
QPM analysis			
20×_0.7NA	Olympus		*Microscopy of sample*
60×_0.9NA	Olympus		*Microscopy of sample*
60×_1.2NA	Olympus		*Microscopy of sample*
Digital camera C11440	Hamamatsu		*Video or photography of samples*
Components of microscope	ThorLabs		*Majority of components needed to build the microscope*

S 3 Basic evaluation of Spermatozoa

Table below contains the standards World health organization has for spermatozoa differentiation

Table: ***World health organization (WHO) standards for healthy semen samples from 1980 to 2021.*** *Table containing the criteria needed categorize a given spermatozoa sample. Parameters are presented in the left column and range from, Volume, Spermatozoon concentration ($x10^5$/ml), Total spermatozoon number ($x10^6$), Progressive motility (%), total motility (%), Vitality (%), and Normal morphology (%). The (a+B) sub-criteria in 2010 issue for progressive motility (%) differentiates spermatozoa moving fast and straight in one direction sorted as A, while B spermatozoa are slower spermatozoa moving in a curved line. The corresponding annotation is used in the 1992. The topmost row contains the year each issue was published. The Figure is reproduced from (49).*

Spermatozoa parameter	**WHO 1980**	**WHO 1987**	**WHO 1992**	**WHO 1999**	**WHO 2010**	**WHO 2021**
Volume (ml)	ND	≥2	≥2	≥2	1.5	1.4
Spermatozoon concentration ($x10^5$/ml)	20-200	≥20	≥20	≥20	15	16
Total spermatozoon number ($x10^6$)	ND	≥40	≥40	≥40	39	39
Total motility (%)	≥60	≥50	≥50	≥50	40	42
Progressive motility (%)	≥2	≥25	≥25(grade a)	≥25	32 (a+b)	30
Vitality (%)	ND	≥50	≥75	≥75	58	54
Normal morphology (%)	80.5	≥50	≥30	-14	4	4

S4 Lipid peroxidation (MDA) Assay kit protocol

Technical Bulletin

Lipid Peroxidation (MDA) Assay Kit

Catalog Number MAK085

Product Description

Lipid peroxidation is the degradation of lipids that occurs as a result of oxidative damage and is a useful marker for oxidative stress. Polyunsaturated lipids are susceptible to an oxidative attack, typically by reactive oxygen species, resulting in a well-defined chain reaction with the production of end products such as malondialdehyde (MDA). Lipid peroxidation may contribute to the pathology of many diseases including atherosclerosis, diabetes, and Alzheimer's.

In this kit, lipid peroxidation is determined by the reaction of MDA with thiobarbituric acid (TBA) to form a colorimetric (532 nm) / fluorometric (λ_{Ex} = 532/λ_{Em} = 553 nm) product, proportional to the MDA present.

Components

The kit is sufficient for 100 colorimetric or fluorometric assays in 96-well plates.

- MDA Lysis Buffer 25 mL
  Catalog Number MAK085A
- Phosphotungstic Acid Solution 12.5 mL
  Catalog Number MAK085B
- BHT, 100× 1 mL
  Catalog Number MAK085C
- TBA 4 bottles
  Catalog Number MAK085D
- MDA Standard, 4.17 M 0.1 mL
  Catalog Number MAK085E

Reagents and Equipment Required but Not Provided

- Pipetting devices and accessories (e.g., multichannel pipettor)
- 96-well flat-bottom plate – It is recommended to use black plates with clear bottoms for fluorescence assays and clear plates for colorimetric assays. Cell culture or tissue culture treated plates are **not** recommended.
- Fluorescence or spectrophotometric multiwell plate reader
- Glacial acetic acid (Catalog Number A6283 or equivalent)
- Perchloric acid (Catalog Number 244252 or equivalent)
- Sulfuric acid (Catalog Number 258105 or equivalent)
- 1-Butanol (Catalog Number 360465 or equivalent)

Precautions and Disclaimer

For R&D Use Only. Not for drug, household, or other uses. Please consult the Safety Data Sheet for information regarding hazards and safe handling practices.

Storage/Stability

The kit is shipped on wet ice. Store components at -20 °C, protected from light.

Preparation Instructions

Briefly centrifuge vials before opening. To maintain reagent integrity, avoid repeated freeze/thaw cycles. Use purified water for the preparation of all reagents. Allow all components to come to room temperature before starting.

TBA Solution: Reconstitute a bottle with 7.5 mL of Glacial Acetic Acid, then adjust the final volume to 25 mL with water. Sonication can be used to assist dissolution if necessary. Store at 4 °C and use within 1 week of preparation.

Procedure

All samples and standards should be run in duplicate.

Use purified water for the preparation of all standards and samples.

MDA Standards for Colorimetric Detection

1. A new standard curve must be set up each time the assay is run.
2. Dilute 10 µL of the 4.17 M MDA Standard Solution with 407 µL of purified water to prepare a 0.1 M MDA Standard Solution.
3. Further dilute 20 µL of the 0.1 M MDA Standard Solution with 980 µL of purified water to prepare a 2 mM MDA Standard.
4. Prepare MDA standards in 1.5 mL microcentrifuge tubes according to Table 1.

Table 1.

Preparation of MDA Standards for Colorimetric Assay

Well	2 mM MDA Standard	Purified Water	MDA (nmole/well)
1	10 µL	190 µL	20
2	8 µL	192 µL	16
3	6 µL	194 µL	12
4	4 µL	196 µL	8
5	2 µL	198 µL	4
6	-	200 µL	0

MDA Standards for Fluorometric Detection

1. A new standard curve must be set up each time the assay is run.
2. Prepare a 2 mM Standard Solution as for the Colorimetric assay Steps 1 and 2.
3. Dilute 100 µL of the 2 mM MDA Standard Solution with 900 µL of water to make a 0.2 mM MDA standard solution.
4. Prepare MDA standards in 1.5 mL microcentrifuge tubes according to Table 2.
5.

Table 2.

Preparation of MDA Standards for Fluorometric Assay

Well	0.2 mM MDA Standard	Purified Water	MDA (nmole/well)
1	10 µL	190 µL	2.0
2	8 µL	192 µL	1.6
3	6 µL	194 µL	1.2
4	4 µL	196 µL	0.8
5	2 µL	198 µL	0.4
6	-	200 µL	0

Sample Preparation Serum or Plasma

1. Gently mix 20 µL of serum or plasma samples with 500 µL of 42 mM sulfuric acid in a microcentrifuge tube.
2. Add 125 µL of Phosphotungstic Acid Solution and mix by vortexing.
3. Incubate at room temperature for 5 minutes and then centrifuge the samples at 13,000 × *g* for 3 minutes. Remove supernatant and retain pellet for assay.
4. In a separate tube, add 2 µL of BHT (100×) to 100 µL of purified water.
5. Resuspend the pellet on ice with the water/BHT solution. Adjust the volume to 200 µL with water.

Tissue or Cells

1. Homogenize tissue (10 mg) or cells (2×10^6) on ice in 300 µL of the MDA Lysis Buffer containing 3 µL of BHT (100×).
2. Centrifuge the samples at 13,000 × g for 10 minutes to remove insoluble material.

   Alternatively, protein can be precipitated by homogenizing 10 mg of sample in 150 µL of purified water containing 3 µL of BHT (100×) and adding 1 volume of 2 N perchloric acid, vortexing, and centrifuging to remove precipitated protein.

3. Place 200 µL of the supernatant from each homogenized Sample into a microcentrifuge tube.

Assay Reaction

1. To form the MDA-TBA adduct, add 600 µL of the TBA solution into each vial containing Standard and Sample.
2. Incubate at 95 °C for 60 minutes.
3. Cool to room temperature in an ice bath for 10 minutes.
4. Pipette 200 µL from each Standard and Sample reaction mixture, except for Serum or Plasma Samples (see Step 5), into a 96-well plate for analysis.

   Note:

   a. To enhance sensitivity, add 300 µL of 1-butanol to extract the MDA-TBA adduct from the 800 µL reaction mixture. If separation does not occur, add 100 µL of 5 M NaCl and vortex vigorously. Centrifuge at 16,000 × *g* for 3 minutes at room temperature to separate the layers. Transfer the 1-butanol layer (the top layer) to another tube and evaporate the 1-butanol. The 1-butanol can be removed either by freeze-drying or heating on a hot block at 55 °C. Dissolve the residue containing the MDA-TBA adduct in 200 µL of purified water, and then transfer to a 96-well plate for analysis.

   b. Occasionally samples will exhibit turbidity, which can be eliminated by filtering through a 0.2 µm filter.

   c. TBA can react with other compounds in Samples to produce other colored products. These should not generally interfere with quantitation of the TBA-MDA adduct.

5. For Serum or Plasma Samples, mix each reaction mixture with 300 µL of 1-butanol and 100 µL of 5 M NaCl. Vortex and then centrifuge for 3 minutes at 16,000 × *g* at room temperature. Transfer the 1-butanol layer (the top layer) to a new centrifuge tube and remove the 1-butanol. The 1-butanol can be removed either by freeze-drying, or heating on a hot block at 55 °C. Resuspend the remaining material in 200 µL of ultrapure water. Mix well and add 200 µL into a 96-well plate.

Measurement

For colorimetric assays, measure the absorbance (A) at 532 nm. For fluorometric assays, measure relative fluorescence units (RFU) at λ_{Ex} = 532 nm /λ_{Em} = 553 nm).

Results

1. Calculate ΔA / ΔRFU by subtracting the A / RFU reading of Standard #6 (Blank) from the remaining Standard reading values. Background values can be significant and must be subtracted from all readings. The amount of MDA present in the samples may be determined from the standard curve.
2. Plot the ΔA / ΔRFU values against Standard concentrations and determine the slope of the standard curve.
3. Using the standard curve determine the quantity of MDA in nmole in the Sample.

   a. For Samples without the 1-butanol concentration step, calculate the MDA concentration of the Sample:

   MDA (nmol/mL) =

$$(SA/SV) \times DF = C$$

where:

S_A = Amount of MDA in Sample (nmole) as determined from the standard curve

S_V = Sample volume (mL) or amount (mg) added into the wells

DF = Sample dilution factor (DF = 1 for undiluted Samples)

C = Concentration of MDA in sample

Example Calculation

Amount of MDA (S_A) = 5.84 nmole Sample volume (S_V) = 0.020 mL Concentration of MDA in sample =

(5.84 nmole/0.020 mL) × 1 = 292 nmole/mL

b. For Samples with the 1-butanol concentration step, calculate the MDA concentration of the Sample:

MDA (nmol/mL) =

$$(SA/SV) \times 4 \times DF = C$$

where:

S_A = Amount of MDA in Sample (nmole) as determined from the standard curve

S_V = Sample volume (mL) or amount (mg) added into the wells

4 = Correction factor for using 200 µL of the 800 µL reaction

DF = Sample dilution factor (DF = 1 for undiluted Samples)

C = Concentration of MDA in sample

Example Calculation

Amount of MDA (S_A) = 5.84 nmole Sample volume (S_V) = 0.020 mL Concentration of MDA in sample

(5.84 nmole/0.020 mL) × 4 × 1 = 1,168 nmole/mL

Technical Assistance

Visit the tech service page at SigmaAldrich.com/techservice.

Terms and Conditions of Sale

Warranty, use restrictions, and other conditions of sale may be found at SigmaAldrich.com/terms.

Contact Information

For the location of the office nearest you, go to SigmaAldrich.com/offices.

The life science business of Merck operates as MilliporeSigma in the U.S. and Canada.

4

S4 Zymot differentiation protocol

ZyMōt®
MULTI (850µL)
Sperm Separation Device | ZMH0850

ILLUSTRATED USE STEPS

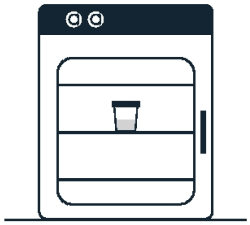

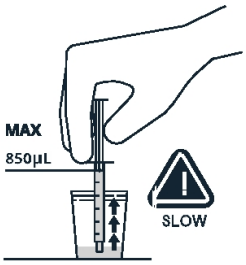

1 | Allow sample to liquify

2 | Draw 850µL of the sample.

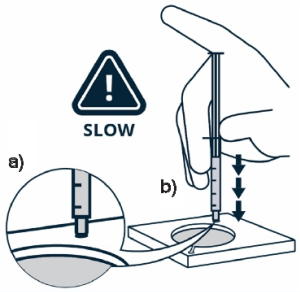

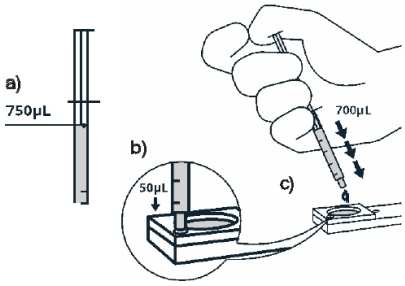

3 | **a)** Achieve seal. **b)** Slowly inject sample.

4 | **a)** Draw 750µL of media. **b)** Prime outlet channel. **c)** Cover membrane surface.

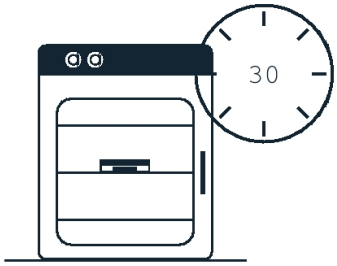

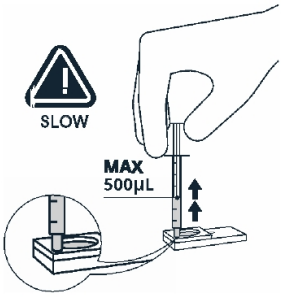

5 | Incubate at 37°C for 30 minutes.

6 | Slowly aspirate a maximum of 500µL

ICSI and IUI
Transfer the collected sample to an appropriate culture tube: a 4mL round bottom culture tube with a snap top or into the bottom of a 15mL conical tube.

Tubes using HEPES-buffered media may be held on the benchtop or tightly capped in an incubator.

Tubes using bicarbonate-buffered media should be st ored in a CO_2 incubator with the lid loosely closed.

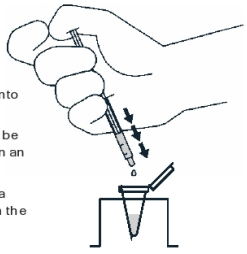

IVF
Transfer the collected sample into a 15ml conical tube.

Add 3ml of bicarbonate-containing media (whatever media is usually used for the final suspension of sperm for conventional insemination) to the conical tube. Mix gently.

Centrifuge the conical tube for 5min at 300 x g.

Remove the supernatant, being careful to not disturb the lower pellet.

Perform count and motility as usual and dilute if needed to achieve appropriate final insemination concentration.

Store tube in a CO_2 incubator until insemination. Insemination should occur more than 1hr, but less than 4hrs after preparation.

7 | Sample Handling After Collection - **ICSI** and **IUI**

7 | Sample Handling After Collection - **IVF**

S5 OXISPERM II protocol

halotech®

oxiSperm® II

Kit REF HT-OS20II
for 20 determinations

oxiSperm® II is a simple test that allows the assessment of pro-oxidant activity in semen samples.

consult intructions of use
product reference
lot number
use by
manufacturer
in vitro diagnostic
contains sufficient for "n" test
2°C 27°C temperature limitation
keep dry
keep away from direct sunlight
CE

Principle of the method

oxiSperm® II has been developed for the assessment of pro-oxidant activity. However, these test are not habitually used by clinical and andrology laboratories. oxiSperm® II provides the clinicians with an easy, fast, reliable and stablished assay for the determination of pro-oxidant activity at three levels: neat semen, seminal plasma or spermatozoa. The test is based in the Nitro Blue Tetrazolium assay (NBT) in the form of a specifically formulated pre-embedded reactive membrane. This assay is based on the reaction of pro-oxidant molecules with the water soluble tetrazolium salt to form water insoluble blue crystals known as formazan (Baehner et al, 1976). These crystals produce an increasing colour intensity in the membrane that ranges from a pale pink to a dark purple-blue that can be easily and comparatively quantified by visual inspection (see colour palette).

Figure 1. Colour pallet according to NBT- reactivity (according to oxiSperm®II)

Description of kit reagents

Each kit contains reagents to test the pro-oxidant activity in 20 ejaculates (neat semen, seminal plasma, sperm).

OSIIRS: Reactive membranes. 20 units with 4 wells each
(N: Neat Semen; SP: Seminal Plasma; S: Sperm; C: Control).
OSIISI: Sperm reactivity induction solution. 1 vial with 210µl.

Material and equipment required, not provided with the kit

*Micropipettes
*Centrifuge capable of reaching 6000xg
Eppendorf tubes
Phosphate Buffered Saline (PBS)
*** NOTE: All equipment should be calibrated**

Samples

Fresh semen samples are advisable. Frozen semen samples can be used for the analysis of pro-oxidant activity in net semen or seminal plasma but not in spermatozoa

Assay protocol

Use recent ejaculated semen samples to obtain the most realistic information at the time of ejaculation. Frozen semen samples can be used for the analysis of oxidative stress in net semen or seminal plasma, but not in spermatozoa.

1. Add 10 µl of neat semen sample to a clean Eppendorf tube -Neat Semen Sample-.
2. Transfer an additional volume of net semen containing at least 10^6 spermatozoa to a new Eppendorf tube or similar, and centrifuge the sample at 6000xg for 10 minutes Transfer seminal plasma fraction to a clean Eppendorf tube -Seminal plasma sample-.
3. Re-suspend spermatozoa pellet in 50 µl of phosphate buffered saline (PBS) and keep it for 3 min at room temperature.
4. Centrifuge spermatozoa at 6000xg for 10 minutes. Discard supernatant and re-suspend spermatozoa pellet in 50µl of PBS and repeat centrifugation at 6000xg for 10 minutes. Discard supernatant and re-suspend spermatozoa pellet in 5-10 µl of the sperm reactivity induction solution. Keep the sperm in these conditions at room temperature for 5 min -Sperm sample-.
5. Pull out from the envelope the reactive membrane card containing 4 wells, 1 for each sample and control. Avoid direct sunlight exposure on the membrane.
6. Place 5 µl of the content of each Eppendorf tube (Neat seminal sample, Seminal plasma sample, Sperm sample) at the corresponding place on the reactive membrane.
7. Let the membrane at room temperature protected from direct sunlight exposure. Full colour will develop in 15 minutes (colour development in spermatozoa may take a prolonged time).
8. For a negative control, the control well can be used by adding 5 µl of PBS.
9. Compare the colour of the samples with the colour of the scheme (Figure 1).

Precautions

1. All samples should be treated as potentially infectious and users must wear protective gloves, eye protection and laboratory coats when performing the test.
2. Do not touch the membrane directly with the hands or skin. This can modify the expected reaction. Avoid direct exposure of the reactive membrane to sunlight. Keep the unused reactive membranes in the wrapper protected from light.
3. Membranes and all material used to perform the test should be discarded to a proper biohazard container after testing.
4. Do not eat, drink or smoking in the area where samples and assay reagents are handled.
5. Do not use beyond the expiration date, which appears on the package label.
6. Material Safety Data is available upon request.
7. Once the test is performed, do not re-store the card to reuse those wells that have not been used.The reactive support of unused wells may be affected by exposure to artificial light. during incubation for color development in the wells in which the sample has been applied

Safety and the environment

Do not release the products used into the environment. Follow center guidelines for the storage and disposal of toxic substances.
Biological samples must be handled as potentially infectious.

Storage conditions

After receiving the kit, store it between 2°C and 27°C and keep it protected from light. After opening the kit, it is recommended to store it at 4ºC.

Expiration

The reagents supplied are stable for 12 months.

Version 2 / 2020

C/ Faraday, 7 Parque Científico de Madrid / Edificio CLAID / Campus de Cantoblanco / 28049 Madrid
Tel: + 34 91 279 69 50 / www.halotechdna.com / info@halotechdna.com

S6 protocol of DNA fragmentation

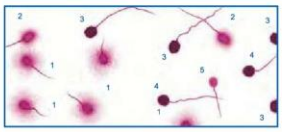

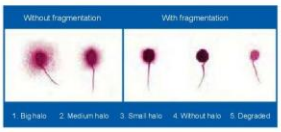

Sperm classification

Count a minimum of 300 sperm per sample following this criteria:

- Spermatozoa without DNA fragmentation:
  - -Spermatozoa with big halo: those whose halo width is similar or higher than the diameter of the core (Fig. 1).
  - -Spermatozoa with medium-sized halo: their halo size is between those with large and with very small halo (Figure 2).
- "others": cell nucleid which do not correspond to spermatozoa. One of the morphological characteristics which distinguish them is the absence of tail. These cells must not be included in the estimation of the frequency of sperm with fragmented DNA.
- Spermatozoa with fragmented DNA:
  - -Spermatozoa with small halo: the halo width is similar or smaller than 1/3 of the diameter of the core (Fig. 3).
  - -Spermatozoa without halo: (Fig. 4).
  - -Spermatozoa without halo and degraded: those that show no halo and present a core irregularly or weakly stained (Fig. 5).

Positive and negative controls

Positive control: all the sperm cells are shown with halo. Follow the instruction for use, skipping step 7.

Negative control: all the sperm cells are shown without halo. Follow the instruction for use, skipping step 8.

Safety and the environment

- Care should be taken to avoid contact with skin or eyes, and to prevent inhalation. The acid solution (DA) contains Hydrochloric acid, and the lysis solution (LS) contains Dithiothreitol and Triton X-100. Work under air removal environment and follow the manufacturer's Material Safety Data regarding safe handling.
- Do not release the products used into the environment. Please follow the specific safety regulation of your laboratory facility with respect to chemicals storage and toxic products disposal as well as the exposure to them.

Precautions

- All patient samples and reagents should be treated as potencially infectious and the user must wear protective gloves, eye protection and laboratory coats when performing the test.
- The test should be discarded in a proper biohazard container after testing.
- Do not eat, drink or smoke in the área where specimens and kit reagents are handled.
- Do not use beyond the expiration date, which appears on the package label.
- The use of gloves and face mask is recommended.
- Material Safety Data Sheet is available on request.

Store conditions

After receiving the kit, store it between 2º and 8ºC.
After opening the kit is stable for 9 months

Version 08.1 / 2018

C/ Faraday, 7 Parque Científico de Madrid / Edificio CLAID / Campus de Cantoblanco / 28049 Madrid
Tel: + 34 91 279 69 50 / www.halotechdna.com / info@halotechdna.com

halotech®

halosperm® G2

Kit REF HT - HSG2
for 10 determinations

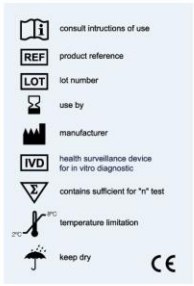

halosperm® G2 has been developed by Halotech DNA in response to the needs of users of the SCD test (Sperm Chromatin Dispersion test) for assessing sperm DNA fragmentation in human.

Principle of the method

Intact unfixed sperm (fresh, frozen/unthawed, diluted samples) are immersed in an inert agarose microgel on a pretreated slide. An initial acid treatment denatures DNA in those sperm cells with fragmented DNA. Following this, the lysis solution removes most of the nuclear proteins, When absence of massive DNA breakage is present, nucleoids from sperm with fragmented DNA either, do not show a dispersion halo or the halo is minimal. The diagnostic sensitivity and specifity is 93%. This test is an aid in the diagnosis. Interpretation of the results will be under medical criteria.

Description of kit reagents

Every kit contains the necessary to perform 10 assays. The components are:

- Agarose Cell Support (ACS); 1 screw tube
- Super-Coated Slides (SCS); 10 units
- Eppendorf Tubes (ETP); 10 units
- Solution 1 (DA) Denaturant Agent, one 10 ml drop bottle
- Solution 2 (LS) Lysis Solution, one 10 ml drop bottle
- Solution 3 (SSA) eosine Staining Solution A, one 10 ml drop bottle
- Solution 4 (SSB) thiazine Staining Solution B, one 10 ml drop bottle
- Float

Material and equipment required, not provided with the kit

Bright field or fluorescence microscope, fridge at 4º C, incubation bath (s) at 37º C and 95-100º C, plastic gloves, glass coverslips (24 x 24 mm). Micropipettes, Petri dishes or similar tray, disposable pipettes, distilled water, ethanol at 70% and 100%. Microwave oven and fume hood (it is recommended the use of fume hood but it is not mandatory because of low reactive concentration). Be ware that all equipment is calibrated

Sperm sample

Fresh semen samples should be collected in a sterile recipient. The sperm DNA fragmentation assay should be performed immediately once the sperm sample has been obtained or thawed after cryopreservation.

Instructions for use

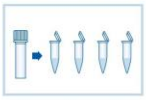

1.

1.1 Place the agarose screw tube (ACS) into the float and melt using a water bath (or a beaker with water on a hot plate) at 95-100°C for 5 minutes or until it is completely melted. Otherwise, if you prefer melting the agarose using a microwave oven, fill 100 ml of water in a beaker. Then, place the ACS slightly opened with the float inside the beaker and heat it at maximum power for 1.5 minutes. Watch constantly and stop the process as soon as the water starts boiling. Please do not keep the ACS boiling inside the microwave! Aliquote 10 eppendorf tubes (ET) with 100 microlitres of the agarose melted. Immediately after, keep the Eppendorf to be used at 37ºC for 5 minutes to prevent the gelification.

1.2 The remaining Eppendorf tubes which are not going to be used at that moment will be storage in the fridge along with the kit.

1.3 Set Solutions 1 and 2 at room temperature (22°C) during the whole process.

1.4 Prepare and select the Super-Coated Slides (SCS) which are going to be used.

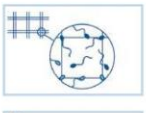

2.

Dilute the sperm sample in an appropriate human sperm extender or PBS to a maximun of 20 million sperm per mililitre

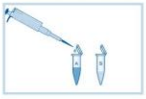

3.

Immediately after, transfer 50 µl of the sperm sample to the Eppendorf tube and mix gently with a micropipette. The formation of bubbles shall be prevented.

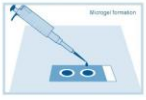

4.

Following, place a drop of 8 µl of the cell suspension onto the centre of sample well ("S"). Cover with a coverslip. Press gently, avoiding air bubbles formation. Slides must be held in a **horizontal position** throughout the entire process. Use the "C" well to process a control sample.

5.

Place the slide on a cold surface (for example, a metal or glass plate pre cooled at 4°C) and transfer into the fridge at 4°C, for 5 minutes to solidify the agarose.

6.

Take the slide out of the fridge and remove the coverslip by **sliding it off gently.** All the processing must be performed at room temperature (22 ºC)

7.

Place the slide horizontally in an elevated position as suggested In the figure into a Petri dish or similar tray.
Apply Solution 1 (DA) on the well making sure **it is fully covered by the reactive during the whole process**. Incubate for 7 minutes. Then, remove the reactive by tilting until completing the drying and place the slide horizontally in an elevated position as suggested in the figure. **It is very important to remove the reactive without shaking. We will perform the removal by tilting and letting it slide.**

8.

Apply Solution 2 (LS) on the well making sure it is fully immersed. Incubate for 20 minutes. Then, remove the reactive by tilting until completing the drying and place the slide horizontally in an elevated position as suggested in the figure. It is very important to remove the reactive without shaking. **We will perform the removal by tilting and letting it slide.**

9.

Wash the slide for 5 min covering with abundant distilled water and using a disposable pipette. Then, remove the reactive by tilting until completing the drying and place the slide horizontally in an elevated position as suggested in the figure. Dehydrate by flooding with 70% ethanol, using a disposable pipette and incubate for 2 minutes.
Drain and apply 100% ethanol for 2 minutes. Drain and allow to dry horizontally on filter paper or similar. After drying, processed slides may be kept in slide boxes at room temperature in a dry and dark place for several months.

10.

Place the slide horizontally in an elevated position into a Petri dish or similar tray. Apply Solution 3 (SSA) on the wells making sure these are fully immersed. Incubate for 7 minutes. Then, remove the stain by tilting until completing the drying and place the slide horizontally in an elevated position.

11.

Apply Solution 4 (SSB) on the wells making sure these are fully immersed. Incubate for 7 minutes. Then, remove the stain by tilting. Remove the excess of stain and allow to dry at room temperature.

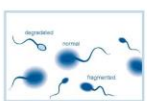

12.

Visualize under bright field microscopy. If the staining is too intense, the slide might be washed in tap water. If the staining is too weak, immerse the slide in 100% ethanol, allow to dry and repeat since step 10. For fluorescence microscopy staining, please contact the authorized dealer.

13.

Calculate the percentage of sperm with fragmented DNA. The results should be evaluated taking into account all clinical and laboratory findings related to the sperm sample. Thresholds for frequency of Sperm DNA Fragmentation (SDF) have been suggested by Dr. Evenson et al. (Evenson and Nixon, Reprod Biomed Online 12:466-472, 2006).

For future assays

Place as many eppendorf tubes as semen samples are going to be evaluated and start the protocol at the point 1.2. Previously, Place the agarose screw tube (ACS) into the float and melt using a water bath (or a beaker with water on a hot plate) at 95-100°C for 5 minutes or until it is completely melted. Otherwise, if you prefer melting the agarose using a microwave oven, fill 100 ml of water in a beaker. Then, place the ACS slightly opened with the float inside the beaker and heat it at maximum power for 1.5 minutes. Watch constantly and stop the process as soon as the water starts boiling.
¡Please do not keep the ACS boiling inside the microwave!

S7 Swim-up protocol

Sædpreparering med swim-up

HELSE NORD

Dokumentansvarlig: Elisabet Tverelv Jakobsen
Godkjent av: Mona Nystad
Gyldig for: IVF-poliklinikk UNN

Dokumentnummer: PR2997
Versjon: 3.6

Papirkopi i linkomat Andrologisk lab

Hensikt

Standardisere preparering av sædprøver til IVF/ ICSI-behandling.

Omfang

Sædprøver til IVF/ ICSI-behandling.

Arbeidsbeskrivelse

Labark, arbeidsskjema tas ut dagen før OPU, se prosedyre
PR4186 Merkeprosedyre før OPU og sædpreparering
Medier forberedes dagen før OPU, se prosedyre
PR9444 Klargjøring/ tillaging av medier
OL2934 Oversikt over medier og forbruksartikler på lab

Prøve mottak

- Mannen leverer prøve helst innen ½ time etter prøvetaking.
- Han identifiseres ved muntlig å oppgi eget navn og fødselsnummer, viser legitimasjon med bilde samt oppgir fødselsdato til kvinnen.
- Bioingeniør signerer på arbeidsskjema for identifikasjon og hvor prøven er tatt.
- Prøveboks merkes med kvinnens navnelapp på boksen og på lokket.

Prøvepreparering

1. To sterile Nunc-rør med spiss bunn og to sterile Falcon 8 ml rør med blå kork merkes med kvinnens navnelapp.
   Bruk eget stativ for hver pasient og ved hver flytting av prøve over i nye rør sjekkes navn og fødselsdato.
2. Boksen med prøvematerialet blandes/ likvifiseres i 10 minutter på vippe, hastighet 20-25 «vipp» pr. min.
3. Prøvens volum, motilitetsgrad og prosent samt viskositet bestemmes. Antall spermier estimeres, dersom lavt antall, <20 mill/ml, tas det av til manuell telling.
   PR5635 Manuell telling av spermier
4. Dersom prøven er svært viskøs, trekkes den opp i sprøyte og sprøytes ut gjennom en kanyle. Dette vil lette videre preparering.
5. Prøven tilsettes 3x volumet SpermWash i prøveboksen, maks tilsetning 10 ml. Prøven vippes 15 min. og helles deretter over i de 2 spissbunna Nunc-rør, sentrifugeres i 10 min. ved 0,4 rcf =1500 rpm.
6. Supernatanten dekanteres slik at pelleten blir så tørr som mulig.
7. Dersom problemer med løs pellet etter 1. sentrifugering:
   Bland prøven opp igjen og trekk den gjennom sprøyte/kanyle, gjenta 1. sentrifugering og dekantering.
8. Med pipette tilsettes 1ml Fertmedium, FM i hvert rør, innholdet blandes godt med pipette, og hele mengden has over i *ett Falcon rør med blå kork.*
9. Røret sentrifugeres 5 min. ved 0,2 rcf =1200rpm.

10. Pipetter forsiktig av supernatanten.
11. Normale prøver: Pipetter 1,5 ml FM meget forsiktig over pelleten.
    Nedsatte prøver: Pipetter 0,5- 1,0 ml FM meget forsiktig over pelleten.
12. Sett prøven til swim-up i 1-2 timer i CO_2- inkubator sammen med det tomme røret med blå kork. **OBS! Løse korker!**

Etter inkubering:

13. Pipetter av 0,7 ml like under toppen av supernatanten, over i det tomme røret. Unngå å ta med det aller øverste laget. Ved nedsatt prøve tas av mindre mengde.
    Ved svært nedsatt prøve tas det ut 5-10 ul like over pellet direkte til bruk ved ICSI.

Bedømming av kvalitet etter swimup.

14. Motilitets-grad og % bedømmes og antallet telles, se prosedyre:
    PR19457 Sædanalysering ved andrologisk lab. : parametre.
15. Det beregnes insemineringsvolum, se prosedyre: *PR3102 Inseminering av egg.*
    ICSI-prøver estimeres på antall.
16. Dersom en ikke er fornøyd med antall spermier, pipetteres 0,5 ml fra neste lag og det telles på nytt.
    Dersom det ennå er for få spermier kan vi blande hele supernatanten og sentrifugere ved 0,2 rcf =1200 rpm i 5 min. og fjerne øverste ½-del for å konsentrere prøven.
17. Den ferdig preparerte prøven oppbevares i CO2- inkubator før inseminering av egg.
    OBS! Løse korker!

    Analyse-verdier noteres på spermprep-skjema og føres inn i LinneFiler under OPU/Spermieanalyse /dagens dato. Husk å krysse av for ID-sjekk.
    Signèr i Linnefiler: OPU/ inseminering. Kryss av for inseminering i bildet Embryo/ D0
    Legg inn alle aktuelle parametere under Spermieanalyse/ før og etter prep og utfør BKM for refusjon fra Helfo.

S8 abnormal spermatozoa

Table showing Criteria of normal and abnormal spermatozoa according to WHO. *For each part of the spermatozoa (i.e., head, midpiece and tail) morphological criteria are presented. Cytoplasmic residues are also included (49).*

Location	Normal (ideal/typical) appearance	Abnormal
Head	The head should be smooth, regularly contoured and generally oval in shape. There should be a well-defined acrosomal region comprising 40–70% of the head area (96). The acrosomal region should contain no large vacuoles, and not more than two small vacuoles, which should not occupy more than one fifth of the sperm head. The post-acrosomal region should not contain any vacuoles.	• acrosome less than 40% or larger than 70% of a normal head area, or • length-to-width ratio less than 1.5 (round) or larger than 2 (elongated), or • shape: pyriform (pear shaped), amorphous, asymmetrical, or non-oval shape in the apical part, or • vacuoles constitute more than one fifth of the head area or located in the post-acrosomal area, or • double heads, or • any combinations
Midpiece	The midpiece should be slender, regular and about the same length as the sperm head. The major axis of the midpiece should be aligned with the major axis of the sperm head.	• irregular shape, or • thin or thick, or • asymmetrical or angled insertion at head, or • sharply bent, or • any combinations
Tail	The principal piece should have a uniform calibre along its length, be thinner than the midpiece and be approximately 45 µm long (about 10 times the head length). It may be looped back on itself, provided there is no sharp angulation indicative of a broken flagellum.	• sharply angulated bends, or • smooth hairpin bends, or • coiled, or • short (broken), or • irregular width, or • multiple tails, or • any combinations
Cytoplasmic residue	Cytoplasmic droplets (less than one third of a normal sperm head size) are normal.	• residual cytoplasm is considered an anomaly only when it exceeds one third of normal sperm head size